Application and Improvement of the Unmanned Aerial System SUMO for atmospheric boundary layer studies

Stephanie Mayer

Geophysical Institute

University of Bergen, Norway

A thesis submitted for the degree of

Philosophiae Doctor (PhD)

June 2011

Coming together is a beginning;
keeping together is progress;
working together is success.
(Henry Ford)

This thesis is written in LaTeX.

Contents

1 Introduction **3**

1.1 In-situ & remote measurement methods 6

1.1.1 Profiling the atmospheric boundary layer 6

1.2 Numerical weather prediction models 9

1.2.1 A short historical overview 9

1.2.2 Parameterizations of physical subgrid-scale processes in numerical weather prediction models 10

1.2.3 The Weather Research and Forecasting model WRF 11

1.3 Motivation & Objectives 12

1.4 The Small Unmanned Meteorological Observer SUMO 15

1.4.1 The airframe 15

1.4.2 Autopilot system 15

1.4.3 Meteorological sensors 17

1.4.4 SUMO operation 17

1.5 Current rules and regulations for unmanned aerial systems 19

1.6 Outlook 21

References **25**

2 Publications **29**

2.1 Summary of Papers 29

2.1.1 Paper I 29

2.1.2 Paper II 30

2.1.3 Paper III 31

Acknowledgements

First of all I would like to thank my supervisors Prof. Dr. Joachim Reuder and Dr. Anne D. Sandvik for supporting and encouraging me during the course of this Ph.D. thesis. My gratitude belows Marius O. Jonassen for being a great fellow during the last years for discussing both technical and scientific topics in a very relaxed and patient way. Many thanks go to the FLOHOF and Svalbard campaign team members for making both field campaigns a success. Without the Paparazzi project mainly provoked by Dr. Pascal Brisset and the working enthusiasm of the model aircraft constructors and pilots Martin Müller and Christian Lindenberg, the realization of SUMO would not have been possible.

GFI's Ph.D. students have developed a great social environment during the last years, especially the Friday's football workout was making 'hard' office work more bearable and mind refreshing. I would like to thank Kristin Richter for being an enjoyable office mate and coffee drinking fellow during the last five years.

Last but not least, I would like to thank my family in Germany for taking care of my daughter while I was spending many weeks abroad on field work and conferences.

Abstract

This synthesis and collection of Papers is submitted for the degree of Philosophiae Doctor (Ph.D.) in experimental meteorology at the Geophysical Institute, University of Bergen, Norway. It consists of two main parts. In the first part, the reader finds an introduction providing the motivation for the study and an overview of measurement methods of the atmospheric boundary layer followed by a brief review on numerical weather prediction modelling. This part also includes a detailed description of the used measurement tool, the Small Unmanned Meteorological Observer SUMO and an overview of Unmanned Aerial Systems used in atmospheric science including regulatory issues. The second part consists of three scientific Papers covering measurements with SUMO and simulations with a numerical weather prediction model. In Paper I and II model and measurements are compared. SUMO system improvements related to wind measurements are addressed in Paper III.

1

Introduction

In this Ph.D. thesis a combination of measurements and integrations with a numerical weather prediction model is presented. The new measurement tool called Small Unmanned Meteorological Observer (SUMO) has been developed for applications in the atmospheric boundary layer (ABL) and numerical model integrations have been performed with the Weather Research and Forecasting model WRF.

With these tools the focus of this study is set on the lowest part of the atmosphere adjacent to the Earth's surface where exchange processes of energy and mass between the surface and the free atmosphere above take place. The air in this layer directly feels the influence of different surface types (sea, land, snow, water, ice) by heating, cooling and friction on a time scale in the order of one hour. According to *Stull* (1988), it typically reaches from bottom up to 100-3000 m and hence represents roughly the lowest 10 % of the troposphere (see Figure 1.1). The ABL is of special interest because it is the part of the atmosphere where forcing mechanisms such as heat transport from and to the ground, frictional drag, evaporation and transpiration, terrain-induced flow modification and pollution emission take place and thereby affect our daily life *Stull* (1988).

The atmosphere and in particular the ABL are a complex dynamical system that cannot be predicted without the use of numerical models. Numerical weather prediction (NWP) models are computer codes based on simplified mathematical representations of physical processes. The output and results of limited area NWP models provide knowledge for daily weather forecasts as well as regional climate

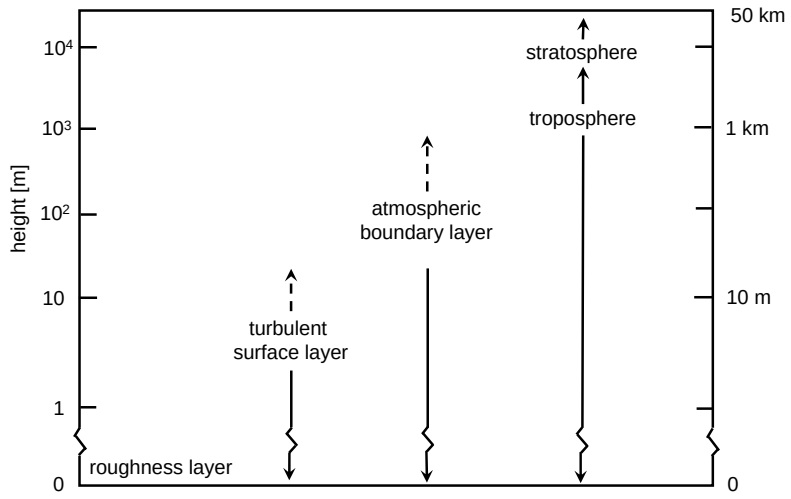

Figure 1.1: *Sketch of the vertical structure of the atmosphere in the lowest 50 km (adapted from Oke (1987)).*

projections for future decades which become increasingly important for planning and adaptation purposes. Hence, the skill and the performance of NWP models are of vital interest for the atmospheric science community as well as for decision makers and planning purposes. The quality of forecasts is highly dependent on reliable observational data for

- the definition of initial and boundary conditions
- the understanding of the physical processes to be mathematically described in the models on an appropriate scale
- the corresponding choice of parameterizations of physical subgrid-scale processes
- the validation, evaluation and further improvement of model physics by intercomparison with measurements.

Large data centres, such as the European Centre for Medium-Range Weather Forecasts (ECMWF) and the National Centers for Environmental Prediction (NCEP), operationally use data from surface-based automatic weather stations,

released radiosondes and satellite-based sensors to monitor the state of the atmosphere. Besides environmental monitoring, the quality of these data sets are crucial for the initialization of NWP models and operational implementation of observational data in data assimilation cycles (e.g. *Hollingsworth et al.* (1986) and *Daley* (1991)).

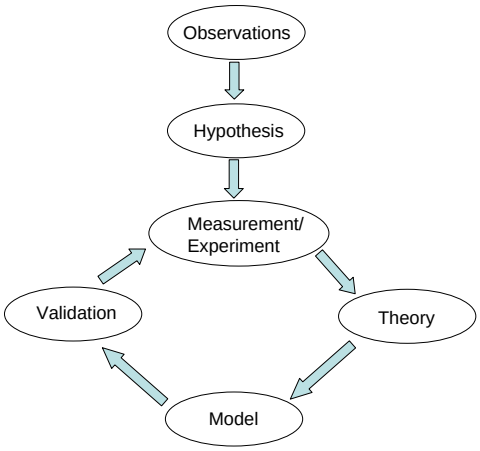

Figure 1.2: *Sketch of the observational and theoretical cycle - showing the equal importance of measurements and models.*

In general, the basic understanding of physical processes in daily weather originates from meteorological measurements. Observations provide the fundament for new hypotheses investigated in targeted meteorological field experiments. Ideally, observational findings can be used to raise new theories or to verify already existing theories, and if necessary to improve such. The theoretical work finds its application in NWP models. To validate NWP models, measurements are always required because they represent the unique source of information on the 'true' state of the atmosphere. However, one should be aware of the measurement methods' limitations and the uncertainties they are afflicted with. Figure 1.2 sketches the continuous interaction between observations, models and theory as tools. The use of measurements and the development and application of models can be considered to be of equal importance in atmospheric sciences (*Warner*, 2011).

The scope of this work is directed towards the meteorological application and improvement of a new measurement tool. This is the unmanned aerial system SUMO. A detailed description of SUMO is provided in section 1.4 followed by an overview of data measured during several field campaigns listed in Table 1.4. These data have been used in case studies for Iceland (Paper I) and Svalbard (Paper II), for evaluation of ABL schemes embedded in the Weather Research and Forecasting model WRF (Paper II) and as a basis for several tests of a new wind algorithm for small unmanned aerial systems (Paper III).

1.1 In-situ & remote measurement methods

A vast variety of measurement methods for atmospheric sciences has grown during the last 140 years. Depending on the demanded variable, available measurement technologies and financial budgets, one can choose from a pool of measurement methods. Atmospheric measurement methods can be divided into two main techniques: i) in-situ and ii) remote techniques as listed in Figure 1.3 which can be surface, airborne or space-based.

1.1.1 Profiling the atmospheric boundary layer

The knowledge of temperature, humidity, wind speed, wind direction and pressure build up the pillars of atmospheric science by being the backbone of the basic governing equations also called the primitive equations. They consist of the equation of state (ideal gas law), the conservation of mass (continuity equation), the conservation of momentum (Newton's second law), the conservation of moisture, the conservation of heat (first law of thermodynamics) and the conservation of a scalar quantity (e.g. *Holton* (1992)).

Measurements on the Earth's surface as well as continuous profiles of temperature, humidity and wind in the vertical dimension are indispensable to monitor and understand physical processes in the atmosphere and to verify, evaluate and improve NWP models. By measuring these variables, the ABL's stability and height can be determined and mean fluxes of heat and momentum can be

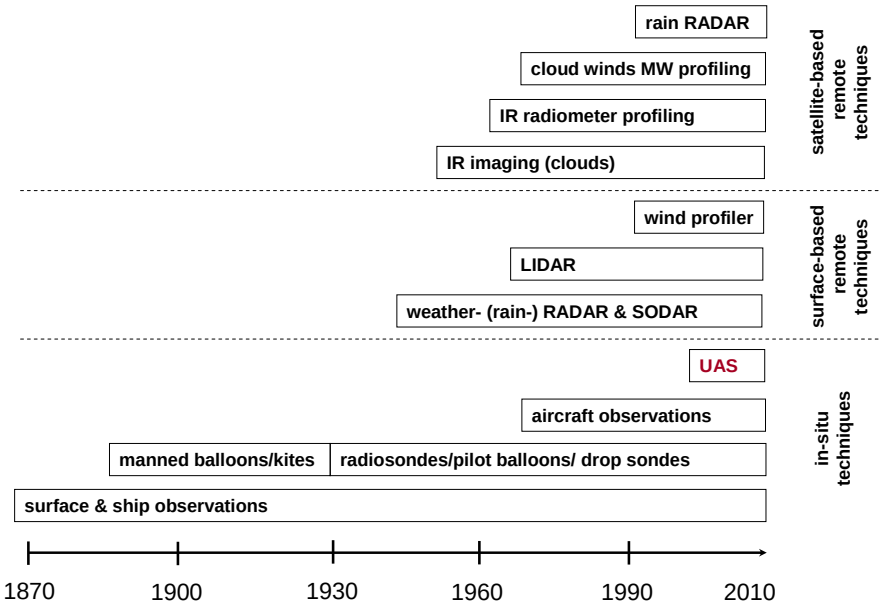

Figure 1.3: *Timeline of meteorological observation techniques (extended from Uppala et al. (2005)).*

estimated. Currently available in-situ measurement platforms are typically automatic weather stations, masts, radiosondes, tethered balloon systems, kites, and research aircraft equipped with meteorological sensor packages.

Historically seen, the first airborne meteorological measurements were performed by using kites in the 18th century by Ben Franklin who flew a kite to study lightning and tracked the direction of a storm impinging the US East Coast in 1743. George Washington and Thomas Jefferson kept logs of atmospheric conditions each day at Mount Vernon and Monticello, Virginia, USA. Kites are still used in single meteorological field campaigns (*Balsley et al.* (1998)), although they have mostly been replaced by tethered balloons in the 20th century. Tethered balloons are large helium-filled balloons attached to a rope which is fixed to an electrical winch on the ground. They are usually equipped with a sensor package consisting of temperature, humidity and pressure sensors and an anemometer for wind measurements to monitor the dynamics and stratification of the ABL. They can be additionally equipped with chemical sensors to measure the chemical composition of the ABL (e.g. *Spirig et al.* (2004)). The balloon's

ascending and descending rate can be controlled by the ground-based winch. Operating the balloon with very slow ascending or descending rates, measurements in very high vertical resolution can be achieved. Meeting very strong inversions, smaller-sized tethered balloons can have troubles to penetrate such layers as it may lack enough buoyancy force. Such a situation was encountered in the field campaign in Svalbard 2009 (Paper II). Tethered balloons are limited in reaching high ceiling heights depending on the length of the rope and prevailing wind conditions. Avoiding such limitations, radiosondes can be an alternative measurement method because they are not attached to a winch. They can profile the lower and upper atmosphere and they are operationally used all over the world. However, they are directly influenced by the wind and thus they do not represent a column measurement in reality. In addition, they are not very suitable for ABL studies because of their lack in vertical resolution due to a fast ascent rate and they can be uneconomical when using them in high frequency because the instrument package cannot be recovered.

Quite new in the aspect of monitoring the atmosphere and especially the ABL, is the use of unmanned aerial systems (UAS). A UAS is an airplane which flies without a human crew onboard. They are mostly known for their military applications but become increasingly important for civil and scientific purposes. Due to their high flexibility, in particular UAS are of great value in areas considered too dangerous for manned aircraft (such as polar environments or flights at low altitude). During the last decade, the application of UAS as alternative in-situ measurement tools has become very popular to fill the observational gap between surface-based measurements and satellites.

The idea to equip a simple model aircraft with a meteorological sensor package is not new. Probably the first ones to use a remotely piloted model aircraft equipped with a temperature, humidity and pressure sensor were *Konrad et al.* (1970) in the late 1960s. During the last 10-15 years the use of UAS has gained popularity in the field of atmospheric science due to an enormous engineering progress in electronical miniaturization of meteorological sensors, data logging systems and highly accurate navigation systems. Small UAS are a very cost-efficient alternative compared to the previously mentioned measurement systems. Of course, all measurement methods have their advantages and shortcomings,

Table 1.1: *An intercomparison of in-situ profiling systems (partly adapted from Balsley et al. (1998)).*

ITEM	radiosonde	tethered balloons	kites	masts	manned research aircrafts	UAS SUMO
max. alt. coverage [km]	> 30	$<$ 1-2	> 5	< 0.4	< 18	< 4
max. payload weight [kg]	< 3	≈ 100	≈ 10	large	≈ 500	< 1
vertical resolution [m]	50	$<$ 1-10	$<$ 1-10	≈ 1	< 10	$<$ 1-50
system costs [k$]	10	10-200	10-20	1-800	50-6000	6
cost per profile	low-high	low	very low	low	high	very low
wind speed limits [m s^{-1}]	$<$ 10 (launch)	< 12	$>$ 5-7	none	minimal	$<$ 15-18
continous data output	no	no	no	yes	no	no
all weather?	yes	no	no	yes	typically yes	no

therefore they are subject to a trade-off process deciding which profiling system is most appropriate in a specific case. Corresponding characteristics of in-situ profiling systems are summarized in Table 1.1.

1.2 Numerical weather prediction models

1.2.1 A short historical overview

The roots of numerical weather prediction (NWP) can be traced back to the work of the Norwegian physicist Vilhelm Bjerknes. In 1904, he published a paper suggesting that the state of the atmosphere can be predicted by solving a system of thermodynamic and hydrodynamic equations under the assumption that the current state of the atmosphere is well known (*Bjerknes*, 1904). This implied

firstly, the diagnosis to comprise the initial state from a set of observations and secondly, the prognosis where the state of the atmosphere is calculated by applying the system of thermodynamic and hydrodynamic equations. Two decades later *Richardson* (1922) tried to carry out Bjerknes theoretical work by developing the first NWP system. He divided a limited area into grid cells, as initial conditions he used data from synoptic weather maps published by V. Bjerknes, and finally he computed the finite differences solutions of differential equations. He formulated a set of primitive equations of motion and solved them numerically for a six hour forecast. This calculation took him several weeks and resulted in failure.

After the Second World War, more (upper-air) observations (see Figure 1.3) became available and first electronic computers were developed. These were two important technological developments enabling further progress in NWP. In the early 1950s, Charney, Fjørtoft and von Neumann were the first ones in this field who could compute a first one day forecast using a one-layer model (*Charney et al.*, 1950). In 1966, the first operational global NWP model was put into practice with a grid size of 300 km in the horizontal dimension including six vertical levels (*Shuman and Hovermale*, 1968). In the 1970s and 1980s NWP models progressed further on and the use of limited area models with higher resolution became feasible using data from global models as boundary conditions. During recent years numerous limited area models have been developed to run on supercomputers at national research centres. Some examples of commonly used limited area models are the HIRLAM model (*Källén*, 1996), the MesoNH model (*Lafore et al.*, 1997), the RAMS model (*Pielke et al.*, 1992), the MM5 (*Grell et al.*, 1994) and the WRF model (*Skamarock et al.*, 2001).

1.2.2 Parameterizations of physical subgrid-scale processes in numerical weather prediction models

Besides numerical techniques, data assimilation techniques and grid sizes, the formulation of physical subgrid-scale processes is a key component in NWP models (*Stensrud*, 2007). Due to the fact that the real state of the atmosphere is only an approximation in a numerical model, it can never be represented perfectly.

The number of discrete grid points governs the representation of atmospheric features by the model. With an increasing number of grid points, the structures (e.g. topographically modified flows) can be resolved with increasing accuracy. Nevertheless, there are always structures too small to be resolved by the model (e.g. turbulent eddies). Such structures can be very crucial for the performance of a viable weather forecast. The mathematical description of these subgrid-scale processes in models are called parameterizations. Physical processes that are typically parameterized in modern NWP models are soil-vegetation processes, surface layer processes, turbulent exchange processes in the ABL, micro-physics, convection and radiation. All these parameterizations are important because they have a strong influence on the skill of a weather forecast by interacting indirectly with each other by changing model variables. Their interrelation can lead to feedbacks causing non-linear effects which makes it a challenge to distinguish between cause and effects.

Most parameterization schemes focus on the effects of physical processes within the vertical column for each grid box. The vertical orientation originates from the consideration that many of these physical processes naturally rearrange energy in the vertical dimension. The model has no direct information of subgrid-scale physical processes, thus in parameterization schemes they have to be related to known model variables, empirically determined relationships and constants. Relationships between subgrid-scale processes and the known model variables define parameterization scheme closures. It is important to be aware of that parameterizations are simplified and idealized representations of complex processes and may therefore not always be appropriate. However, without parameterizations NWP may not be useful because most subgrid-scale processes are key factors in weather forecasts that concern our daily life (*Stensrud*, 2007).

1.2.3 The Weather Research and Forecasting model WRF

In the performed studies in Paper I and Paper II the Weather Research and Forecasting model WRF has been used as a modelling tool. Its model code and documentation as well as pre- and post-processing tools are freely available on `www.wrf-model.org`. The model is used by a rapidly increasing user community

that continuosly contributes to model improvements. To date, it is used by over 14000 registered users in 144 countries for operational weather forecasts, various atmospheric research purposes (including atmospheric chemistry and wildfire research) as well as for dynamical downscaling of future climate projections for limited areas. The application of the WRF model is mainly made for simulations in the order of mesoscale (10-200 km), although it can also be run in higher-resolution configuration by using the one-way or even two-way nesting option (*Skamarock et al.*, 2008). Hence, particularly for case studies, WRF is a formidable tool to be used in higher-resolution as is reflected in its appearance in a great variety of atmospheric science literature for example hurricane studies (e.g. *Davis et al.* (2008)) as well as applications in the Arctic and Antarctic (*Bromwich et al.*, 2009; *Hines and Bromwich*, 2008; *Hines et al.*, 2011) and in complex terrain such as steep mountains in the Himalaya region (e.g. *Medina et al.* (2010)).

1.3 Motivation & Objectives

With operational mesoscale NWP progressing towards kilometre and even sub-kilometre resolution, more detailed forecasts of circulation patterns and boundary layer structures can be produced down to regional and even local scales. Caused by this advancement the quality and performance of parameterization schemes appear in a new spotlight. Are they regardlessly valid when increasing the horizontal resolution in models from tenths of kilometres to scales in the order of one kilometre? This is the scale when physical processes, such as turbulent eddies in the ABL (scales of 10^{-3} to 10^{3} m) and cumulus convection (scales of 10^{2} to 10^{3} m) are being partially resolved in NWP models (e.g. *Klemp* (2007); *Stensrud* (2007); *Warner* (2011)). Thus, NWP models are operated in a twilight zone which consequently increases the demand for appropriate measurement tools for evaluation and verification purposes. This arrogates the need for new flexible and affordable measurement strategies accounting for such scales.

So far, there has been a lack of cost-efficient measurement systems appropriate for the ABL covering a horizontal range of 100 m to 10 km. Therefore, there is

a need for alternative measurement systems to bridge the gap between surface measurements and already existing in-situ and remote measurement systems. As described in section 1.1.1, UAS can be a helpful tool to complement space-based and ground-based measurement systems. Nowadays, there are numerous activities in using UAS for atmospheric research. The biggest UAS in use are the Global Hawk (National Aeronautics and Space Administration (NASA) and National Oceanic and Atmospheric Administration (NOAA)) (Figure 1.4a)) and the Zephyr (Figure 1.4b)) which can remain in the air for several hours to days (QinetiQ press release, Aug 2008). Due to their size, they are, however, not suited for ABL research. Smaller sized UAS as the Manta (Figure 1.4c)) and Aerosonde (Figure 1.4d)) have been used in various missions as over the Indian Ocean to investigate global dimming (*Ramanathan et al.*, 2007), hurricanes over the Atlantic Ocean (*Cascella*, 2008) and katabatic flows in the Antarctic (*Cassano and Knuth*, 2010). An even lighter UAS such as M^2AV (Figure 1.4f)) has been used for profiles and horizontal surveys in the ABL (*Spiess et al.*, 2007; *van den Kroonenberg et al.*, 2008). The UAS Kali (Figure 1.4e)) has been successfully used in very steep mountainous terrain in the Kali Gandaki Valley in Nepal (*Egger et al.*, 2002) and in the Andes (*Egger et al.*, 2005). These UAS have shown their excellent capabilities in being additional valuable measurement tools in meteorological field campaigns due to their flexible manoeuvrability.

In this context, the main motivation for developing SUMO has been to build a small and cost-efficient UAS that can be used as 'controllable and recoverable radiosonde' for atmospheric boundary layer research purposes by enabling in-situ measurements of temperature, humidity and wind with high spatial and temporal resolution (*Reuder et al.*, 2009). Especially, the field campaigns in Central Iceland (Paper I) and Svalbard (Paper II) have proven the operation of SUMO in mountainous and Arctic environment where observations are generally rare and thus highly demanded. Therefore, the SUMO system can be regarded as an additional measurement tool that has been made available for various applications in atmospheric boundary layer research.

Since SUMO has a very limited payload in the order of grams, an alternative wind estimation method had to be found to replace sophisticated onboard wind measurement devices. The so called 'no-flow sensor' wind estimation method is

described and elaborated on in Paper III of this Ph.D. thesis. For quality control and validation purposes of the wind estimation algorithm, data from several field campaigns listed in Table 1.4 have been used.

Table 1.2: *Overview of six exemplary UAS used in atmospheric sciences.*

	name	wing span [m]	weight [kg]	typical endurance
a)	Global Hawk	35	5000	$\approx$ 30 hours
b)	Zephyr	18	30	days-weeks
c)	Manta	2.6	27	hours
d)	Aerosonde	3	14	hours
e)	Kali	2	3	minutes-hour
f)	M^2AV	2.8	5	minutes-hour

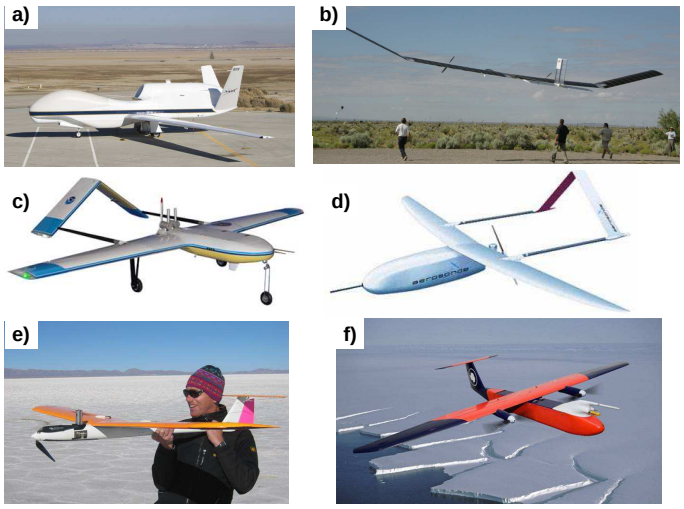

Figure 1.4: *Examples of UAS used in atmospheric science. a) Global Hawk (NASA/NOAA) b) Zephyr (Qiniteq) c) Manta (NOAA) d) Aerosonde (NASA/NOAA) e) Kali (University of Munich, Germany); f) M^2AV (Technical University of Braunschweig, Germany).*

1.4 The Small Unmanned Meteorological Observer SUMO

1.4.1 The airframe

The current version of SUMO is based on a commercially available model aircraft construction kit by Multiplex (see Figure 1.5). It is equipped with an open source autopilot system and a meteorological sensor package. It is a delta-wing pusher prop jet made of the light-weight foam material expanded propylen. The aircraft is electrically powered by a motor driving a 9"x 6" propeller. A lithium polymer battery package enables a typical endurance of 20 minutes full power motor time, enabling flight missions up to 45 minutes. Technical characteristics for the airframe are summarized in Table 1.3. The FunJet airframe is quite robust and rather inexpensive with approximately 60 €. With its take-off weight of 0.58 kg, it is very light weight compared to the previously described UAS. Low speed during landing minimizes the risk of structural damage (*Reuder et al.*, 2009).

Figure 1.5: *The FunJet airframe from Multiplex. An overview of its characteristics is shown in Table 1.3.*

1.4.2 Autopilot system

For autonomous flight capability of SUMO, the open source autopilot system Paparazzi schematically shown in Figure 1.6 has been adapted. Paparazzi provides a flexible hard- and software structure for autonomous aircraft operation. It consists of an airborne processor board with sensors for the determination of the

Table 1.3: *Overview of SUMO's characteristics and flight performance.*

length	0.75 m
wingspan	0.80 m
weight	0.58 kg
av. air speed	12-18 m s^{-1}
max. air speed	35 m s^{-1}
av. ascent rate	7-10 m s^{-1}
max. ascent rate	15 m s^{-1}
max. ceiling height	$\geq$ 3500 m agl
max. endurance	45 min

aircraft's attitude including a global positioning system (GPS) for navigation and ground speed information as well as a set of three pairs of infrared sensors used for aircraft stabilization. The Paparazzi system also incorporates the airborne autopilot software, the ground control station (GCS), an on-line communication hardware and corresponding communication protocols. A standard remote control (RC) transmitter system realizes a safety-link option (*Brisset et al.*, 2006).

Figure 1.6: *A sketch o the Paparazzi autopilot system Brisset et al. (2006).*

1.4.3 Meteorological sensors

SUMO is equipped with sensors for the measurements of pressure, temperature and relative humidity. The pressure sensor is mounted inside the fuselage, while the sensors for temperature and humidity can be attached either on top of the fuselage to minimize contamination and damage by sand and snow during landing, or under the wings to minimize radiation errors due to solar heating. Pressure is measured by the miniaturized (diameter 6.1 mm, height 1.7 mm) SCP1000 Absolute Pressure Sensor from VTI Technologies. Its measurement range covers 300 to 1200 hPa with a resolution of 0.015 hPa and an absolute pressure accuracy of 1.5 hPa in the range 600 to 1200 hPa. The relative pressure accuracy relevant for atmospheric profiling is 0.5 hPa. The pressure sensor is equipped with a temperature sensor that provides onboard temperature information during flight. This is an important information for the estimation of battery capacity under cold environmental conditions. Temperature and humidity are measured by the combined sensor SHT75 by Sensirion. The sensor element has a temperature range between -40 and 124 °C and a resolution of 0.01 K. The absolute and relative accuracies are given as ±0.5 K respectively ±0.1 K. The humidity sensor covers 0-100 % relative humidity with an absolute accuracy of ±1.8 % and a reproducibility of ±0.2 %. The ±0.5 K accuracy is valid for the temperature range between 0 and 45 °C and increases to ±0.7 K at -20 °C. The humidity sensor is temperature compensated. The given accuracy is expected to be independent of temperature and valid for the humidity range 10 to 90 % (*Reuder et al.*, 2009).

1.4.4 SUMO operation

The Paparazzi autopilot system enables manual as well as autonomous flight capabilities of SUMO. For security reasons SUMO is flown manually by a human pilot using a standard remote control transmitter during take-off and landing. In heights greater than 100 to 200 m above ground level (agl), the flight mode is switched from manual to autonomous mode. In autonomous mode, SUMO is controlled by the onboard autopilot, constantly linked to the GCS via a radiomodem data link as sketched in Figure 1.6. On the GCS's display shown in

Figure 1.8a) the operator can monitor and modify SUMO's flight parameters such as climb speed, pitch angle, etc. at any time. The Paparazzi software also enables the on-line display of the atmospheric parameters, such as temperature, humidity, wind speed and direction. The stabilization of SUMO by infrared sensoric requires a temperature difference of 8 K between ground and sky (`http://paprazzi.enac.fr/wiki/Infrared_Sensors`). This has limited SUMO to dry and clear sky weather conditions in the field campaigns listed in Table 1.4, while very cold conditions are not a limitation (see Paper II). It can be flown in wind conditions up to 15-18 m s^{-1}.

Using SUMO for vertical profile measurements, the aircraft is operated in a helical flight pattern during ascent and descent with a radius of typically 100 to 200 m (see Figure 1.7a)). This flight pattern enables a 'no-flow-sensor' wind estimation method. Figure 1.7b) presents the varying ground speed (indicated by the colour code) which the aircraft experiences during head, cross- and tail-wind conditions. Ground speed is measured by the onboard GPS. By taking advantage of this, a minimization algorithm can be applied to estimate wind speed under the assumption that the aircraft is operated with constant true airspeed using constant throttle and pitch angle. This is described explicitly and tested in detail in Paper III.

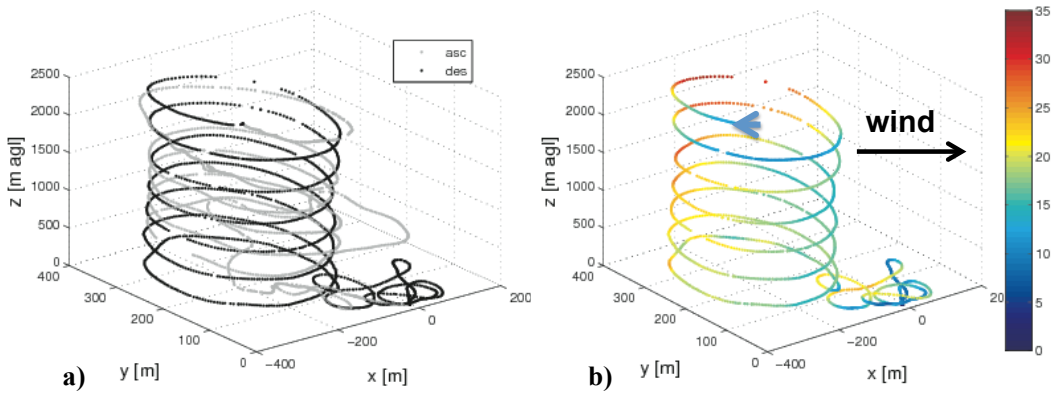

Figure 1.7: *A typical flight track for ABL profiling with SUMO; a) grey dots show ascent and black dots descent. b) The corresponding ground speed in m s^{-1} during descent is indicated by the colour code.*

Table 1.4: *Overview of scientific missions performed with SUMO. It has been used in eight field campaigns performing approximately 350 flight missions.*

campaign region	**scientific topic**	**No. flights**	**max. alt [m agl]**	**year**
FLOHOF, Central Iceland	first flights, instationary gravity waves, evaluation of ABL schemes	30	3580	2007
Svalbard	system test polar region	44	1470	2008
Coburg, Germany	nocturnal ABL	25	2450	2008
FLUXPAT III, Jülich, Germany	ABL; inhomogenous surfaces	34	800	2008
Svalbard	Arctic ABL, simultaneous flights; evaluation of ABL schemes in WRF	85	1500	2009
MOSO, Iceland	orographic flow modification and land-sea breeze	68	2990	2009
Andfjorden, Norway	characterization of marine ABL for search and rescue applications	4	1600	2009
Denmark	wind and turbulence structure in a wind park	65	100	2011

1.5 Current rules and regulations for unmanned aerial systems

In most scientific missions UAS are operated in flight levels going beyond the height limits for ordinary model aircraft activities (150 m agl). Civil Aviation Agencies (CAAs) have become aware of the need to recognize UAS equivalent to manned rotary and fixed-wing aerial systems in civil airspace. Currently, the regulations for UAS operations are rather unclear. The following paragraph attempts to summarize the actual legal situation for the operation of UAS in civil airspace. In general, the International Civil Aviation Organization (ICAO) is responsible for the flight mission clearance for UAS with a take-off weight larger than 150 kg (*ICAO*, 2011). In weight classes below 150 kg national authorities

carry responsibility for the authorization of UAS missions. To date, there is neither an international nor a European harmonization of rules and regulations for UAS missions. Even the harmonization on a national level is not given in every country. In federal states such as Germany various contact points (in the case of Germany, 17(!)) exist to apply for flight permission.

In principal, all UAS below 150 kg take-off weight have to be treated equally following the actual regulations. However, most countries have separate treatment for systems with a take-off weight below 25-30 kg. Recently, several countries (e.g. the United States, the United Kingdom, Sweden, Netherlands, Switzerland) consider an extra weight class of inherently unharmful UAS (< 1 kg, < 2 kg) with a specifically tailored set of regulations. The rule of sense and avoid is not realistic for those light-weight systems in the near future.

During the FLOHOF (Flow over and around Hofsjökull) field campaign in Central Iceland in 2007 (Paper I), flight permission was given by the Icelandic CAA for the area around Hofsjökull upto a flight level FL120 ($\approx$ 3600 m agl). The operation of SUMO was issued in a Notice To Airmen (NOTAM) by the responsible CAA. Two years later during the Svalbard field campaign (Paper II) rules were interpreted in a stricter manner by the Norwegian CAA. Flight permission for operating SUMO at Longyear airport (LYR) was given to FL50 which is in practice 1500 m agl with the limitation that the airspace around LYR had to be clear off other air traffic. The final permission decision was given to the local air-traffic controllers at LYR. They decided to allow SUMO operation only during periods when the airport was officially closed; i.e. mainly during nighttime and most parts of the weekends. This was an unfortunate constraining factor for the amount of sampled data during the field campaign in 2009.

In summary, the most critical and challenging part in operating UAS for scientific purposes today is to obtain the corresponding flight permission from CAAs even for a small and light-weight UAS as SUMO. In the future, there will be even stricter rules and regulations for UAS operations with new requirements for pilots and operators to obtain e.g. a UAS specific pilot's licence. In addition, stricter requirements on documentation of procedures, operations and maintenance will be required as well as the reporting of accidents or dangerous situations similar to manned aircraft traffic.

1.6 Outlook

One major step will be the use of several UAS at the same time to expand single point-column measurements into measurements covering areas of several square kilometres. This will enable the collection of new comprehensive observational data sets in areas that are difficult to access by conventional observational methods. With this further step, the use of UAS data for evaluation purposes of NWP and climate models can be broadened. Such an approach is in particular suited for the investigation of surface heterogeneity effects on the ABL on different scales. Typical phenomena to be studied in more detail in this context are internal boundary layers and transitions, for instance occuring at coastlines (land-sea-breezes) or at the ice edge (marginal ice zone, leads and plynyas), between rural and urban areas (mega-cities) as well as mountain-valley circulations.

The Paparazzi software enables a flexible operation of several SUMOs simultaneously. A first test of simultaneously profiling the ABL by using two SUMOs at the same time have been performed during the Svalbard field campaign in 2009 (`www.svalbardscienceforum.no/pages/news333.htm`). Thereby, one SUMO was flown above the apron of Longyear airport, while the other one was flown over Adventfjorden (see Figure 1.8). In Figure 1.9 the corresponding temperature, humidity and wind profiles are shown.

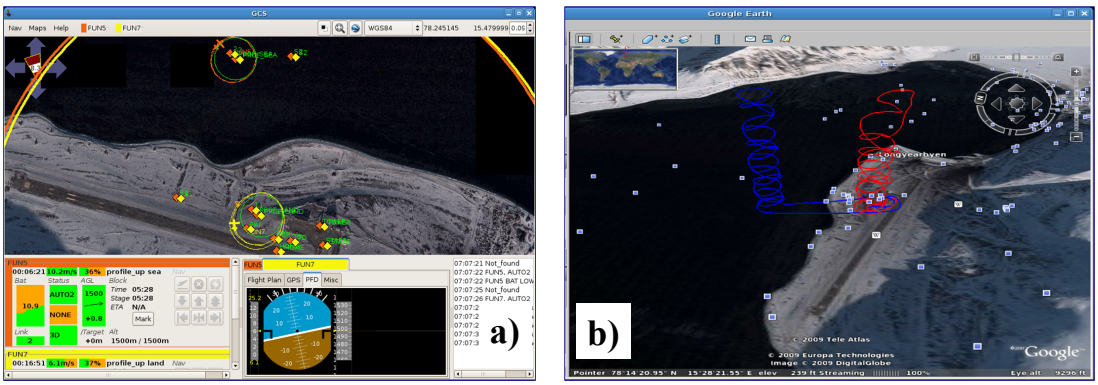

Figure 1.8: *a) A screenshot of the GCS showing two SUMOs simultaneously in the air at Longyear airport. The yellow and orange circles indicate the aircraft's flight path projected to the Earth's surface. b) SUMO flight tracks in Google Earth; the blue line indicates SUMO flying above water.*

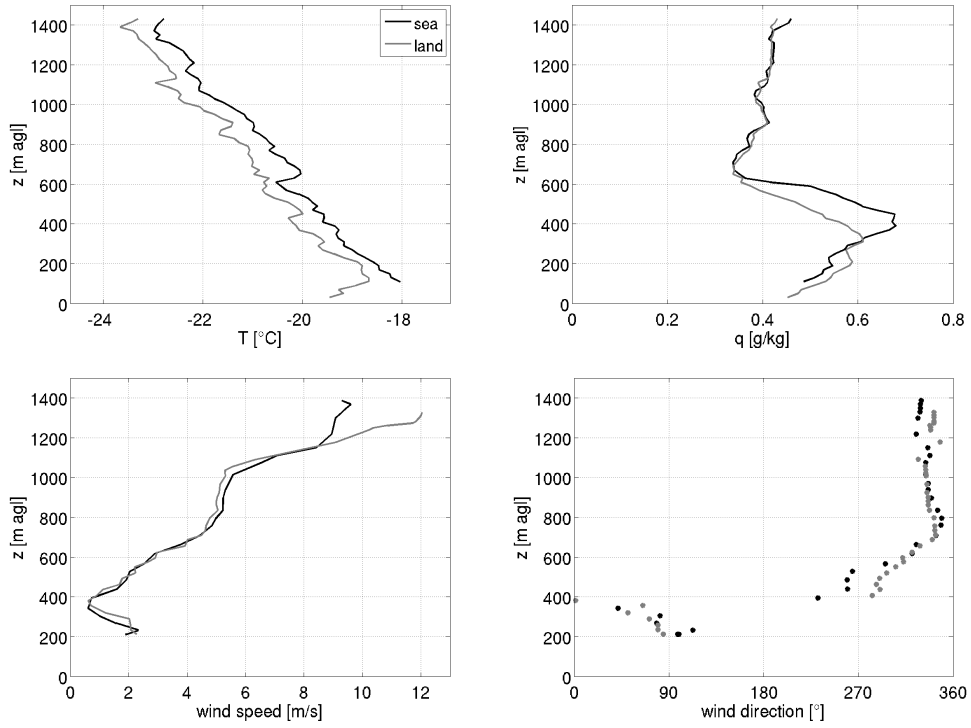

Figure 1.9: *Simultaneous temperature, specific humidity, wind speed and wind direction profiles at Longyear city airport on 02.04.2009 at 04:22 UTC; black: profile over sea; grey: profile over land.*

In a first approach, SUMO data has been successfully used for data assimilation purposes in WRF (*Jonassen et al.*, 2011). This gives the opportunity to improve local weather forecasts, which is especially useful when considering wind fields in the vicinity of potentially dangerous sites such as vulcanoes, chemistry factories and nuclear power stations.

A search and rescue application by using SUMO data has been recently made available by a group of Icelandic researchers (*Rögnvaldsson et al.*, 2010).

Recently, a five-hole probe from Air Data shown in Figure 1.10 has been installed in the nose of SUMO. This enables turbulence measurements (100 Hz) and can provide a data basis for the evaluation of simulated turbulent kinetic energy in the ABL parameterization schemes in NWP models.

As mentioned in subsection 1.4.4 a stable operation of SUMO depends on fair visibility conditions with an infrared temperature difference of 8 K between

ground and sky. The very recent installation of an inertia measurement unit (IMU) enables now flights also under and in clouds.

As tethered balloons, UAS can be equipped with chemistry sensors to monitor the chemical composition of the ABL. In cooperation with Universities of Reading and Cambridge, chemistry sensors (CO_2, SO_2 and NO_x) are under current development to be implemented on SUMO.

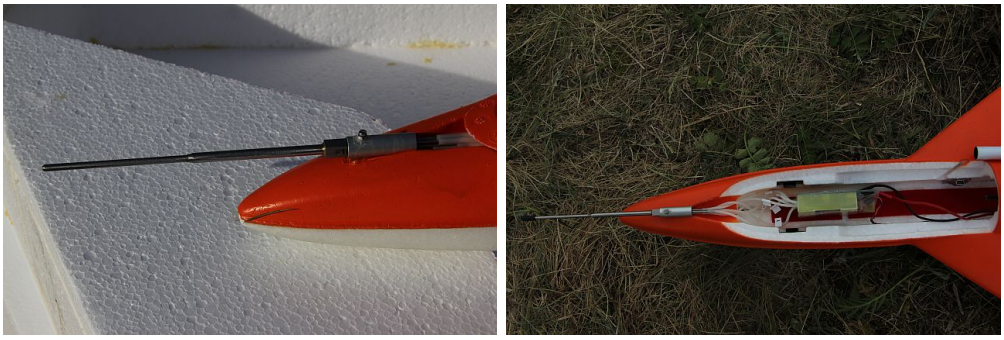

Figure 1.10: *The turbulence probe from Air Data installed in the nose of SUMO.*

With these improvements becoming realized in the near future, SUMO will have more application possibilities by providing a broader spectrum of meteorological variables and by progressing from single point-column measurements to multiple measurements covering larger areas. This can both contribute to better understanding of ABL processes as well as further NWP model validation and finally to the improvement of NWP models. Such activities highly depend on the undergoing actions on national and international level to establish rules and regulations tailored for the scientific operation of UAS in civil airspace.

References

Balsley, B., M. Jensen, and R. Frehlich, The use of state-of-the-art kites for profiling the lower atmosphere, *Boundary-Layer Meteorology*, *87*(1), 1–25, 1998.

Bjerknes, V., Das Problem der Wettervorhersage, betrachtet vom Standpunkt der Mechanik und Physik, *Metorologische Zeitschrift*, *21*, 1–7, 1904.

Brisset, P., A. Drouin, M. Gorraz, P. Huard, and J. Tyler, The Paparazzi Solution, *ENAC*, `http://www.recherche.enac.fr/paparazzi/papers_2006/mav06_paparazzi.pdf`, 2006.

Bromwich, D., K. Hines, and L. Bai, Development and testing of Polar Weather Research and Forecasting model: 2. Arctic Ocean, *Journal of Geophysical Research*, *114*, 2009.

Cascella, G., Identifying the Inner-Core Characteristics of Hurricane Noel (2007) via the Unmanned Aerial Vehicle, the Aerosonde, *28th Conference on Hurricanes and Tropical Meteorology, American Meteorological Society*, 2008.

Cassano, J., and S. Knuth, UAV observations of the wintertime boundary layer over the Terra Bay Polynya, Antarctica, EGU General Assembly Vienna, 2010.

Charney, J., R. Fjørtoft, and J. von Neumann, Numerical integration of the barotropic vorticity equation, *Tellus*, *2*, 237–254, 1950.

Daley, R., *Atmospheric Data Analysis*, 457 pp., Cambridge University Press, 1991.

Davis, C., et al., Prediction of Landfalling Hurricanes with the Advanced Hurricane WRF Model, *Monthly Weather Review*, *136*, 1990–2005, 2008.

REFERENCES

Egger, J., et al., Diurnal Winds in the Himalayan Kali Gandaki Valley. Part III: Remotely Piloted Aircraft Soundings, *Monthly Weather Review*, *130*, 2042–2058, 2002.

Egger, J., et al., Diurnal Circulation of the Bolivian Altiplano. Part I: Observations, *Monthly Weather Review*, *133*(4), 911–924, 2005.

Grell, G., J. Dudhia, D. Stauffer, N. C. for Atmospheric Research. Mesoscale, and M. M. Dicision, A description of the fifth-generation Penn State/NCAR Mesoscale Model (MM5), 1994.

Hines, K., and D. Bromwich, Development and Testing of Polar Weather Research and Forecasting (WRF) Model. Part I: Greenland Ice Sheet Meteorology, *Monthly Weather Review*, *136*(6), 1971–1989, 2008.

Hines, K., D. Bromwich, L.-S. Bai, M. Barlage, and A. Slater, Development and testing of Polar WRF. Part III. Arctic land, *Journal of Climate*, *24*, 26–48, 2011.

Hollingsworth, A., D. Shaw, P. Lönnberg, L. Illari, K. Arpe, and A. Simmons, Monitoring of observation and analysis quality by a data assimilation system, *Monthly Weather Review*, *114*(5), 861–879, 1986.

Holton, J. R., *An Introduction to Dynamic Meteorology*, vol. 48, third edition ed., 511 pp., Academic Press, Inc., 1992.

ICAO, Unmanned Aircraft Systems (UAS), circular 328, `icao.int/cgi/isbn_txt.pl?1761`, 2011.

Jonassen, M., H. Ágústsson, and H. Ólafsson, Improving a numerical weather prediction model by assimilating unmanned aerial vehicle data, EGU General Assembly Vienna, 2011.

Källén, E., *HIRLAM Documentation Manual: System 2.5*, Swedish Meteorological and Hydrological Institute, 1996.

Klemp, J., Research-community priorities for WRF-system development, `wrf-model.org/development/wrab/docs/RAB-plan-final.pdf`, 2007.

Konrad, T., M. Hill, J. Rowland, and J. Meyer, A Small, Radio-Controlled Aircraft As A Platform For Meteorological Sensors, *Applied Physics Laboratory Technical Digest*, *10*, 11–19, 1970.

Lafore, J., et al., The Meso-NH atmospheric simulation system. Part I: Adiabatic formulation and control simulations, in *Annales Geophysicae*, vol. 16, pp. 90–109, 1997.

Medina, S., J. R. A. Houze, A. Kumar, and D. Niyogy, Summer monsoon convection in the Himalayan region: Terrain and land cover effects, *Quarterly Journal of the Royal Meteorological Society*, *136*(648), 593–616, 2010.

Oke, T. R., *Boundary layer climates*, 435 pp., Routledge, 1987.

Pielke, R., et al., A comprehensive meteorological modeling system - RAMS, *Meteorology and Atmospheric Physics*, *49*(1), 69–91, 1992.

Ramanathan, V., M. Ramana, G. Roberts, D. Kim, C. Corrigan, C. C., and D. Winker, Warming trends in Asia amplified by brown cloud solar absorption, *Nature*, *448*(7153), 575–578, 2007.

Reuder, J., P. Brisset, M. Jonassen, M. Müller, and S. Mayer, The Small Unmanned Meteorological Observer SUMO: A new tool for atmospheric boundary layer research, *Meteorologische Zeitschrift*, *18*(2), 141–147, 2009.

Richardson, L., *Weather prediction by numerical process*, 236 pp., Cambridge University Press, 1922.

Rögnvaldsson, Ó., E. Einarsson, H. Águstsson, M. Joassen, M. Edwardsdóttir, S. Vilhjálmsson, T. Sigurdsson, and Ö. Rögnvaldsson, SARWeather - High-resolution and On-Demand Weather Forecasts in Search and Rescue, WRF workshop in Bergen, Norway, 2010.

Shuman, F., and J. Hovermale, An operational six-layer primitive equation model, *Journal of Applied Meteorology*, *7*, 525–547, 1968.

REFERENCES

Skamarock, W., J. Klemp, J. Dudhia, D. Gill, D. Barker, M. Duda, X.-Y. Huang, W. Wang, and J. Powers, A description of the Advanced Research WRF Version 3, *Tech. rep.*, 2008.

Skamarock, W. C., J. B. Klemp, and J. Dudhia, Prototypes for the WRF (Weather Research and Forecasting) model, preprints, Ninth Conference on Mesoscale Processes, 2001.

Spiess, T., J. Bange, M. Buschmann, and P. Vörsmann, First application of the meteorological Mini-UAV M^{2}AV, *Meteorologische Zeitschrift*, *16*(2), 159–169, 2007.

Spirig, C., A. Guenther, J. Greenberg, P. Calanca, and V. Tarvainen, Tethered balloon measurements of biogenic volatile organic compounds at a Boreal forest site, *Atmospheric Chemistry and Physics*, *4*(1), 215–229, 2004.

Stensrud, D. J., *Parameterization Scheemes - Keys to Understand Numerical Weather Prediction Models*, 459 pp., Cambridge University Press, 2007.

Stull, R. B., *An Introduction to Boundary Layer Meteorology*, 666 pp., Kluwer Academic Publishers, 1988.

Uppala, S. M., et al., The ERA-40 re-analysis, *Quarterly Journal of the Royal Meteorological Society*, *131*(612), 2961–3012, 2005.

van den Kroonenberg, A., T. Martin, M. Buschmann, J. Bange, and P. Vörsmann, Measuring the wind vector using the autonomous Mini Aerial Vehicle M^{2}AV, *Journal of Atmospheric and Oceanic Technologies*, *25*, 1969–1982, 2008.

Warner, T., *Numerical Weather and Climate Prediction*, 526 pp., Cambridge University Press, 2011.

2

Publications

2.1 Summary of Papers

This part of the thesis consists of three Papers addressing the SUMO system, measurements performed by SUMO in different geographical areas (see Table 1.4) and a detailed description and tests of a new wind estimation algorithm which is especially suited for small UAS (Paper III). In Paper I and II, SUMO data are used as a reference to evaluate the quality of NWP simulations using the numerical weather prediction model WRF with different ABL paramterization schemes.
In Paper I, the potential of using SUMO data as a reference for the evaluation of high-resolution WRF integrations is shown in two case studies. In Paper II, numerous SUMO profiles measured in Advent Valley, Svalbard are used to evaluate ABL schemes in WRF. A 'no-flow-sensor' wind estimation algorithm for small UAS is introduced in Paper III. In the following subsections the main results of the three Papers are summarized.

2.1.1 Paper I

In Paper I, the first SUMO flights performed during the FLOHOF field campaign in Iceland in summer 2007 are presented. The Paper discusses the potential of the SUMO system for being used as an alternative tool for the evaluation of NWP models. Highlights of this study are

- two days when SUMO could be operated in high temporal frequency. The first case addresses the performance of WRF and SUMO in calm wind conditions. The second case addresses a more dynamic situation with a mountain-induced gravity wave;

- the thermal stratifiation of the ABL as well as meso-scale features residing above the ABL, such as a subsidence inversion could be identified.

2.1.2 Paper II

In Paper II, results from a two weeks field campaign conducted in Svalbard in early spring 2009 are described and summarized. The Paper addresses

- the successful operation of SUMO in Arctic conditions;

- a direct comparison of SUMO data and measurements from a tethered balloon;

  - The SUMO system provides comparable data quality to the tethered balloon for heights above 200 m agl.
  - The strenghts and shortcomings of both systems are discussed.

- the evaluation of WRF ABL parameterization schemes under conditions when the ABL was stable stratified;

  - a warm bias close to the surface and a cold bias above the ABL could be identified in the tested schemes.

- high frequency profiles during one night providing deeper insight in the complex interaction between atmosphere and underlying topography in Advent Valley, Svalbard;

  - subgrid-scale processes such as strong surface inversion in the valley and an inertia oscillation in summit height could be observed.

2.1.3 Paper III

In Paper III the 'no-flow-sensor' wind estimation algorithm is described and investigated on. The main results from this study can be summarized as follows:

- The 'no-flow-sensor' wind estimation algorithm is an appropriate alternative to bypass the installation of sophisticated onboard wind measurement devices (such as flow sensor and gyroscope). This is especially important for small UAS with limited payload capabilities.
- The algorithm can be applied when the UAS is flown in auto mode, performing a helical flight pattern with constant pitch angle and throttle.
- One important finding is that wind information can be gained in comparable quality to other well established measurement tools such as radiosondes. This is feasible by flying the aircraft with low climb speed. As low climb speed is rather inefficient in reaching high ceiling height, SUMO is typically operated with high vertical velocity during ascent (8-10 $\mathrm{m\,s^{-1}}$) but distinctly lower values (ca. 2 $\mathrm{m\,s^{-1}}$) during descent.
- The presented 'no-flow-sensor' wind estimation algorithm has been implemented in the SUMO data post-processing routine.

Paper I

Mayer, S. Jonassen, M. Sandvik, A. Reuder, J. [2010], Atmospheric profiling with the UAS SUMO: a new perspective for the evaluation of fine-scale atmospheric models, Meteorology and Atmospheric Physics, doi: 10.1007/s00703-010-0063-2.

Paper II

Mayer, S. Jonassen, M., Sandvik, A., Reuder, J. [2011], Profiling the Arctic stable boundary layer in Advent Valley, Svalbard - measurements and simulations, Boundary-Layer Meteorology, under revision.

Paper III

Mayer, S. Hattenberger, G. Brisset, P. Jonassen, M. Reuder, J. [2011], A 'no-flow-sensor' wind estimation algorithm for Unmanned Aerial Systems, submitted to International Journal of Micro Aerial Vehicles.

Paper I

Atmospheric profiling with the UAS SUMO: a new perspective for the evaluation of fine-scale atmospheric models

Mayer, S. Jonassen, M. Sandvik, A. Reuder, J. (2010)

Meteorology and Atmospheric Physics
DOI: 10.1007/s00703-010-0063-2

Meteorol Atmos Phys
DOI 10.1007/s00703-010-0063-2

ORIGINAL PAPER

Atmospheric profiling with the UAS SUMO: a new perspective for the evaluation of fine-scale atmospheric models

Stephanie Mayer · Anne Sandvik · Marius O. Jonassen · Joachim Reuder

Received: 13 February 2009 / Accepted: 17 January 2010

Abstract For the first time, unmanned aerial system measurements collected by the small unmanned meteorological observer (SUMO) are used to evaluate atmospheric boundary layer (ABL) parameterization schemes embedded in the Advanced Weather Research and Forecasting model (AR-WRF). Observation sites were located in the vicinity of the almost idealized shaped mountain Hofsjökull, Central Iceland. SUMO profiles provided temperature, relative humidity and wind data to maximum heights of 3 km above ground. Two cases are investigated, one with calm wind conditions and development of a convective ABL and one with moderate winds and gravity waves over Hofsjökull. For the high-resolution simulation with AR-WRF, three two-way nested domains are chosen with a grid size of 9, 3 and 1 km. During its first meteorological test, SUMO has proved its great value for the investigation of the diurnal evolution of the ABL and the identification of mesoscale features residing above the ABL, such as subsidence.

Keywords Unmanned aerial system · ABL · Fine-scale numerical simulation · ABL parameterization schemes · WRF · Hofsjökull · Central Iceland

S. Mayer (✉) · M. O. Jonassen · J. Reuder
Geophysical Institute, University of Bergen,
Allégaten 70, 5007 Bergen, Norway
e-mail: stephanie.mayer@gfi.uib.no

A. Sandvik
Institute of Marine Research, PO Box 1870,
Nordnesgate 50, Nordnes, 5817 Bergen, Norway

1 Introduction

The vertical structure as well as the spatial and temporal variability of the atmospheric boundary layer (ABL) is of vital importance in various meteorological disciplines, such as numerical weather prediction (NWP), climate simulation and aeronautical meteorology. The boundary layer profiles of the basic meteorological variables, as temperature, humidity and wind, build up the pillars for the understanding of atmospheric stability and the corresponding turbulent exchange processes between the earth's surface and the atmosphere (e.g. Stull 1988; Garratt 1994). Several boundary layer phenomena, e.g. stable boundary layers or entrainment, are still not well understood, and, therefore, only poorly represented by the recent ABL parameterization schemes (Stensrud 2007; Teixeira et al. 2008).

Nowadays, increased computational capabilities enable operational mesoscale atmospheric model simulations down to a horizontal grid size of 1 km and even distinctly below for limited area and limited time studies. The evaluation of such high-resolution forecasts is a key task for further progress in NWP model development and the improvement of sub-grid parameterization schemes. This demands three-dimensional ABL data sets with high spatial and temporal resolution. The systems typically used for ABL studies, as meteorological towers, tethered balloons and profilers based on Sodar, Lidar or Radar can give valuable information on the status of an atmospheric column in the ABL, but they are rather demanding considering costs and infrastructural requirements and they only provide single column measurements. Radiosoundings are not appropriate when only interested in the ABL. Besides the costs, ascents are time limited and, therefore, constrain temporal resolution. Manned aircraft missions allowing flexible probing of the ABL, e.g. Ahmadov et al. (2007),

Published online: 12 March 2010

are highly expensive. Moreover, the surface layer close to the ground is hardly reachable due to flight regulations and safety reasons.

Beginning of the late 1960s (Konrad et al. 1970), small, remotely controlled aircrafts have been proposed as useful ABL observation tools. Technical progress and miniaturization in the field of electronics have enabled the development of smaller autonomous unmanned aerial systems (UAS) for atmospheric research in the last decade (Holland et al. 2001; Egger et al. 2002; Ma et al. 2004; Spiess et al. 2007). These systems, with weights between 3 and 50 kg and a wingspan in the order of 2–3 m, still need substantial infrastructure for operation. In addition, the costs for fully equipped meteorological versions are in the order 50–100 k€ per unit, led by the Geophysical Institute at the University of Bergen, the small and light-weight autonomous UAS small unmanned meteorological observer (SUMO) has been designed as 'recoverable radiosonde' for ABL research (Reuder et al. 2009b; Jonassen 2008). The system is intended to close the existing gap of in situ ABL observations covering horizontal scales from several tenths of meters up to around 10 km. SUMO provides a highly mobile, flexible and cost-efficient platform (below 3€ per unit) for the determination of temperature, humidity and wind profiles. It can be used without extensive infrastructure and is, therefore, especially well suited for applications in remote areas.

A first prototype of SUMO has been operated as a part of the field campaign FLOHOF (Reuder et al. 2009a). At 6 days during this 5-week campaign, around 30 profiles of temperature, relative humidity, horizontal wind speed and wind direction up to 3,500 m above ground have been measured with SUMO around Hofsjökull glacier in Central Iceland.

In this study, the SUMO measurements are used for the evaluation of high resolution runs performed with the state-of-the-art numerical Advanced Research Weather Forecasting (AR-WRF) model and Version 3.0.1 offers four different ABL schemes. In a sensitivity study, these ABL schemes are tested and compared with the corresponding SUMO soundings. Thereby, the focus is set on 2 days of different synoptic situation. 18 August 2007 with calm wind conditions and convection; and 13 August 2007 with moderate wind conditions imposing gravity waves over Hofsjökull.

Section 2 is reserved for a short description of the field experiment FLOHOF in Iceland and profile measurements with the UAS SUMO. In Sect. 3, the AR-WRF model setup is explained. Simulated and observed data are presented in Sects. 4 and 5 as case studies. Finally, the results are summarized followed by an outlook into future meteorological applications of SUMO.

2 The FLOHOF field experiment and the UAS SUMO

During July and August 2007, the field experiment FLow Over and around HOFsjökull (FLOHOF) was conducted in the vicinity of the mountain Hofsjökull, an isolated, glacier covered mountain (1,782 m) in Central Iceland (Fig. 1). At a diameter of about 30 km, it rises approximately 1,000 m above its soundings. This mountain is unique due to its nearly circular shape and rather smooth, ice-covered surface. Hence, the area around Hofsjökull is an ideal field laboratory for validation of orographic effects simulated by mesoscale models. The border of permanent ice and snow cover corresponds closely to the 1,000 m contour line. Below this altitude, the ground consists mostly of rocks and lava partly covered by sparse vegetation.

The main camp of the experiment was located at Ingólfsskáli (65.01°N, 18.89°W, 845 m a.s.l.), about 5-km north of the ice edge of the glacier (denoted by the northernmost red dot in Fig. 1). Here, a cabin with accommodation capacity for around 20 people provided the basic infrastructure for the field experiment. During the campaign, a total of 18 automatic weather stations (AWS) for the measurement of temperature(T), humidity (rh), wind speed (f), wind direction (dir), pressure (p) and precipitation (P) were deployed on and around the glacier. In addition, atmospheric surroundings were performed north and south of Hofsjökull by a tethered balloon, pilot balloons and two measurement systems based on unmanned aerial vehicles. A detailed description of FLOHOF and the performed measurements can be found in Reuder et al. (2009a) and on the project homepage (http://www.flohof.uib.no).

SUMO is based on a small model aircraft equipped with an autopilot system that can be operated as 'recoverable radiosonde' for ABL studies. The SUMO airframe has a length of 75 cm, a wingspan of 80 cm and an overall take-off weight of 580 g. It is electrically powered and has an endurance of up to 20 min motor time. The system has been equipped with sensors for pressure, temperature and humidity. The absolute accuracy for the temperature is given by the manufacturer with 0.5 K and for the relative humidity with 1.8%. Unfortunately, the pressure sensor did not work properly during the FLOHOF campaign, consequently altitude information has been taken from the GPS data set. The GPS height information has an accuracy of ± 10 m. Flying SUMO in autonomous mode in a helical flight pattern enables also the determination of wind speed and wind direction profiles. Near-constant values of the true air speed can be assumed, when operating SUMO with constant pitch angle and constant throttle. Headwind reduces the ground speed measured by the GPS system, tailwind increases it. The average wind speed over one circle of the flight pattern can be determined from these

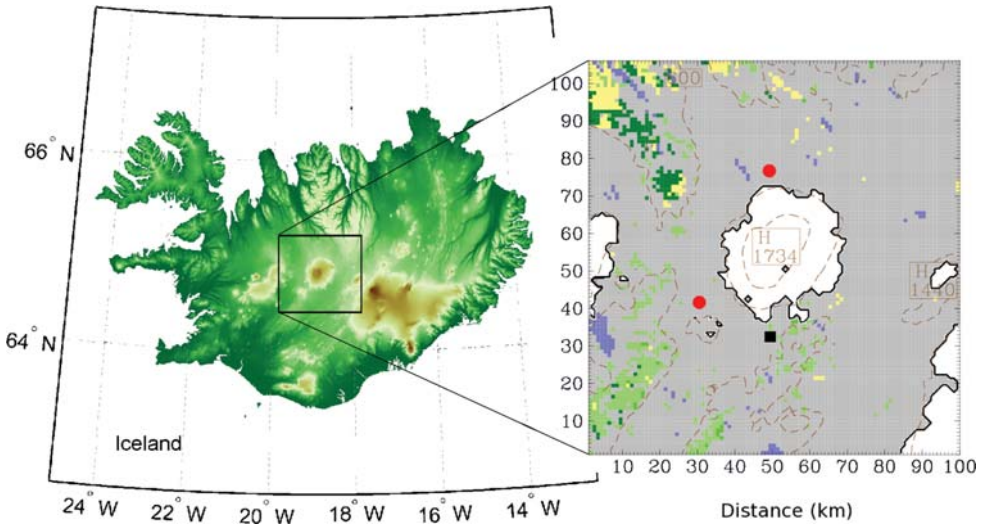

Fig. 1 Iceland with the Hofsjökull area (*black box*) where the FLOHOF campaign took place in summer 2007. The *right panel* zooms into the Hofsjökull area. *Dashed lines* are contour lines with height intervals of 400 m. *White areas* are snow/ice covered. *Gray areas* represent bare lava ground. *Red dot* SUMO launch sites; *black square* site of AWS S2. The improved landuse data set is kindly provided by the Icelandic Institute for Meteorological Research

ground speed differences, and the average wind direction from the position of the corresponding ground speed minimum and maximum. These wind profiles are a running mean over a full circle of the helical path. The accuracy of the wind speed is indicated by error bars in Fig. 8c and 14c. It is important to note that the wind determination only works in autonomous flight mode. For safety reasons, SUMO is operated manually at altitudes below 150 m. As a result, wind data of the SUMO system during the FLOHOF campaign are available for altitudes of above ca. 300 m. Owing to the changes in pitch angle and throttle from ascent to descent at the ceiling of the profile, it is also not possible to derive wind data for the uppermost 200 m of the soundings. More details on the system and the wind algorithm can be found in Reuder et al. (2009b).

In its current version, the stabilization of the aircraft is done by an array of infrared sensors. Therefore, a safe SUMO operation requires a radiation temperature difference of around 8 K between ground and sky. This limits the operation of SUMO in clouds and under low, warm clouds. This is the reason why all measured SUMO profiles taken during the campaign correspond to an atmospheric column without or only with rather thin higher level clouds. Two days with good SUMO data coverage and interesting meteorological situations have been selected for the comparison with AR-WRF fine-scale numerical simulations presented in this paper (see Table 1 for corresponding flights).

Table 1 Overview over SUMO flights, start locations and achieved maximum altitude above the ground level

Date	Start time	End time	Altitude (m)	Location
13.08.07	13:11	13:28	2,601	64.67°N
13.08.07	13:48	14:10	1,865	19.23°W
13.08.07	17:25	17:49	3,484	773 m a.s.l.
18.08.07	08:16	08:39	3,034	65.01°N
18.08.07	08:53	09:14	3,344	18.89°W
18.08.07	10:04	10:27	3,321	840 m a.s.l.
18.08.07	11:28	11:50	2,036	
18.08.07	15:22	15:40	1,505	
18.08.07	17:56	18:12	2,567	

Time is given in UTC

3 WRF model configuration and experiment design

The non-hydrostatic Advanced Weather Research and Forecasting Model AR-WRF version 3.0.1 has been used for the numerical simulations. The AR-WRF accommodates multi-nested domains, and various physical parameterizations. For a detailed description, see Skamarock et al. (2005). In the present study, the model has been configured with three domains with a horizontal grid resolution of 9, 3 and 1 km which have been two-way nested. The outermost nest covered Iceland and parts of the North Atlantic Ocean (1,080 × 990 km^2), while the innermost nest covered Hofsjökull and its surroundings (100 × 110 km^2) as shown in the right panel of Fig. 1. Analysis data from the European Centre for Medium Range Weather Forecasts (ECMWF) have been used as initial conditions, as well as forcing of the AR-WRF at its boundaries. The lateral boundary values have been included every 6 h during the simulation. The AR-WRF runs can, therefore, be considered as downscaling runs. The time step has been set to 54 s and output has been taken every 15 min. The numerical simulation started at 00 UTC and lasted for 24 h. The simulations have been performed with 61 vertical levels, where the lowermost level for the main prognostic variables has been set at about 39 m above the ground. The vertical grid spacing

gradually increased with height, with seven levels below 400 m. This setup with a relatively low-vertical resolution of the surface layer has been chosen because SUMO could not be operated in autonomous mode in altitudes below 150 m above ground level. The model top level has been set to 50 hPa. Owing to the focus on measurements in the ABL, we have used most AR-WRF default physical parameterizations, but sensitivity experiments have been made with the four ABL scheme options available in the present model version (see Fig. 2a, b).

Option one is the Medium Range Forecast Model (MRF) scheme from MM5 (Hong and Pan 1996). Second is the MRF successor, the Yonsei University (YSU) ABL scheme (Hong et al. 2006; Hong and Kim 2007). These schemes are based on the original work of Troen and Mahrt (1986) which consider countergradient fluxes, diagnoses the ABL height and finally prescribe the K profile over the ABL depth. A detailed description about the development from Troen and Mahrt (1986), through MRF and finally to YSU can be found in Hong et al. (2006). Following Stull (1988) these two schemes are first order and nonlocal. Third is the MYJ (Mellor-Yamada-Janjic, Eta/NMM) ABL scheme (Janjic 1990, 1996, 2002), which can be classified as a 1.5 order local scheme, where the turbulent kinetic energy (TKE) is computed through a prognostic equation and the diffusion coefficient as a function of the Richardson number and TKE. Fourth is the Asymmetrical Convective Model version 2 (ACM2) scheme, where nonlocal mixing is combined with the local eddy diffusion in a first-order scheme (Pleim 2007). A schematic representation of turbulent exchange between layers in local and nonlocal schemes can be found in Stull (1988) and Pleim (2007). More details can also be found at http://www.mmm.ucar.edu/wrf/users/docs/arw_v3.pdf.

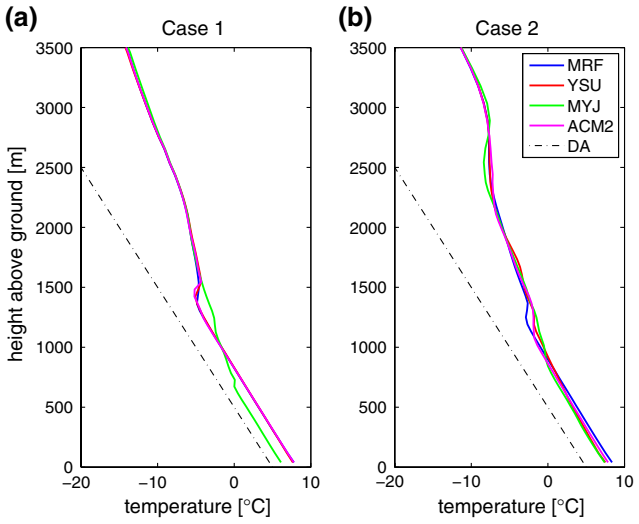

Fig. 2 Simulated temperature profiles. *Black dashed line* dry adiabate (DA). **a** Case 1, 18 August 2007 at 18:00 UTC. **b** Case 2, 13 August 2007 at 17:30 UTC

Furthermore, the following physical parameterizations have been applied: micro-physics has been parameterized with the so-called simple ice scheme with cloud water/ice, and rain/snow as prognostic variables (Dudhia 1989; Hong et al. 2004), the RRTM longwave radiation scheme (Mlawer et al. 1997) and the Dudhia shortwave scheme (Dudhia 1989), a snow/soil surface model that predicts the temperature in five layers using a vertical diffusion equation. Cumulus convection has been neglected in the present model simulations.

When the flow is connected to complex topography, the forecast skill will generally improve with increased model resolution (Sandvik and Furevik 2002; Ágústsson and Ólafsson 2007; Ágústsson et al. 2007). Details in the flow pattern, such as jets and wakes not seen in the meteorological analysis, will become visible when the horizontal resolution is sufficiently high. For the present cases, the results from the 9-km simulation show synoptic scale features, such as mean wind speed and direction, while the results from the 3- and 1-km simulations show spatial details connected to the topography. The similarity between the results from the 3- and 1-km simulations indicate that the flow is well represented on the 1-km grid. From theory, two-way nesting should perform better and also provide more consistent boundary data for the 3 and 1-km simulation. Some test integrations have been performed using both one- and two-way nesting option. Additional test simulations have been performed with variable vertical resolution as well as initial and boundary data from ECMWF on 91 model levels and 22 pressure levels. Differences have been found between these simulations, mainly due to the spatial displacement, but no significant differences have been found at the observation sites. The results presented are from the two-way nested simulations, with 61 vertical model levels and initial and boundary conditions taken from the ECMWF pressure levels. Model values selected at the actual hour of measurement correspond to a prognostic time of between 8 and 18 h, allowing for a model spin-up (dates and flight times in UTC can be found in Table 1).

Figure 2 presents modeled temperature profiles for 18 August (case 1) and 13 August (case 2) at the corresponding SUMO observation sites (see Fig. 1). The profiles show the performance of the four different ABL schemes offered in AR-WRF. The nonlocal schemes MRF, YSU and ACM2 show almost identical behavior in case 1 (Fig. 2a) while the local scheme MYJ calculates a colder ABL. For case 2 (Fig. 2b), all ABL schemes show similar temperatures from ground up to 900 m, but deviate in the representation of the ABL height by 300–400 m as well as in the strength of the ABL capping inversion. These disparities show the need for a tool to decide which ABL scheme is most appropriate for a certain synoptical situation.

4 Case 1: 18 August 2007

4.1 Synoptic situation

During 18 August, Iceland was influenced by the formation of a high-pressure ridge over the Northern North Atlantic. Winds in the Hofsjökull region were weak (≤5 m/s) from westerly directions (Fig. 3a) during most of the day (see Fig. 4). Slight convective activity could be observed in the form of stratocumulus clouds in the afternoon. Figure 3b shows a north–south cross-section at 18:00 UTC with a well mixed layer and calm wind conditions up to 1,400 m above ground. The SUMO observation site was located north of the mountain (65°00′46″N, 18°53′37″W), indicated with a red dot in Fig. 3a.

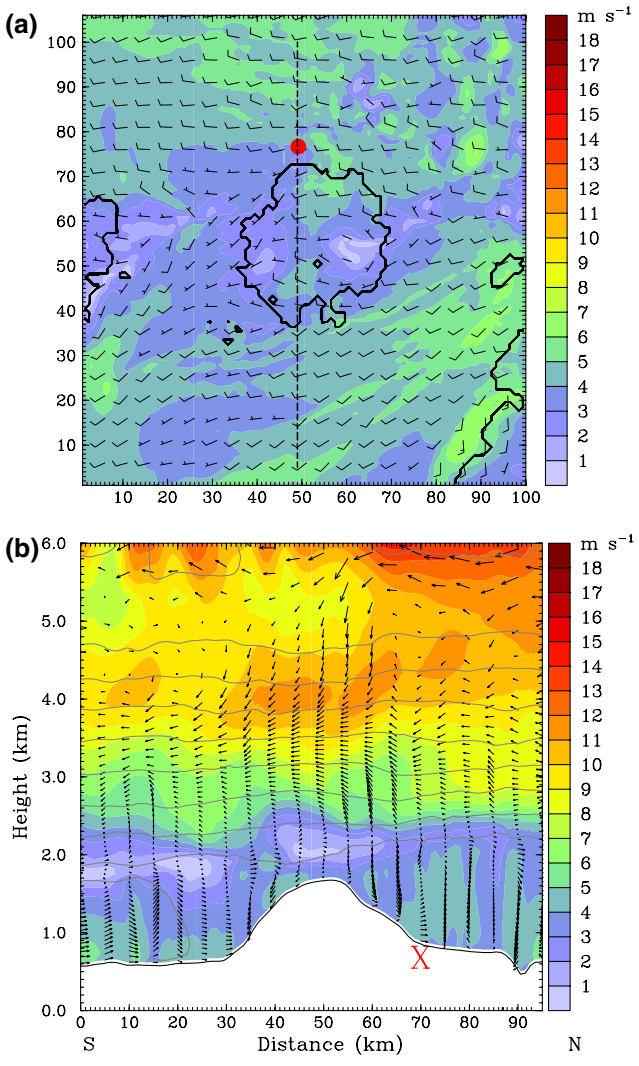

Fig. 3 Case 1, 18 August at 18:00 UTC: Domain 3 with default ABL scheme. **a** Wind speeds in the first layer above ground are shown in *color code*. The *arrows* indicate the wind direction. *Black solid line* ice/snow border; *black dashed line* indicates the cross-section shown in **b**). *Red dot* SUMO launch site. **b** *Gray contour lines* represent potential temperature in the cross-section. *X* SUMO launch site

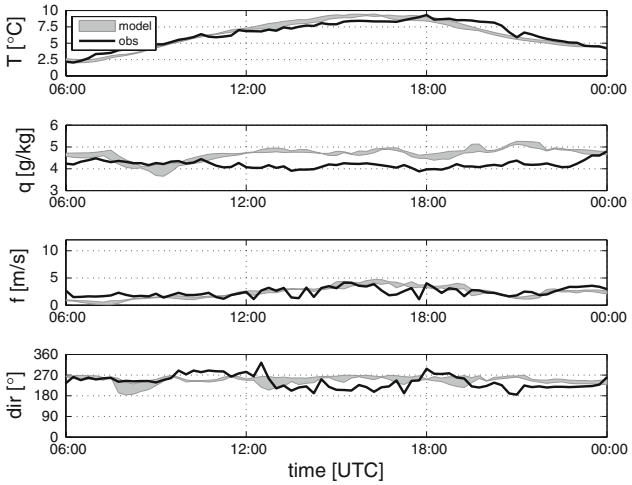

Fig. 4 Case 1, 18 August 2007: WRF versus AWS N3b for temperature (*T*), specific humidity (*q*), wind speed (*f*) and wind direction (*dir*) in 2 m

4.2 Surface observations

Figure 4 shows a time series of temperature, specific humidity and wind as measured at the AWS N3b (black) averaged over 15 min. Correspondingly, AR-WRF output is shown with a temporal resolution of 15 min in a gray band which indicates the variability of the 1 km run in an area of 5 × 5 km^2 with the location of the AWS N3b in the center of this area. With sunrise, the observed temperature started to increase from 2°C until it reached its maximum value of 9°C at 18:00 UTC. The wind speed was below 5 m/s from westerly directions turning to southerly in the afternoon. The specific humidity was almost constant during the whole day with values between 4 and 5 g/kg. Overall, the 1-km AR-WRF run agrees very well with the surface observation (obs) at AWS N3b.

4.3 SUMO observations and WRF output

Figure 5 presents the temperature and humidity profiles of all SUMO ascents during the day. At 8:00, about 3 h after sunrise, there is a well mixed layer in the lowest 200 m, capped by a weak remainder of the nocturnal inversion. Above and up to an inversion at 1,000 m, a neutral to slightly stable residual layer can be identified. The free atmosphere above is slightly stable stratified and shows the signature of a subsidence inversion at 2,800 m. The profiles during the next hours document continuous warming from the ground and a corresponding increase of the ABL depth (around 500 m at 9:00 and 800 m at 10:00). Around 11:30, the ABL inversion of the day before has been eroded, the

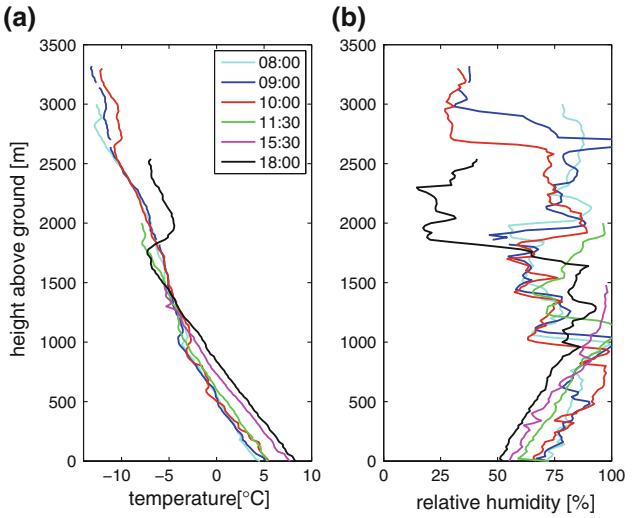

Fig. 5 Case 1, 18 August 2007: SUMO profiles of temperature and relative humidity from 08:00 to 18:00

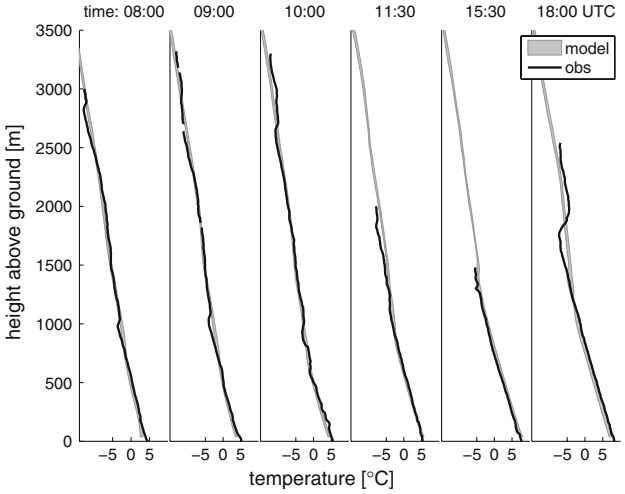

Fig. 6 Case 1: temperature evolution during 18 August 2007. The *gray band* represents the horizontal variability of the model output considering a square of 3.5 × 3.5 km centered at the closest grid point to the observation site

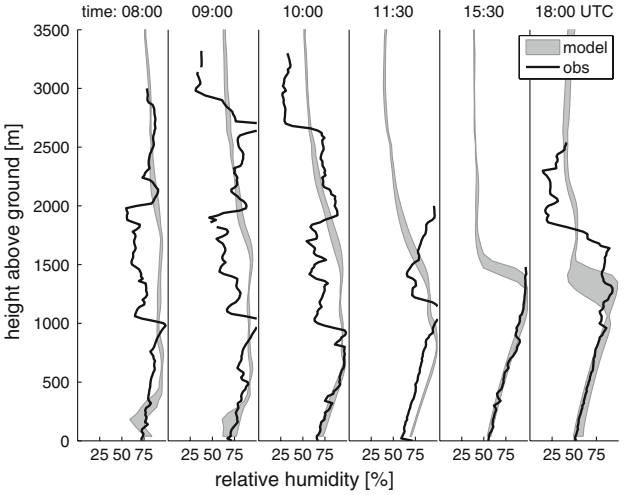

Fig. 7 Case 1: relative humidity evolution during 18 August 2007. *Gray band* as in Fig. 6

ABL extends to 1,100 m now. During the afternoon, the whole ABL is warmed by about 3 K and reaching a maximum depth of 1,300 m, indicated by a weak temperature inversion and a slight reduction in humidity. The well pronounced inversion around 1,800 m in the 18:00 ascent is not related to diurnal ABL development, but is likely the signature of ongoing rapid subsidence related to the increasing influence of a high pressure system. During the observation period, the altitude of this inversion has decreased by around 1,000 m from 2,800 m at 8:00 and 2,600 m at 10:00 to the value of 1,800 m observed in the last ascent. The subsidence process is also confirmed by the 12:00 radiosounding of Keflavk (around 260-km southwest of Hofsjökull) which reports a strong inversion at 700 hPa, i.e. around 3 km above the sea level or 2,200 m above the site of the SUMO measurements.

Figures 6 and 7 show the temperature and humidity profiles presented above in comparison with the temporal closest model calculation of AR-WRF with 1-km horizontal resolution using the YSU scheme. The YSU scheme, which is the default ABL scheme in AR-WRF, has been chosen because this model run was in best agreement to the measured profiles. Model data are presented as a gray band. This represents the output of the modeled profile at the grid point nearest to the SUMO ascent and of four modeled profiles at surrounding points with a horizontal distance of 3.5 km. These four points have been chosen at the outer corners of a square centered at the SUMO nearest grid point. Therefore, the gray band can be considered as horizontal variability in the model output. Except for the last profile at 18:00, measurements and model calculations for the temperature are in very good agreement. However, the model does not reproduce the capping inversion of the residual layer at around 1,000 m and the descending subsidence inversion aloft. During the morning, the modeled humidity in the ABL is also very close to the observations, as it is in the layer between 2,000 m and the subsidence inversion. However, the measurements reveal a drier layer between 1,000 and 2,000 m which is not captured by the model. In general, the simulations are able to reproduce the humidity profiles quite well. The only distinct deviation occurs at 11:30, where the model simulations of relative humidity are biased by around 15%, while they fit nearly perfectly before and after. This can be explained by the growth of the ABL into the dry layer above 1,000 m and corresponding mixing of drier air throughout the whole

ABL below. The model does not have this dry intermediate layer and is, therefore, unable to reproduce this feature.

The series of profiles taken in the daytime enable to give a rather clear picture of all important dynamic and thermodynamic processes affecting the lower atmosphere. The example makes clear on how important the availability of atmospheric measurements with reasonable high-temporal resolution will be for the validation and future improvement of corresponding model parameterization schemes. Looking at the last profile at 18:00 alone would most probably lead to the erroneous conclusion that the model has clearly overestimated the development of the well mixed ABL, misinterpreting the subsidence inversion at around 1,700 m as capping inversion of the mixed layer.

Figure 8 shows the modeled and measured profiles for T, rh and wind at 18:00. As in Figs. 6 and 7, the gray band represents the horizontal variability from the AR-WRF run with the YSU parameterization. When considering the SUMO profile as a reference, one can decide which ABL scheme suits best for this particularly calm situation. The nonlocal MRF, YSU and ACM2 schemes perform very well in T and rh, while the local MYJ scheme underestimates T by 2 K and overestimates rh by approximately 25%. As can be seen in Fig. 5, the relative humidity is rather high in parts of the atmosphere. Thus, it is reasonable to speculate that clouds can have formed at different levels and with time lags in the experiments. A closer look on the evolution of the ABL during the morning hours revealed a high level cirrus cloud in the YSU experiment, which likely has led to less evaporation from the surface. In the MYJ experiment, on the other hand, the higher solar downward flux seems to have increased the evaporation from the surface. For this experiment, a lower ABL height has also been found, which is in agreement with the findings in both Hong and Pan (1996) and Steeneveld et al. (2008), where it was reported that local TKE closure models produced shallower and more humid boundary layers than nonlocal schemes. The increase in evaporation and the relatively thin ABL both contributed to increased rh and the formation of a low level cloud with substantial cloud water content at 10:30. This cloud was also found at 12:00, but had disappeared at 18:00. The appearance of this low level cloud is the most likely reason for the T bias at 18:00 seen in Fig. 8.

Looking at the wind profiles, all ABL schemes behave quite similar. When compared with the measurement, the model slightly overestimates the wind speed in the lower ABL. The wind direction in the model is west while it is more southwest in the measurement. The increase in wind speed and the slight veering in the wind direction correspond satisfactory well with the observed inversion in Fig. 8a at 1,700 m.

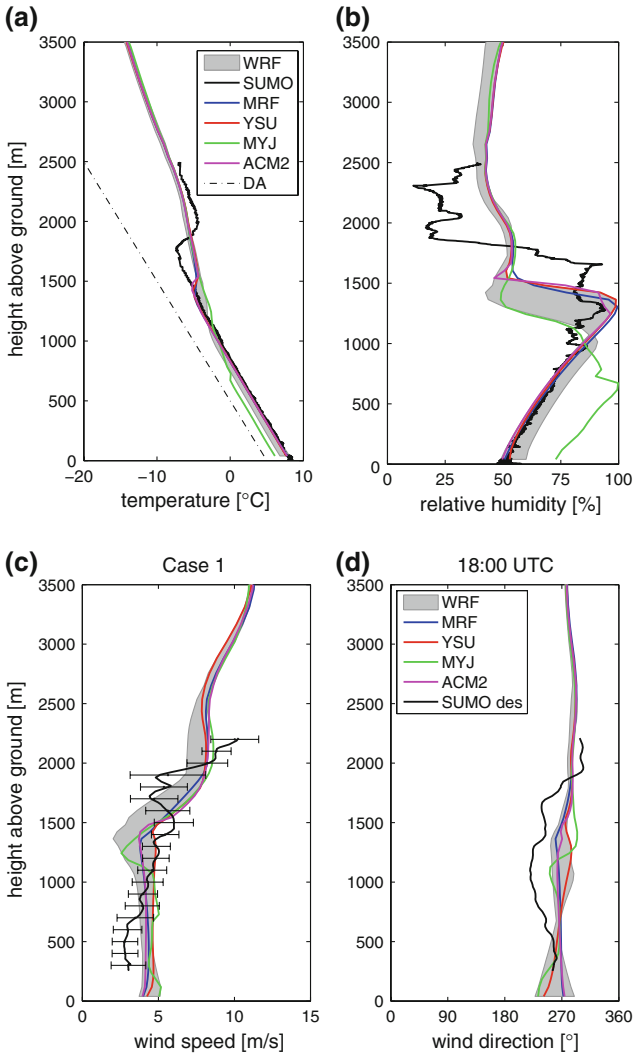

Fig. 8 Case 1, 18 August 2007 at 18:00 UTC: WRF temperature, relative humidity and wind profiles, in comparison with SUMO (*black line*). *Dashed line* indicates the dry adiabat (DA) in the temperature profile. **c** *Error bars* represent the mean error over height intervals of 100 m. *Gray band* as in Fig. 6

5 Case 2: 13 August 2007

5.1 Synoptic situation

On August 13, Iceland was influenced by an approaching high-pressure system from South Greenland, while a low-pressure system was active with its center located at the Shetland Islands. This constellation caused a rather strong pressure gradient across Iceland imposing moderate winds between 5 and 10 m/s from northeast, especially over the southeastern part of the country. These wind conditions led to mountain wave activity in the lee of Hofsjökull accompanied by downslope winds close to the surface (Fig. 9b). Figure 9a and b shows a tail-shaped wake

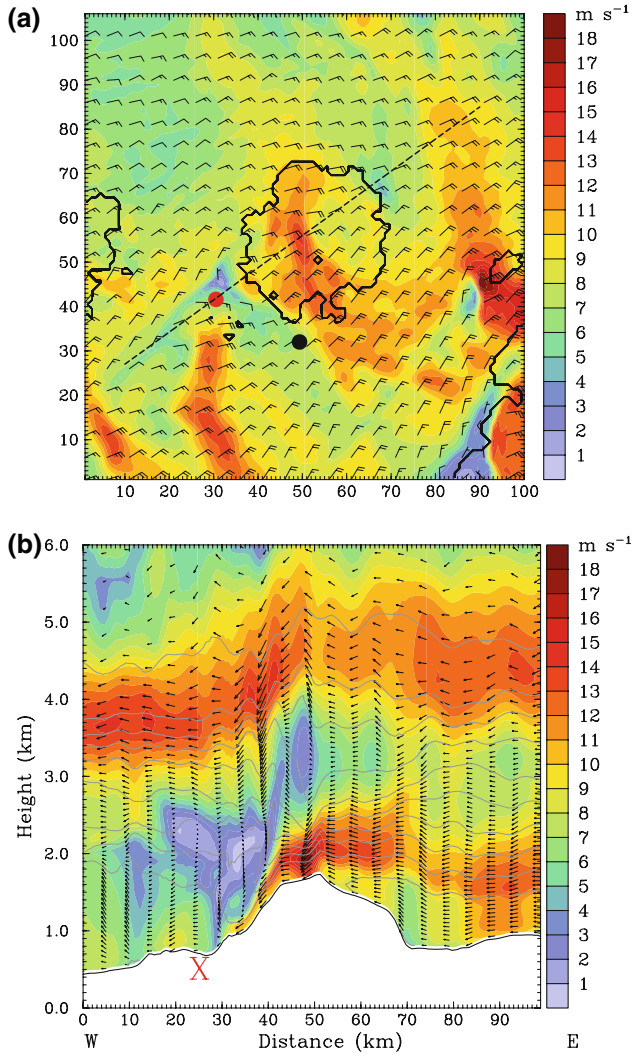

Fig. 9 As Fig. 3, for Case 2 at 17:30 UTC. *Black dot* in **a** indicates the location of the AWS S2. *X* SUMO launch site

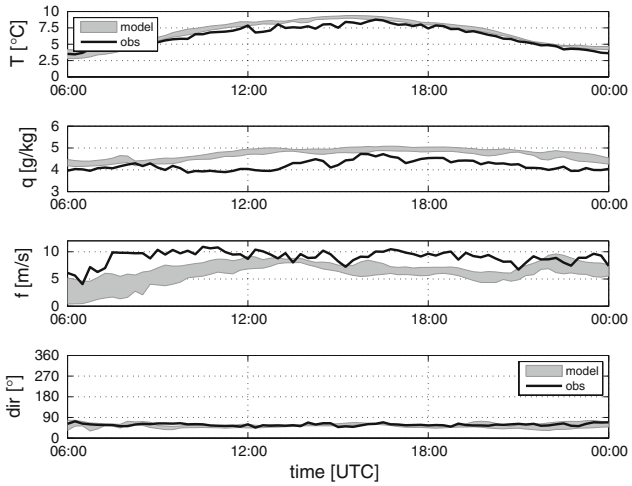

Fig. 10 Case 2, 13 August 2007: WRF versus AWS S2 for temperature, wind speed, wind direction and specific humidity in 2 m

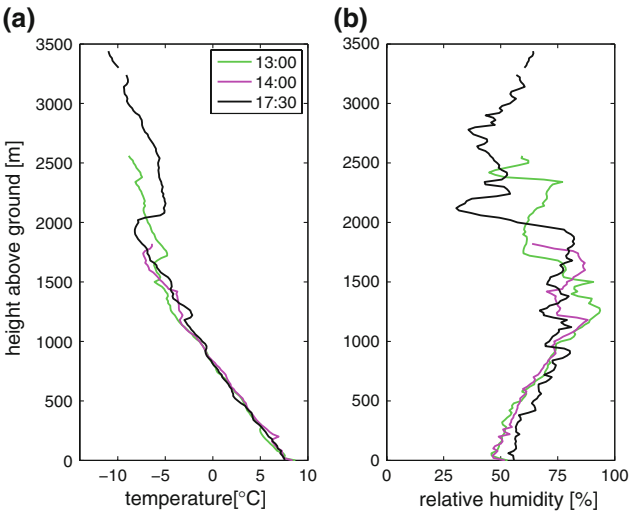

Fig. 11 Case 2, 13 August 2007: SUMO profiles of temperature and relative humidity. *Gray band* as in Fig. 6

located approximately 25-km southwest of the Hofsjökull summit. Lenticularis-shaped clouds at different levels, which are a strong indicator for mountain wave activity, have been observed continuously during that day.

5.2 Surface observations

Figure 10 shows a time series of modeled and observed temperature (T), specific humidity (q) and wind at AWS S2 (indicated with a black dot in Fig. 9a) approximately 23-km southeast of the SUMO observation site. T, q and the wind direction (dir) are captured very well by AR-WRF as compared to the AWS S2, while AR-WRF underestimates the wind speed (f) by 2–5 m/s. Looking at Fig. 9a, this is probably caused by a slight dislocation by the model of the rather strong wind field approximately 5–10-km northeast of AWS S2.

5.3 SUMO observations and AR-WRF output

Owing to the fact that this day was characterized by high spatial and temporal variability in the atmosphere, the interpretation of the SUMO profiles is rather difficult. Corresponding to Fig. 5, Fig. 11 presents the temperature and humidity profiles of all SUMO ascents during the day. Unfortunately, only afternoon ascents could be performed. All temperature profiles show mainly neutral conditions up to height of 1,600 m, but they are interrupted by more stable conditions as e.g. in 900 m at 17:30 or at 1,200 m in all three profiles. In addition, the SUMO temperature profiles show a rather bumpy behavior as compared to the ones in case 1 which can be most likely associated with atmospheric wave activity.

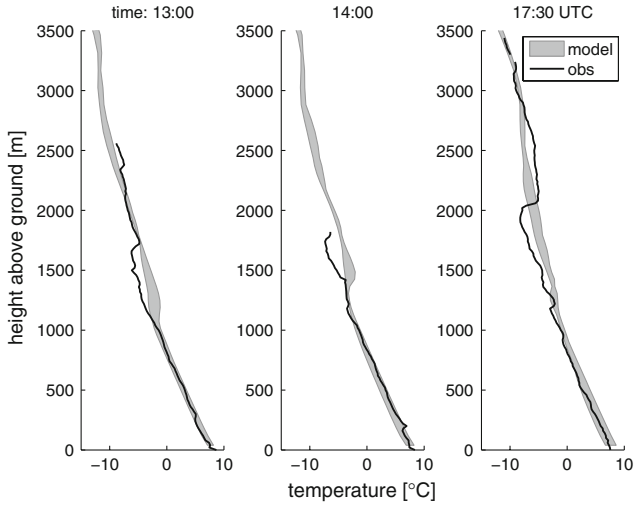

Fig. 12 Case 2: temperature evolution during 13 August 2007

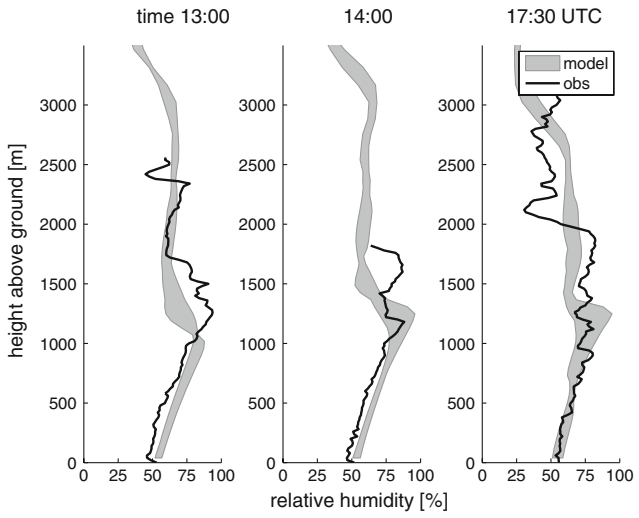

Fig. 13 Case 2: relative humidity evolution during 13 August 2007. *Gray band* as in Fig. 6

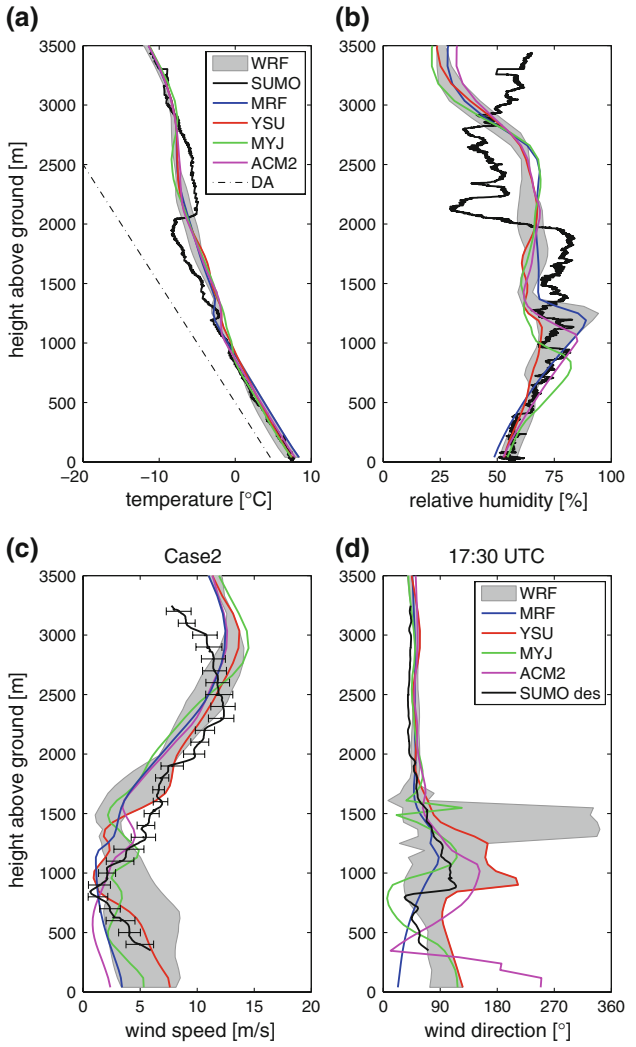

Fig. 14 Case 2, 13 August 2007 at 17:30 UTC: WRF temperature, relative humidity and wind profiles, in comparison with SUMO (*black line*). *Dashed line* indicates the dry adiabat (DA) in the temperature profile. **c** *Error bars* represent the mean error over height intervals of 100 m. *Gray band* as in Fig. 6

The humidity profiles at 13:00 and 14:00 show relatively dry conditions close to the surface and increasing with height to values of 75% in 1,200 m. An inversion can be identified at 2,400 m in the 13:00 ascent which is also visible in the corresponding humidity profile. At 17:30, the ABL has approximately the same depth as seen in the previous soundings. In addition, a strong inversion can be pinpointed at 2,000 m where T increases by 5 K and rh decreases by 50% in a layer of 100 m thickness. As in Figs. 6 and 7, Figs. 12 and 13 show measurements and model calculations for T and rh. Overall, they are in very good agreement considering the mean vertical gradients in the ABL as well as surface values. However, the model does not reproduce several small inversions measured by SUMO at heights of 200–500 m and 1,000–1,300 m in the 17:30 UTC ascent. The rather strong inversion at 2,000 m (17:30 UTC ascent) is most likely caused by the subsidence of dry air from a layer above due to the approach of a high-pressure system. An inversion at approximately 3-km height is documented by the Keflavk radiosonde at 12 UTC. The model identifies this subsidence, but less intense and 500 m higher as compared to SUMO (see 17:30 profile).

Figure 14 shows the modeled and measured profiles for T, rh and wind at 17:30. As in case 1, the MRF, YSU and ACM2 schemes show satisfying results for temperature and humidity. In this case, MYJ performs better than in case 1. But it still shows a slightly lower temperature and a higher relative humidity in the ABL. Considering the great spatial and temporal variability in the atmosphere in this case, the

simulated wind speed using the ABL scheme YSU is in satisfactory agreement with the SUMO wind profile. It captures the decrease of wind speed from the surface up to 1,000 m accompanied by veering of the wind with height. This can be associated with the wake in the lee of Hofsjökull. Above that level, the wind backs to east and increases with height to values of 12 m/s in 2,300 m above the ground. The width of the gray band represents the large variability of the wind conditions in this area. The ABL scheme ACM2 shows very low wind speeds close to the surface and probably, therefore, it fails to reproduce the wind direction at the surface by almost 180°.

6 Summary and outlook

For the first time, atmospheric soundings performed by an UAS have been used for the validation of fine-scale numerical simulations. During the FLOHOF campaign on Iceland, the UAS SUMO has been operated to retrieve profiles of temperature, relative humidity and wind. Together with the surface stations, these measurements are the basis for an evaluation of four different ABL schemes embedded in AR-WRF. For this purpose, two situations with different large scale synoptic situations have been selected. The investigations indicate that, in general, hourly soundings seem to be appropriate to capture the relevant features of the diurnal evolution of the ABL as well as large-scale synoptic influences. For very dynamical situations, e.g. in case of mountain-induced gravity waves, soundings every half an hour are desirable to monitor the enhanced variability in the lower atmosphere.

The comparisons show in general a satisfying agreement between model and surface observations. One exception is case 2 where the model underestimates the wind speed at surface level as compared to AWS measurements by 2–5 m/s. However, it has to be mentioned that the model shows a very strong horizontal gradient in the wind speed field, a rather small positioning error in the model could, therefore, be responsible for this large deviation. Looking into the vertical structure of the atmosphere, both cases indicate that the model simulations seem not to be able to resolve the time development of the synoptic scale subsidence inversion properly. This is most likely due to the too coarse vertical resolution of ECMWF analysis data used for the model initialization. In general, the nonlocal AR-WRF ABL schemes MRF, YSU and ACM2 are able to reproduce the temporal development of the ABL in both cases satisfactory. The local MYJ scheme tends to underestimate ABL depth and the low-level temperatures in the convective case 1. In particular, it shows a cold (−2 K) and wet (+25 %) bias in the lower ABL which is probably due to excessive evaporation from the ground in the morning. This leads to the erroneous formation of a shallow low level cloud layer in the model in the morning that distinctly reduces the incoming solar radiation and corresponding ground heating in the afternoon.

Overall, SUMO has proved its great value not only for the investigation of the diurnal evolution of the ABL in difficult mountainous area, but also for the identification of mesoscale features residing above the ABL, such as subsidence inversions. The system turns out to be a greatly valuable tool for the evaluation of fine-scale atmospheric models and their ABL parameterization schemes and can serve to gain increased knowledge of the ABL structure and development, especially in areas with limited infrastructure, such as remote mountain regions and the Arctic.

The further improvement of fine-scale atmospheric model capabilities is strongly dependent on the availability of appropriate four-dimensional data sets with high temporal and spatial resolution. With such new data sets, a number of well-known problems in the state-of-the-art NWP and climate modeling can be addressed in novel ways. Typical examples of not yet well understood phenomena are in general stable boundary layers, both night time and during winter in the Arctic, or entrainment processes at the top of the ABL.

For case studies, SUMO data will also be highly beneficial, e.g. for model initializations in complex terrain where model runs based on coarser scale analysis data (e.g. ECMWF) are not able to reproduce all relevant structures (e.g. inversions) in the lower parts of the atmosphere.

The SUMO system has the potential to close the obviously existing observational gap. The possibility of getting profiles of the lower atmosphere up to about 3 km above ground every 30 min provides the temporal resolution to investigate the relevant physical processes in the ABL. This will be crucial for the detailed validation and further development of the corresponding parameterization schemes used in numerical models. Owing to its freely programmable flight patterns and its horizontal range of about 10 km, the SUMO system is also well suited for the study of horizontal variability, which will enable a more realistic and reliable comparison of numerical grid point calculations and environmental measurements. With its capability of performing vertical profiles, horizontal surveys and complex, freely programmable flight patterns, SUMO clearly outperforms tethered balloon systems. During parallel operation of SUMO and a tethered balloon system at Longyearbyen airport on Spitsbergen at temperatures between −10°C down to −35°C in spring 2009, SUMO proved a distinctly higher data availability. This is mainly due to the very short preparation time of the SUMO system. In contrast to the balloon, SUMO could also be operated at wind speeds exceeding 10 m/s. During this

campaign, the most serious disadvantage of the tethered system was due to the fact that the balloon was unable to penetrate stable inversion layers of the Arctic ABL, limiting the available atmospheric profiles in several cases to only a few hundreds of meters at Longyear airport. In contrast, SUMO reached nearly for each ascent a ceiling of 1,500 m above ground, the maximum altitude approved by the Norwegian Civil Aviation Authority for this experiment. Nevertheless, both systems should not be seen as competitors, but used to complement each other. Tethered balloons are able to measure atmospheric profiles with distinctly higher vertical resolution, particularly in the lowest 150 m above ground.

A further big step toward real high-resolution four-dimensional atmospheric data sets will be the simultaneous operation of several SUMO aircrafts in so-called swarms or flocks. The autopilot software of the SUMO system is capable for this type of operations. First simultaneous atmospheric measurements with two SUMO aircrafts, e.g. performing parallel profiles over land and open sea in a horizontal distance of 1–2 km, as well as simultaneous horizontal survey flights at different levels, have been successfully performed during the 2-week field campaign on Svalbard in March/April 2009.

Acknowledgments Supercomputing resources, on a Cray XT4 computer at Parallab at the University of Bergen, have been made available by the Norwegian Research Council. The observational data used in this study were collected as part of the field campaign FLOHOF. The authors wish to acknowledge all participants of FLOHOF, especially Martin Müller, Pascal Brisset and Christian Lindenberg. The improved landuse data set has been kindly provided by Reiknistofa i veðurfræði (Icelandic Institute for Meteorological Research).

References

Ágústsson H, Ólafsson H (2007) Simulating a severe windstorm in complex terrain. Meteorol Z 16(1):111–122

Ágústsson H, Cuxart J, Mira A, Ólafsson H (2007) Observations and simulation of katabatic flows during a heatwave in Iceland. Meteorol Z 16(1):99–110

Ahmadov R, Gerbig C, Kretschmer R, Koerner S, Neininger B, Dolman A, Sarrat C (2007) Mesoscale covariance of transport and CO_2 fluxes: Evidence from observations and simulations using the WRF-VPRM coupled atmosphere–biosphere model. J Geophys Res Atmos 112(D22):14

Dudhia J (1989) Numerical study of convection observed during the winter monsoon experiment using a mesoscale two-dimensional model. J Atmos Sci 46(20):3077–3107

Egger J, Bajrachaya S, Heinrich R, Kolb P, Lämmlein S, Mech M, Reuder J, Schäper W, Shakya P, Schween J, Wendt H (2002) Diurnal winds in the Himalayan Kali Gandaki Valley. Part III: remotely piloted aircraft soundings. Mon Weather Rev 130:2042–2058

Garratt J (1994) The atmospheric boundary layer. Cambridge University Press, Cambridge

Hong S, Kim S (2007) Stable boundary layer mixing in a vertical diffusion scheme. The Korea Meteorological Society, Fall conference, Seoul, Korea, Oct 25–26

Hong S, Pan H (1996) Nonlocal boundary layer vertical diffusion in a medium-range forecast model. Mon Weather Rev 124(10):2322–2339

Hong S, Dudhia J, Chen S (2004) A revised approach to ice microphysical processes for the bulk parameterization of clouds and precipitation. Mon Weather Rev 132(1):103–120

Hong S, Noh Y, Dudhia J (2006) A new vertical diffusion package with an explicit treatment of entrainment processes. Mon Weather Rev 134(9):2318–2341

Holland G, Webster P, Curry J, Tyrell G, Gauntlett D, Brett G, Becker J, Hoag R, Vaglienti W (2001) The Aerosonde robotic aircraft: a new paradigm for environmental observations. Bull Am Meteorol Soc 82(5):889–901

Janjic Z (1990) The step-mountain coordinate: physical package. Mon Weather Rev 118(7):1429–1443

Janjic Z (1996) The surface layer in the NCEP eta model. 11th conference on numerical weather prediction, American Meteorological Society, pp 354–355

Janjic Z (2002) Nonsingular implementation of the Mellor-Yamada Level 2.5 Scheme in the NCEP meso models. NCEP Office Note No. 437, 61 p

Jonassen M (2008) The small unmanned meteorological observer (SUMO)—characterization and test of a new measurement system for atmospheric boundary layer research. Master's thesis, Geophysical Institute, University of Bergen

Konrad T, Hill M, Rowland J, Meyer J (1970) A small, radio-controlled aircraft as a platform for meteorological sensors. Appl Phys Lab Tech Digest 10:11–19

Ma S, Chen H, Wang G, Pan Y, Li Q (2004) A miniature robotic plane meteorological sounding system. Adv Atmos Sci 21(6): 890–896

Mlawer E, Taubman S, Brown P, Iacono M, Clough S (1997) Radiative transfer for inhomogeneous atmosphere: RRTM, a validated correlated-k model for the longwave. J Geophys Res 102(D14):16,663–16,682

Pleim J (2007) A combined local and nonlocal closure model for the atmospheric boundary layer. Part I: model description and testing. J Appl Meteorol Climatol 46(9):1383–1395

Reuder J, Ablinger M, Águstsson H, Brisset P, Brynjólfsson S, Garhammer M, Johannesson T, Jonassen M, Kühnel R, Lämmlein S, de Lange T, Lindenberg C, Malardel S, Mayer S, Müller M, Ólafsson H, Rögnvaldsson O, Schäper W, Spengler T, Zängl G, Egger J (2009a) FLOHOF 2007: an overview of the mesoscale meteorological field campaign at Hofsjökull, Central Iceland. Meteorol Atmos Phys (this issue)

Reuder J, Brisset P, Jonassen M, Müller M, Mayer S (2009b) The small unmanned meteorological observer SUMO: a new tool for atmospheric boundary layer research. Meteorol Z 18(2):141–147

Sandvik A, Furevik B (2002) Case study of a coastal jet at Spitsbergen—comparison of SAR and model estimated wind. Mon Weather Rev 130:1040–1051

Skamarock W, Klemp J, Dudhia J, Gill D, Barker D, Wang W, Powers J (2005) A description of the advanced research WRF version 2. NCAR Tech Notes 468+ STR

Spiess T, Bange J, Buschmann M, Vörsmann P (2007) First application of the meteorological Mini-UAV M^2AV. Meteorol Z 16(2):159–169

Steeneveld G, Mauritsen T, de Bruijn E, Vilà-Guerau de Arellano J, Svensson G, Holtslag A (2008) Evaluation of limited-area models for the representation of the diurnal cycle and contrasting nights in CASES-99. J Appl Meteorol Climatol 47(3):869–887

Stensrud D (2007) Parameterization schemes: keys to understanding numerical weather prediction models. Cambridge University Press, Cambridge

Stull R (1988) An introduction to boundary layer meteorology. Kluwer Academic Publishers, Dordrecht

Teixeira J, Stevens B, Bretherton C, Cederwall R, Doyle J, Golaz J, Holtslag A, Klein S, Lundquist J, Randall D, Siebesma A, Soares P (2008) Parameterization of the atmospheric boundary layer: a view from just above the inversion. Bull Am Meteorol Soc 89(4):453–458

Troen I, Mahrt L (1986) A simple model of the atmospheric boundary layer; sensitivity to surface evaporation. Bound Layer Meteorol 37:129–148

Paper II

Profiling the Arctic stable boundary layer in Advent Valley, Svalbard - measurements and simulations

Mayer, S. Jonassen, M. Sandvik, A. Reuder, J. (2011)

Boundary-Layer Meteorology
status: under revision

Boundary-Layer Meteorology manuscript No.
(will be inserted by the editor)

Profiling the Arctic stable boundary layer in Advent Valley, Svalbard - measurements and simulations

Stephanie Mayer · Marius O. Jonassen · Anne Sandvik · Joachim Reuder

Received: June 20, 2011/ Accepted: date

Abstract The unmanned aerial system SUMO (Small Unmanned Meteorological Observer) has been used for the observation of the structure and behaviour of the atmospheric boundary layer in Advent Valley, Svalbard during a two weeks period in early spring 2009. Temperature, humidity and wind profiles measured by the SUMO system have been compared with measurements of a tethered balloon system which has been operated simultaneously. It is shown that both systems complement each other. Above 200 m, the SUMO system outperforms the tethered balloon in terms of flexibility and the ability to penetrate strong inversion layers of the Arctic boundary layer. Below that level, the tethered balloon system provides the atmospheric profiles with higher accuracy, mainly due to its ability to operate at very low vertical velocities. For the observational period the meso-scale model has been run in high-resolution and evaluated with SUMO profiles reaching up to a height of 1500 m above ground level. The sensitivity to the choice of atmospheric boundary-layer schemes and horizontal resolution has been evaluated. A new scheme especially suited for stable conditions improves the temperature forecast slightly in stable conditions. However, all schemes show a warm bias close to the surface and a cold bias above the ABL. During one cold and cloudless night the SUMO system could be operated nearly continuously (every 30-45 minutes). This allowed for a detailed case study addressing the structure and behaviour of the air column inside and above Advent Valley and its interaction with the local topography. The SUMO measurements in conjunction with a meteorological 10 m mast enabled the identification of a very stable nocturnal surface layer adjacent to the valley bottom, a stable air column in the valley and a strong inversion layer above the summit heights. The results indicate the presence of inertial-gravity waves during the night, a feature not captured by the model.

Keywords Atmospheric profiles · Evaluation of boundary-layer schemes · High-resolution numerical model · Inertia-oscillation · Small Unmanned Meteorolical Observer measurements · Stable Arctic atmospheric boundary layer

S. Mayer
Geophysical Institute, University of Bergen
now: Uni Bjerknes Centre for Climate Research
Allegaten 70
5007 Bergen
Norway
Tel.: +47-55 58 87 13
Fax: +47-55 58 98 83
E-mail: stephanie.mayer@uni.no

M. O. Jonassen
Geophysical Institute, University of Bergen
Allegaten 70
5007 Bergen
Norway

A. Sandvik
Institute of Marine Research
Nordnesgate 50, PO Box 1870 Nordnes
5817 Bergen
Norway

J. Reuder
Geophysical Institute, University of Bergen
Allegaten 70
5007 Bergen
Norway

1 Introduction

In numerical weather prediction (NWP) there is a continuous demand for meteorological observations for the initialization of the models and data assimilation, as

well as for model evaluation and validation purposes. Commonly, surface observations, satellite data and radiosonde data are used for this purpose. To asses smaller-scale atmospheric boundary- layer (ABL) phenomena, special in-situ measurement tools are required, such as masts, radiosondes, tethered ballones, kites or aircrafts, and remote measurement techniques (e.g. sodar or lidar). These methods have all their advantages and shortcomings (e.g. Seibert et al. (2002)).

During the last decade the utilization of remotely piloted vehicles, also called unmanned aerial systems (UAS), has become increasingly popular in atmospheric sciences as a cost-efficient and flexible measurement alternative. So far, UAS of different size and complexity have been developed and applied for atmospheric measurements. Several of those UAS, like the Aerosonde (Curry et al., 2004), the Micro Aerial Vehicle (M^2AV) (van den Kroonenberg et al., 2008) and the Small Unmanned Meteorological Observer (SUMO) (Reuder et al., 2009) have already been successfully used for missions in polar regions. UAS have a huge potential to improve our limited observational capabilities in Arctic regions where the observational network is sparse. In addition to the usual atmospheric profiling, that can be done rather fast and with high repetition frequency in a well-defined atmospheric column, UAS are also capable of flying arbitrary user-defined flight patterns, as e.g. horizontal surveys at a given altitude or transects over surface inhomogeneities, adding at least one dimension to the observational potential. Compared to other profiling platforms, as kites, tethered balloons or radiosondes, small UAS require significantly less infrastructure. Provided that a UAS is equipped with a temperature, humidity and pressure sensor, numerous ABL phenomena can be observed by flying subsequent vertical profiles. These are besides the general thermal stratification, in particular inversion layers and subsidence. Adding a wind measurement system enables the identification of low level jets as well as orographically induced gravity waves. Mayer et al. (2010) used SUMO data measured during the FLOHOF field campaign in Central Iceland in summer 2007 (Reuder et al., 2011) to show the potential of using UAS data for the evaluation of ABL parameterization schemes in the state-of-the-art Weather Research and Forecasting model WRF. NWP and climate models often fail to appropriately reproduce the stable ABL in polar regions (Mahrt, 1998; Dethloff et al., 2001; Tjernström et al., 2005). This shortage in forecast skill for Arctic regions is well documented by Tjernström et al. (2004) and Galperin et al. (2007). The latter defined the so-called 'nordic temperature problem' where NWP forecasts notoriously result in a warm bias in predicting near surface temperatures in weather situations when temperature sinks below -25°C. The observed deviations between model and measurements in intensity and development of the stable ABL are caused by a combination of an insufficient coverage in the observational network to minimize the model initialization errors and the limited understanding and representation of the relevant atmospheric key processes in particular in the presence of strong or extreme surface inversions and the corresponding reduced vertical exchange of heat. During Arctic winter and early spring the absence or low level of solar radiation and the high albedo of snow and ice minimize the influence of solar heating from the ground, creating extended periods of high static stability and strong surface inversions. Such very stable boundary layers are in general poorly understood (Mahrt, 1998). Under such conditions additional pathways of energy transfer are not sufficiently covered by the models, e.g. by the interaction between atmospheric turbulence and gravity waves, are expected to be relatively more important (Zilitinkevich and Baklanov, 2002) compared to the other processes as advection, radiative cooling or the heat exchange between the atmosphere and the open or ice covered ocean. In particular, in complex terrain close to the coast, as in the Svalbard fjords, where mountains of ca. 1000 m height will trigger gravity waves in the stable atmosphere, those effects should be considerable. Further improvement of our understanding of these processes and the ability to improve the corresponding model parametrization schemes in the future is strongly dependent on the availability of in-situ atmospheric measurements.

So far, there are some evaluation studies using WRF focusing on regions influenced by cold weather conditions, e.g. Schicker and Seibert (2009) focus in their study on the Inn Valley in the Austrian Alps. Mölders and Kramm (2010) investigated on a larger scale on Alaska. Polar WRF has been evaluated for Greenland (Hines and Bromwich, 2008), the Arctic ocean (Bromwich et al., 2009) and the Arctic land (Hines et al., 2011).

The capability of SUMO to measure profiles with high vertical and temporal resolution and its proved functionality in Arctic regions encouraged the authors to use the system for investigations of the stable ABL on Svalbard. In this study, SUMO data are used to evaluate the representation of the vertical structure of the stable ABL in WRF for two locations on Svalbard.

The archipelago of Svalbard is a distinguished location due to its high latitude and adjacency to the Arctic Ocean. It stretches from 76°-81°N and from 10-28°E (see Figure 1). In general, atmospheric observations are quite rare in the Arctic due to harsh weather conditions and the lack of sufficient infrastructure. However, the settlement of Longyearbyen provides a unique in-

frastructural and scientific environment due to its airport and the University Centre in Svalbard (UNIS). Longyearbyen is located at the mouth of Advent Valley (AV) which leads to Isfjorden (see Figure 1b)). Svalbard's topography is characterized by mountain ranges (reaching a maximum altitude of around 1700 m above sea level) and deep fjords. Due to the adjacency to the Arctic Ocean and the Fram Strait, the climate and weather conditions of Svalbard are additionally influenced by rapid changes in sea-ice conditions around the archipelago and inside the fjords. Overall, this results in rapid changes of different land surface types (e.g. snow covered land, sea-ice, open water) over small horizontal distances. Typically, the Isfjorden region is influenced by two main flow conditions; either by southwesterly winds which advect relatively warm and humid air from Fram Strait or by north-easterly winds which transport cold and dry air from the Arctic Ocean over the archipelago (Hanssen-Bauer and Førland, 2001) resulting in high dynamical variability (such as gravity waves) induced by the complex mountainous topography. In low wind and clear sky situations during nighttime, cold pools associated with extreme surface inversions can build up in the mountain valleys. Such cold pools are especially well investigated in Alpine valleys and basins (e.g. Zängl (2005); Whiteman et al. (2001)) and can cause air quality problems in populated areas (e.g. Mölders and Kramm (2010)).
The remainder of this paper has the following structure. Section 2 describes the field campaign and observational setup. The SUMO system is described in Section 3; regulatory issues as well as data quality compared to a tethered balloon system are discussed. In Section 4, the numerical model setup and chosen physical options for the model integrations are described. The model simulations are evaluated for each model level below 1500 m by using the SUMO profiles as reference (see Section 5). In Section 6, we discuss a set of subsequent SUMO profiles during clear and calm conditions in AV. Results are summarized and discussed in Section 7.

2 The field campaign

The field campaign has been conducted in the period of 21 March until 5 April 2009, which is the late winter season on Svalbard. After the three months long polar night, direct solar insolation returns to Longyearbyen and AV in March. AV is a nearly east-west orientated valley which has its exit at Longyear airport where it leads to Isfjorden (Figure 1b)), the largest fjord at the western coast of Svalbard. Two main measurement sites have been chosen for investigating the stable Arctic ABL. Site one was located at Longyear airport (LYR) at 78°14'46"N, 15°27'56"E in close vicinity to the sea, enabling easy profiling access for the SUMO system over open or sea-ice covered ocean. Site two was set up at the old Auroral Station about 15 km to the east of LYR. Both sites provided the infrastructure for a relatively comfortable performance of the SUMO flight missions, as availability of a workshop, electricity and office space with internet connection, and routine basic meteorological recordings.

2.1 Measurement site 1: Longyear airport

At LYR the Norwegian Meteorological Institute (met.no) operates routine meteorological measurements of 2 m temperature (T), 10 m wind speed (f) and direction (dd) and pressure (p) (see black dots in Figure 4). At this site, 41 SUMO flights were operated up to a height of 1500 m above ground level (agl) which was the maximum altitude approved by the Norwegian Civil Aviation Authority (Luftfartstilsynet). From 23. March - 05. April 2009 UNIS operated a tethered balloon system at the northern end of the runway. With the tethered balloon system, 27 temperature, humidity, wind speed and wind direction profiles have been measured during this period (Manninen, 2009). Figure 2a) shows a cross section of the valley topography at Longyear airport (black diamond).

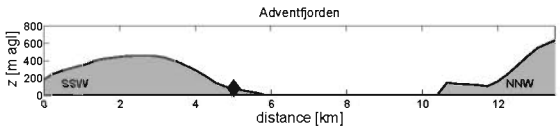

Figure 2 Cross sections at LYR which is indicated by number 1 in Figure 1b).

2.2 Measurement site 2: Old Auroral station

The old Auroral station (OAS) is located at 78°12'08"N, 15°49'42"E, about 15 km east of LYR. OAS is an abandoned research station which could be used during the field campaign. It is located close to sea level roughly in the middle of the ca. 4 km wide AV, to the north and south surrounded by mountain ranges reaching about 800 m in a distance of ca. 5 km (see Figure 3b)). AV's main orientation is east-west (appproximately 120°). Several smaller side-valleys open into the main valley close to the station area, making OAS a rather orographically complex site that seems to be well suited for investigations of orographic modification of flows, e.g.

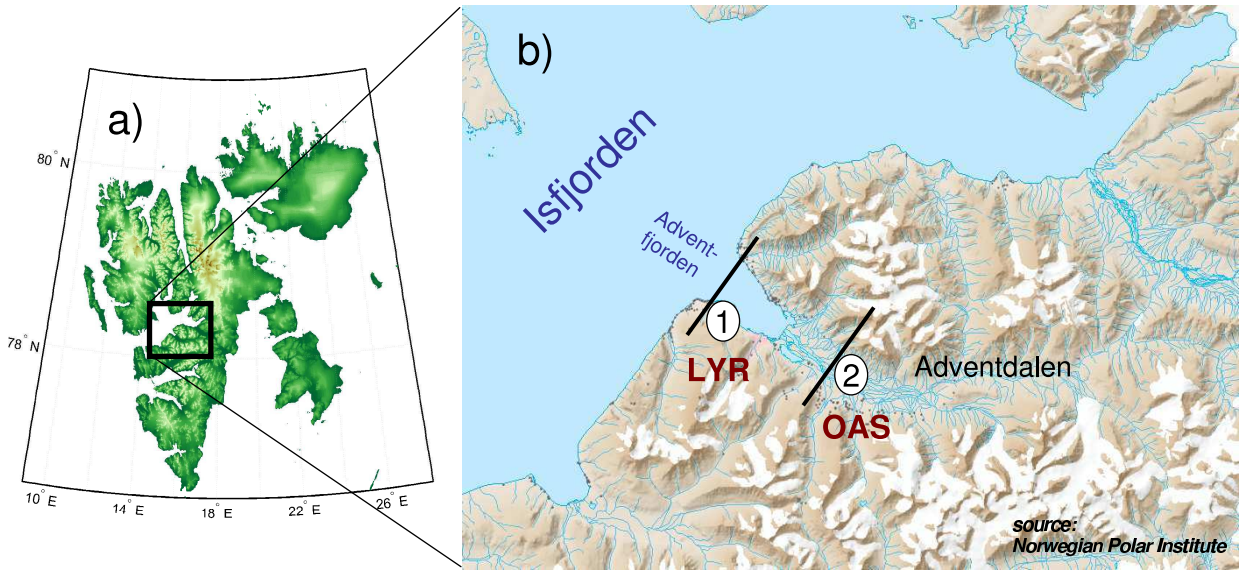

Figure 1 a) Topographic map of Svalbard. b) Region of Isfjorden; numbers indicate the measurement sites; 1: Longyear airport (LYR) at the coastline of Isfjorden and 2: the old Auroral station (OAS) in Advent Valley.

the influence of gravity waves on atmospheric profiles or katabatic and drainage inflow close to the ground. For the field experiment a 10 m mast equipped with temperature, humidity sensors and anemometers (2 m, 6 m and 10 m) has been set up (see Figure 4, grey dots). Figure 3b) displays the topography at OAS (black diamond) in AV. At this site, 46 SUMO flights were performed.

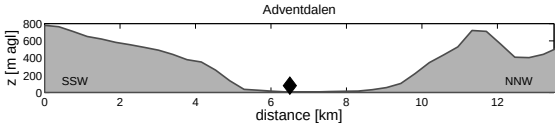

Figure 3 Cross sections at OAS which is indicated by number 2 in Figure 1b).

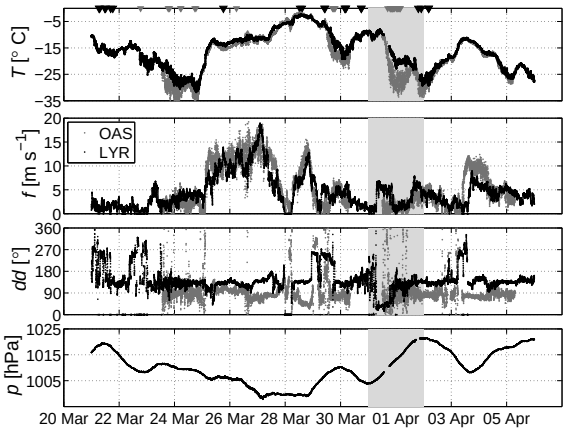

Figure 4 Automatic weather station measurements (temporal resolution: 1 minute) during the field campaign at the old Auroral station (grey line) and at Longyear airport (black line). SUMO flights at the two locations listed in Table 2 are indicated in the corresponding colour in the top panel.

2.3 Synoptic situation during the field campaign

During the field campaign, fair weather conditions with clear sky, calm wind and low temperature have been interrupted by the passage of a low pressure system accompanied by warm air advection and strong winds from 25 to 29 March 2009 (see Figure 4). In nights with clear sky and calm wind, the surface observations from the OAS station shows substantially lower temperatures compared to LYR (see Figure 5). This might be due to drainage flows from snow covered sidevalleys and mountain slopes contributing to continuous cooling and the built up of a cold pool in AV.

3 Measurements with the Small Unmanned Meteorological Observer SUMO

3.1 The SUMO system

The SUMO (Small Unmanned Meteorological Observer) system used in this study has been developed at the Geophysical Institute at the University of Bergen in cooperation with Müller Engineering (www.pfump.org) and the Paparazzi Project (http://paparazzi.enac.fr). It consists of an airframe based on the FunJet construction kit by Multiplex (see Figure 6). To our knowl-

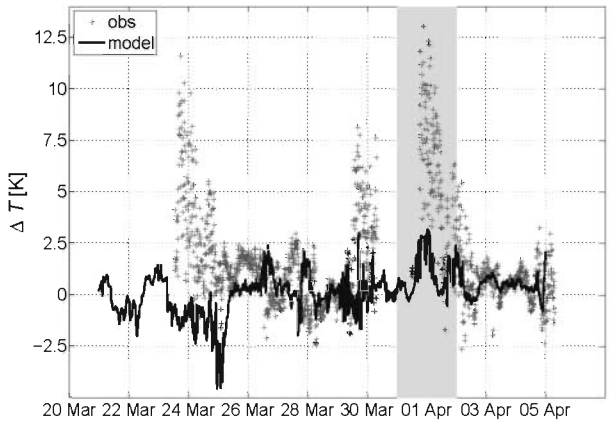

Figure 5 Temperature difference ΔT between Longyear airport and the old Auroral station.

edge, the SUMO system is at the moment the smallest and lightest UAS (0.8 m in length and wingspan, 0.580 kg take-off weight) in operation for atmospheric research worldwide and therefore unique in the category of light UAS (weight $<$ 150 kg [1]). SUMO is electrically powered by rechargeable Lithium-Polymer batteries with a pusher propeller in the rear of the aircraft. For autonomous operation, SUMO is equipped with the Paparazzi autopilot system (Brisset et al., 2006). Currently, SUMO carries a basic meteorological sensor package consisting of a combined temperature and humidity sensor mounted in a radiation shield tube on the wing of the aircraft and a pressure sensor located inside the fuselage. To avoid additional sophisticated measurement equipment, SUMO has, in its recent version, no flow sensors on board. Thus, wind speed and wind direction are not measured directly but estimated by using a minimization algorithm. For this, SUMO is operated with constant throttle and pitch angle in a helically shaped flight pattern with a radius of 100-200 m for vertical profiles. Flying in circular or helical flight patterns with constant throttle and constant pitch angle will result in approximately constant true air speed. Thus, the speed over ground, continuously recorded by the autopilot's GPS receiver, can be used to calculate wind speed and direction by applying the Nelder-Mead minimization algorithm (Mckinnon, 1996).
With its capability of reaching altitudes above 3500 m agl, SUMO is as a 'recoverable radiosonde' an excellent tool for atmospheric boundary-layer research. Besides regulatory issues, the operation of SUMO is in its actual version limited to wind speeds below 18 m s^{-1}. The SUMO version used in the Svalbard field campaign has not had a turbulence probe yet. As the in-flight stabilization of SUMO in autonomous flight mode is done by a set of infrared sensors using the difference in radiation temperature between ground and sky to define a flight horizon, SUMO can not fly autonomously in weather situations with a radiation temperature difference $<$ 8 K. That prevents operation in or under clouds. An improved version of the autopilot, using an inertial measurement unit (IMU) for stabilization and attitude control, is under development and will overcome this limitation. SUMO has proved its functionality in more than 300 scientific mission flights (Jonassen, 2008; Reuder et al., 2009).
Typically, SUMO is operated in a helical flight pattern with a climb speed of 6-10 m s^{-1} during ascent and 2-4 m s^{-1} during descent. Raw data are sampled and stored with a frequency of 2 Hz which results in a vertical resolution of $<$ 5 m during ascent and $<$ 2 m during descent. In the post-processing routine, data are averaged over height intervals Δz = 20 m, starting at z = 10 m agl. Therefore the effective vertical resolution is slightly lower than tethered balloons or masts. Due to the relatively fast climb speed of SUMO, the temperature and humidity measurements have to be corrected for a sensor time-lag error. A numerical correction scheme based on digital filters is applied to correct for the sensor response. This correction is performed in the post-processing routine thoroughly described by Jonassen (2008). In this study, we present data measured in descent mode when SUMO is operated with a slower climb speed which ensures a better data quality. SUMO's wind information is only shown for heights between 200 and 1250 m agl. Below 200 m agl, SUMO is operated manually and thus the wind algorithm is not working. At ceiling altitude SUMO switches from ascent to descent mode and the assumption of constant throttle and pitch angle is violated. Therefore, wind data for levels above 1250 m are not evaluated. For more technical details of the SUMO system the reader is refered to Reuder et al. (2009) and Jonassen (2008).

3.2 Regulatory issues

For the SUMO missions during the field campaign, flight permission had to be approved by Luftfartstilsynet, the Norwegian Civil Aviation Authority (CAA) in Bodø. A general permission to operate SUMO up to heights of 1500 m agl was issued by CAA with the constraint that every flight had to be cleared by the tower at LYR. This meant in practice that SUMO flights were only permitted when LYR was officially closed and no other irregular air traffic, as manned research flights

[1] European Commission; Directorate-General Mobility and Transport; Directorate E - Air Transport; Brussels, TREN E2/LT/GF/gc D(2010) Hearing on Light Unmanned Aircraft Systems, 08 October 2009 - Brussels

Figure 6 The SUMO airframe (based on FunJet construction kit by Multiplex). The airframe has a wingspan of 0.8 m. Its take-off weight is 0.58 kg.

and search and rescue operations were ongoing. As a result, most SUMO flights have been conducted during night-time and during the weekends. From the authors' point of view this was a very strict and unnecessary limitation which unfortunately disabled subsequent profiles by SUMO during a whole diurnal cycle in order to monitor the development of the ABL. A typical profiling mission of SUMO takes around 20 minutes and the aircraft's autopilot provides an emergency descent function for a safe recovery from 1500 m agl within less than 3 minutes at any time of the mission. As LYR tower is informed about any kind of air traffic approaching LYR well in advance (one hour or more, except for emergency rescue operations) a good deal more SUMO missions could have been performed without any violation of general aviation safety.

3.3 Comparison with tethered balloon measurements

During the field campaign, a tethered balloon (tethered balloon) system has been operated in the vicinity of the SUMO measurement site 1 at LYR, directly at the coast just ahead of the runway. These data are used for a comparison and data quality control of the SUMO measurements. Defining a maximum acceptable time slot of one hour between SUMO and tethered balloon ascents, 15 out of a total of 27 tethered balloon profiles could be used for inter-comparison purposes. One typical example is shown in Figure 7. The tethered balloon data have a vertical resolution of 1 m, while the SUMO data are averaged over 20 m, therefore the SUMO profiles (black line) have a smoother structure. It can be seen that the tethered balloon observations connect the surface measurements nearly perfect to the SUMO profiles. Overall, both measurement systems agree reasonably well. The temperature profiles show a good agreement with maximum deviations less than 1 K. The gradients and fine scale structures are matching well. A slight bias in altitude occurs which can be associated to the sensor time-lag in combination with the higher descending velocity of the SUMO system for the presented profile. The relative humidity measurements (Figure 7b) of both systems show the same structure and slope in the profile, but distinctly lower absolute values of the tethered balloon compared to SUMO and surface measurements are obvious. This was most likely caused by a calibration offset in the tethered balloon system. The wind speed profiles agree well (Figure 7c). Both wind speed profiles show values between 2-4 m s^{-1} with some differences in the vertical structure. SUMO shows a stronger vertical shear in 400 m agl. This might be due to the horizontal distance between the measurement systems as well as unsteady wind conditions caused by the complex topography. It can be clearly seen that the tethered balloon system has not been able to penetrate the second layer of a stronger wind shear in 600 m agl where SUMO measured a wind speed of 6 m s^{-1}. This height corresponds to the temperature inversion in Figure 7a. The wind direction profile agrees quite well in the shown profile (Figure 7d).

The strength of the tethered balloon system is the low vertical velocity that can be realized, which is in particular important for the resolution of e.g. strong to extreme shallow surface inversion layers. Such inversions are at the moment not appropriately resolvable with SUMO. Here, the SUMO system has further potential of improvement concerning data quality for temperature and humidity measurements below approximately 50 m. Due to the flow-sensor-less wind determination algorithm that is only working in autonomous flight mode, wind could only be measured for $z > 200$ m agl. In general, tethered balloon and SUMO should not be seen as competitors for the purpose of ABL measurements, but as two systems that highly complement each other, mainly using data from the tethered balloon system to fill the gap of information from reliable SUMO measurements down to the operational surface measurements at 2 m, respectively 10 m for wind. The experience with SUMO and tethered balloon during the campaign also clearly showed that SUMO outperforms the tethered balloon system when it comes to flexibility of measurements, the required infrastructure and in situations with elevated inversion layers that could not be penetrated by the tethered balloon. One prominent example can be seen in Figure 7, where SUMO easily reached 1500 m, while the tethered balloon was not able to ascent higher than approximately 600 m due to a marked temperature inversion and wind shear layer.

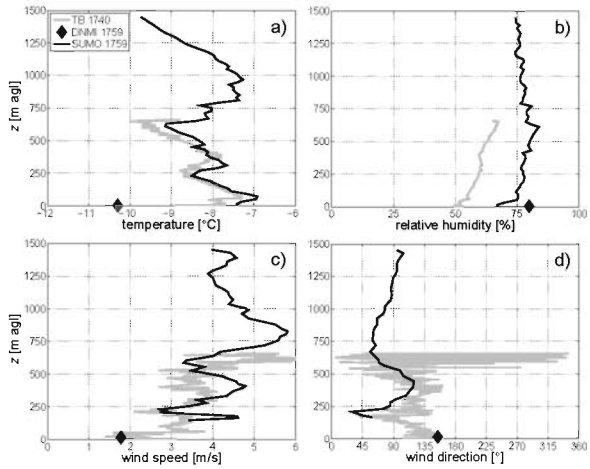

Figure 7 Profiles measured on 30 March 2009 at 1800 UTC. a) Temperature, b) relative humidity c) wind speed and d) wind direction profiles measured with the tethered balloon system (grey line) and the SUMO system (black line).

4 Model Configurations

For the modeling part of this study, the Advanced Weather Research and Forecasting model WRF version 3.1.1 developed by the National Center of Atmospheric Research (NCAR) has been used. WRF integrates fully compressible non-hydrostatic equations on terrain-following hydrostatic-pressure vertical coordinates. It provides multi-nested domains and a large number of physical parameterizations. For a further detailed description of the model we refer the reader to Skamarock et al. (2008).
The sensitivity to horizontal resolution due to the close coherency of wind and complex topography is a well known feature (e.g. Sandvik and Furevik (2002) and Schicker and Seibert (2009)). Due to Svalbard's complex topography, a high horizontal resolution setup of 9 km - 3 km -1 km centered at 78.5°N, 17.0°E has been chosen. The inner domains are two-way nested to their mother domain. The locations of the domains are sketched in Figure 8. The outer domain covers 120 x 120 grid points stretching from the north-east corner of Greenland in the west to Franz-Josef-Land in the east. The second domain covers most parts of the archipelago with 130 x 155 points. The innermost domain covers 160 km in the east-west and 175 km in the north-south direction including the region of Isfjorden, Longyearbyen and AV. All three domains have a high vertical resolution by containing 61 vertical terrain-following sigma levels, with the top at 50 hPa (approximately 15.5 km). The lowest 1500 m include 29 model levels, with the lowest full level at 36 m. A sensitivity test on the vertical resolution showed that 61 vertical levels are necessary to resolve ABL phenomena, such as a low level jet. Note that doubling a model's resolution increases the computational time by about $2^4 = 16$ times (roughly a factor of two for the three spatial dimensions and another factor of two for the smaller timestep).
Static fields as landuse and topographical data have been provided by the U.S. Geological Survey in a horizontal resolution of 30" (0.9 km in north-south direction). These latitude-longitude datasets are interpolated into the stereographic domains within the WRF Pre-processing System (WPS).
For initial and lateral boundary conditions, data from the European Centre for Medium-Range Weather Forecasts are used, on a 0.5° x 0.5° grid on 26 pressure levels which is updated every 6 hours. Thus, the WRF integrations can be considered as dynamical downscaling runs. For all three domains the Noah land surface model (Chen and Dudhia, 2001) has been used. For the model integrations a timestep of 36 s has been chosen. The model has been run for the observational period starting on 20 March 2009 0000 UTC to 5 April 2009 0000 UTC allowing for a spin up time of 24 hours as recommended in Hines et al. (2011) for polar environments.
Since the availability of the WRF version 3.1, fractional sea ice can be used in the integrations. As mentioned in Kilpeläinen et al. (2010), sea ice in the ECMWF data are afflicted with errors in fjords and near coastlines. Therefore, the ECMWF sea ice fields have been replaced by daily sea ice concentration data provided by the Advanced Microwave Scanning Radiometer (data available at the National Snow and Ice Data Center http://nsidc.org/data/amsre/). However, after the preprocessing procedure (WPS) in WRF there was still too much sea-ice in Isfjorden. Therefore, sea-ice has been removed manually to be consistent with the daily met.no's sea-ice charts (personal communication with T. Kilpeläinen).

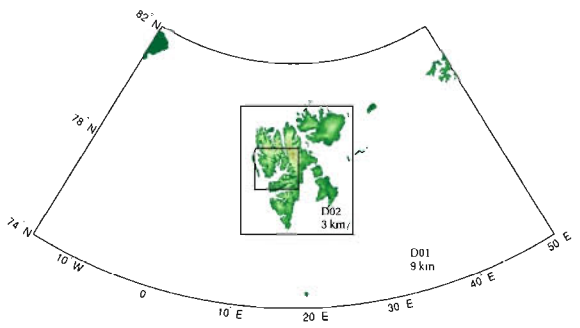

Figure 8 Model set up. The outer domain D01 has a horizontal resolution of 9 km. Domain D02 includes grid boxes of 3 km and the innermost domain has a horizontal resolution of 1 km.

4.1 Model physics

As micro-physical option the single-moment 5-class scheme has been chosen that provides mixed-phase processes and super-cooled water. For the long-wave radiation the Rapid Radiative Transfer Model (RRTM) scheme has been used (Mlawer et al., 1997). The scheme uses lookup tables for efficiency. It accounts for multiple bands, trace gases, and micro-physics species. For the short-wave radiation scheme the Goddard scheme has been activated which is a two-stream multi-band scheme including cloud effects (Chou and Suarez, 1999). Fluxes as well as snow-cover and cloud-effects have been activated. Leaving all physical options constant apart from the choice of ABL scheme, three different ABL configurations have been run. In WRF version 3.1 there are 9 different ABL schemes available. As a standard ABL scheme the Yonsei University (YSU) scheme (Hong et al., 2006; Hong and Kim, 2007) is implemented in the model which is a successor of the Medium Range Forecast Model (MRF) scheme which has been used in the Mesoscale Model MM5. These schemes are based on the original work of Troen and Mahrt (1986) which consider counter-gradient fluxes, diagnoses the ABL height and finally prescribe the K-profile over the ABL depth. A detailed description of the development from Troen and Mahrt (1986), through MRF and finally to YSU can be found in Hong et al. (2006). Following Stull (1988) these two schemes are first order and non-local.

An alternative is the Mellor-Yamada-Janjic (MYJ) ABL scheme (Janjic, 1990, 1996, 2002), which can be classified as a 1.5 order local scheme where the turbulent kinetic energy (TKE) is computed through a prognostic equation and the diffusion coefficient as a function of the Richardson number and TKE.

A new option in WRF version 3.1 is the Quasi-Normal Scale Elimination (QNSE) scheme especially suited for the stable ABL. This scheme is based on the work of Sukoriansky and Galperin (2008) using local TKE-based vertical mixing. It successively eliminates small scales of motion and calculates following corrections to viscosity and diffusivity. It expresses analytically eddy viscosity, eddy diffusivity, kinetic energy and temperature spectra. Scale elimination to some extent provides a subgrid-scale representation of large eddies. The method traces the modification of the flow with increasing stratification and recovers growing anisotropy and the effect of internal waves (Sukoriansky and Galperin, 2008).

Additionally to the three two-way nested runs, one model integration has been performed by using the QNSE scheme in a one-way nested configuration to test the sensitivity of the horizontal resolution. The performed WRF integrations are listed in Table 1.

Table 1 Overview of the performed WRF runs; fb1: two-way nesting has been activated. fb0: two-way nesting has been deactivated. YSU: Yonsei University scheme; MYJ: Mellor Yamada Janjic scheme; QNSE: Quasi Normal Scale Elimination scheme.

run	ABL scheme	two-way nested	horizontal grid size [km]
YSU-fb1-d03	YSU	yes	1
MYJ-fb1-d03	MYJ	yes	1
QNSE-fb1-d03	QNSE	yes	1
QNSE-fb0-d01	QNSE	no	9
QNSE-fb0-d02	QNSE	no	3
QNSE-fb0-d03	QNSE	no	1

5 Evaluation of atmospheric boundary-schemes in high-resolution model runs

For every model level σ from the surface up to 1500 above ground or correspondingly from $\sigma = 1...28$, the mean error (*ME* see eq. 1) and root mean squared error (*RMSE* see eq. 2) for the temperature forecast have been calculated for $N = 52$ SUMO profiles reaching heights $z > 900$ m agl. The corresponding flights are listed in Table 2. The same evaluation has been performed for the wind speed forecast for the levels $\sigma = 4...24$. For the evaluation of the wind information a reduced number of model levels have been used due to the fact that the observed wind is not reliable close to the ground and between the switch of the aircraft between ascent and descent.

$$ME = \frac{1}{N}\sum_{i=1}^{N}(X_{forecast_i} - X_{observed_i}) \tag{1}$$

$$RMSE = \sqrt{\frac{1}{N}\sum_{i=1}^{N}(X_{forecast_i} - X_{observed_i})^2} \tag{2}$$

In Figure 9 the result of the evaluation of WRF integrations is shown. In a)-d) we see the profiles for LYR and in e)-h) for OAS. For both locations the surface layer ($z < 250$ m) in all model integrations (besides QNSE-9km-fb0) shows a warm bias of approximately 1-3 K. In heights above 250 m the mean temperature bias ranges between -1 and 1 K which we consider as a very good agreement of WRF with the SUMO measurements. However, at OAS the model shows too low

temperatures above 1200 m. Overall, we see little sensitivity in the choice of ABL scheme, but high sensitivity to horizontal resolution. The wind profiles for LYR show an overall good agreement with the SUMO measurements. The bias is approximately 1 m s^{-1} from 200 - 800 m agl. The wind profile from the 9 km run shows a substantially poorer result which can be addressed to the smoother topography in the model. For OAS all model integrations show a too strong low level jet in 250 m agl. In heights above 500 m agl all 1 km integrations perform well while the coarser resolution runs overestimate the wind speed in all layers. We see quite little sensitivity in the choice of the ABL parameterization. However, the QNSE scheme performs slightly better in the lowest layers. The increase from 9 to 1 km horizontal resolution in WRF results in a better wind forecast which is a well known feature in the performance of NWP models in complex terrain. Since the three tested schemes show very similar results we cannot conclude that the QNSE scheme is substantially improving the near surface temperature forecast for very stable conditions. Nevertheless, this has to be seen as a subtle hint since the evaluation period was quite limited. This result is not directly comparable with the study of Sukoriansky and Galperin (2008) where the QNSE scheme is used in the High Resolution Limited Area Model (HIRLAM) system and statistically evaluated against pressure, temperature, wind speed and relative humidity observations in France and Scandinavia for a longer period (January 2005). The latter showed that employing the QNSE scheme improved the skill of the 24 h- and 48 h-forecast substantially.

6 Case study 31 March - 01 April 2009

During the campaign minimum surface temperature below -30°C have been measured during nights in fair weather i.e. during high pressure conditions with clear sky and low wind speeds (indicated by grey shading in Figure 4). The development of such low temperatures and corresponding extreme surface inversions, was in addition favored by the fact that Adventfjorden (see map in Figure 1b) was mostly ice-covered during spring 2009. Similar situations have been described by Petersson (2007), for instance.

The lowest temperatures during the campaign (T < -25°C) have been observed in two periods, from 23 to 25 March and from 31 March to 2 April. During both time intervals the 10 m wind speed was mostly below 5 m s^{-1} and the temperature difference between LYR and OAS exceeded 5 K (see Figure 5) due to the proximity of the LYR measurements to a patch of open sea along the coast off the airport. For this case study we have focused on a part of the most extreme cold episode, when the temperature difference between the stations reached values up to 14 K. Here, also numerous SUMO profiles with a typical repetition frequency of about 30-45 minutes could be performed due to nearly perfect flight conditions, i.e. low wind, clear sky and most important no air traffic restrictions during the night from 31 March to 1 April.

6.1 Synoptic weather conditions

During the selected period, the archipelago of Svalbard was influenced by a cold air outbreak which can be easily seen in the cloud streets appearing south of the sea-ice edge in the upper left corner of Figure 10. The cold-air outbreak was triggered by a combination of a high-pressure system over Greenland and a low-pressure system above the Barents Sea. The associated occlusion extended over Svalbard on 31 March 2009 0000 UTC (not shown). This synoptic constellation caused moderate northerly winds over the Svalbard archipelago.

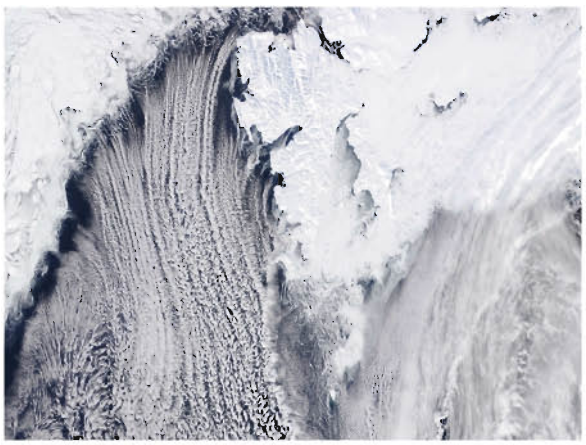

Figure 10 MODIS terra satellite imagery for the region of Svalbard on 01. April 2009 1200 UTC showing the cold-air outbreak influencing the experiment region.

6.2 Profile measurements

Figure 11 shows the subsequently measured profiles of temperature (T), potential temperature (Θ) and specific humidity (q) during the selected case measured by SUMO from one hour before dusk (1700 UTC) until dawn (0400 UTC). Panel b) presents the results of a corresponding WRF simulation of the studied period. In Figure 11a) the near surface temperatures measured by the 10 m mast are added. They show a strong cooling in the 2 m values from -16.5 °C in the afternoon down

Table 2 Overview of 52 SUMO soundings at Longyear airport (LYR) and at the old Auroral station (OAS) reaching heights $z > 900$ m agl.

SUMO ID	Start date, time [UTC]	max. height [m agl]	duration [min]	location
1	21 March 2009, 0636	1495	32	LYR
2	21 March 2009, 0709	1488	28	LYR
3	21 March 2009, 1137	1491	35	LYR
4	21 March 2009, 1214	1495	28	LYR
6	21 March 2009, 1643	1495	25	LYR
8	21 March 2009, 1832	1499	27	LYR
10	22 March 2009, 1837	1495	27	OAS
15	23 March 2009, 1833	1495	32	OAS
16	23 March 2009, 1909	1495	33	OAS
17	23 March 2009, 1944	1407	34	OAS
18	24 March 2009, 0514	1500	22	OAS
19	24 March 2009, 0538	1495	23	OAS
22	24 March 2009, 1737	1493	31	OAS
23	24 March 2009, 1833	1495	30	OAS
27	25 March 2009, 1824	972	14	LYR
30	26 March 2009, 0546	1495	21	OAS
34	28 March 2009, 1251	1413	18	LYR
36	28 March 2009, 1423	1088	27	LYR
37	29 March 2009, 1005	1495	25	LYR
38	29 March 2009, 1030	1495	22	LYR
39	29 March 2009, 1703	1495	26	OAS
40	29 March 2009, 1739	1499	12	OAS
41	29 March 2009, 1813	1495	25	OAS
43	29 March 2009, 1906	1495	27	OAS
44	29 March 2009, 1906	1492	23	OAS
46	30 March 2009, 0343	1495	21	LYR
47	30 March 2009, 0430	1495	17	LYR
48	30 March 2009, 0430	1495	29	LYR
49	30 March 2009, 1759	1495	25	LYR
50	30 March 2009, 1759	1496	23	LYR
53	31 March 2009, 1652	1495	27	OAS
55	31 March 2009, 1853	1495	28	OAS
56	31 March 2009, 1932	1495	33	OAS
57	31 March 2009, 1932	1495	32	OAS
58	31 March 2009, 2005	1496	22	OAS
59	31 March 2009, 2028	1494	20	OAS
60	31 March 2009, 2048	1495	11	OAS
61	31 March 2009, 2100	1495	23	OAS
62	31 March 2009, 2124	1495	29	OAS
63	31 March 2009, 2155	1495	47	OAS
64	31 March 2009, 2242	1495	57	OAS
66	1 April 2009, 0016	1495	41	OAS
68	1 April 2009, 0057	1499	34	OAS
70	1 April 2009, 0134	1495	40	OAS
71	1 April 2009, 0215	1495	40	OAS
72	1 April 2009, 0258	1495	36	OAS
73	1 April 2009, 0334	1494	19	OAS
74	1 April 2009, 0353	1495	38	OAS
76	1 April 2009, 1927	1496	22	LYR
77	1 April 2009, 2156	1495	26	LYR
78	2 April 2009, 0422	1497	23	LYR
79	2 April 2009, 0422	1493	23	LYR

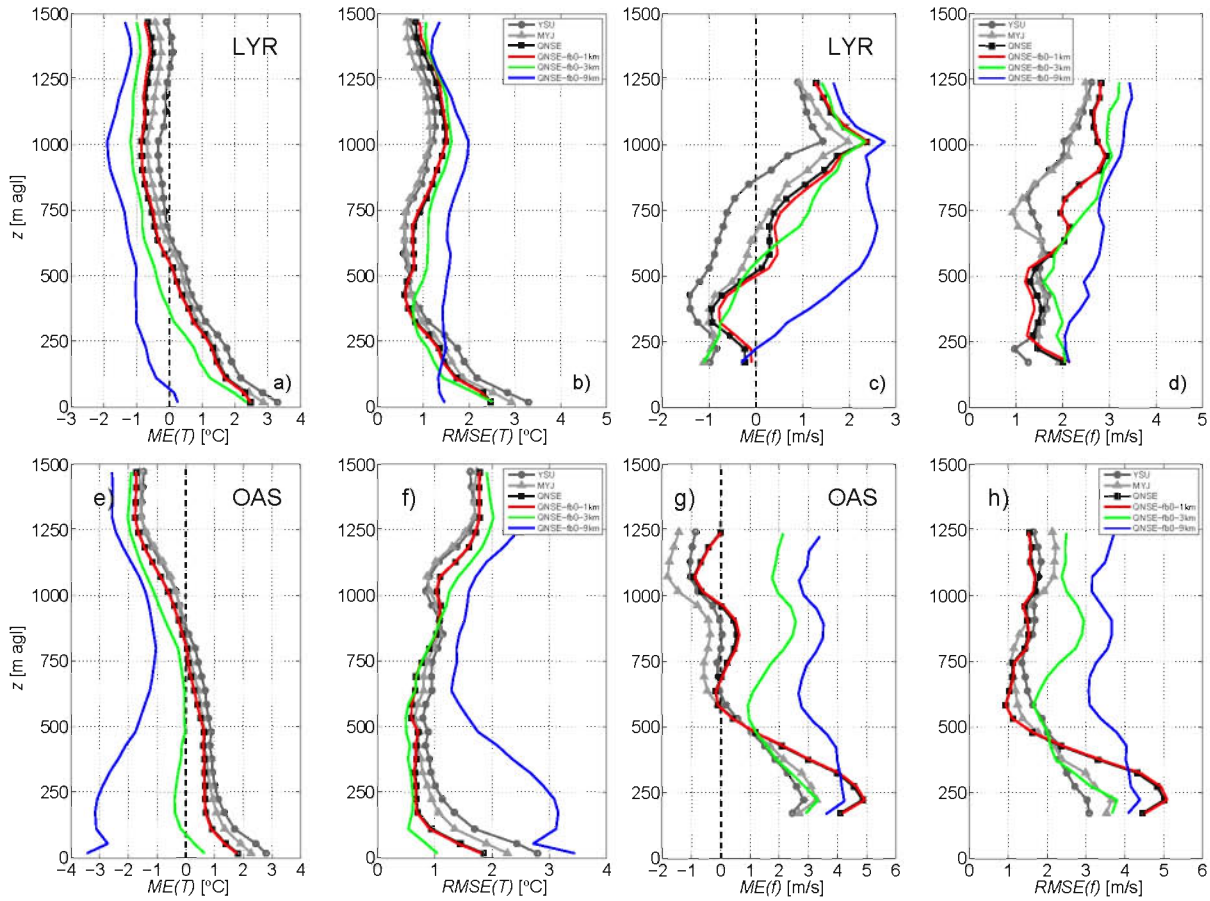

Figure 9 Evaluation of the ABL schemes (YSU, MYJ, QNSE) with respect to temperature and wind speed by using the mean error (eq. 1) and root mean square error (eq. 2) as a measure. a)-d): profiles at LYR; e)-h): profiles at OAS. Coloured profiles show the sensitivity to horizontal resolution (9 km - 3 km - 1 km) with de-activated feedback (fb0).

to values below -30 °C during the night. The lowest layer above the snow covered valley bottom (labelled by I in Figure 11a)) is very stable stratified with a temperature gradient between 2 and 10 m of 2-8 K, also distinctly increasing in time.

Due to the lower vertical velocity of SUMO during descent (ca. 2 m s^{-1} in contrast to typically 6-10 m s^{-1} during ascent), minimizing the effects of the temperature sensor time constant, only the SUMO profiles taken during descent have been used for the following investigations. The SUMO data have been averaged over 20 m intervals, with the lowest SUMO data point at 10 m above ground (see also Section 3). The remaining temperature offset of 2-8 K between SUMO and mast temperatures at this level is a result of the delay due to the time constant of the SUMO T-sensor in the strong inversion layer. The applied correction of the T-sensor's time-lag error is not sufficient to resolve the actual strong temperature gradient in the surface-layer inversion.

The SUMO profiles identify stable stratification ($d\Theta/dz > 0$) in the whole probed column up to 1500 m above ground. The layers II (50 -750 m) and IV (1200-1500 m) are moderately stable, while the marked inversion layer indicated by III (in 800-1200 m) is very stable. It shows at the beginning an increase in Θ of around 5 K over 200 m at around 1000 m. During the night this inversion is weakening ($d\Theta/dz = 4$ K 200 m^{-1}) and finally slightly descending to around 800 m in the morning. The level of the main inversion layer corresponds closely to the altitude of the surrounding mountains in AV, creating a high potential for the formation of internal gravity waves.

The time evolution in the measured temperature profiles reveals an overall cooling of 4-5 K during the course of 11 hours, in particular in the layers II and IV (see Figure 11a)). The strong cooling in layer IV can mainly be addressed to advection related to the cold-air-outbreak which is also reported from tethered balloon profiles in Ny-Ålesund and from the radiosonde on Bjørnøya (not shown). The strong cooling in the valley (0-700 m) is primarily due to enhanced outgoing longwave radiation

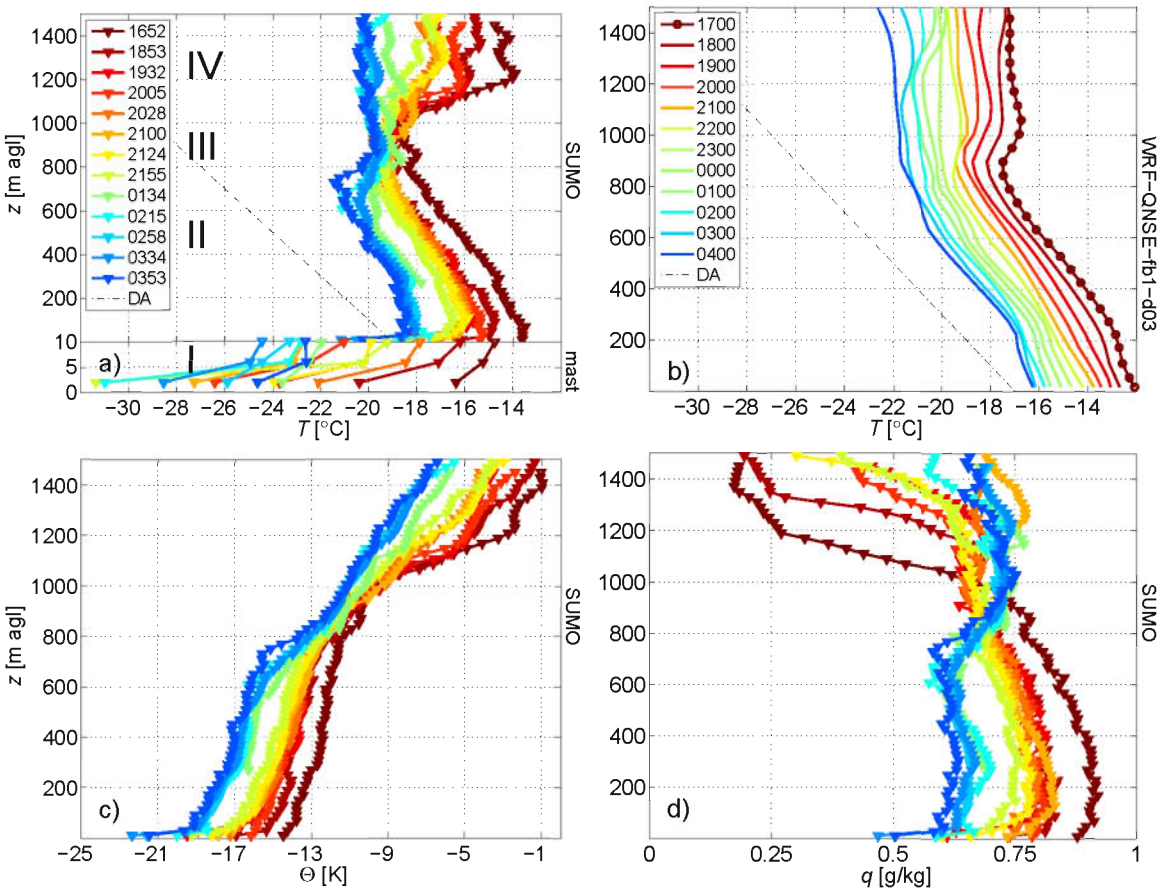

Figure 11 SUMO profiles for a) temperature, c) potential temperature and d) specific humidity profiles at OAS during the course of the night of 31. March until 01. April 2009. The temperature profiles in a) are supplemented by temperature measurements from the 10 m mast. DA: dry adiabate. The Roman numerals in a) indicate distinct layers discussed in Section 6.2. The corresponding WRF temperature profiles are shown in b); red circles indicate vertical model levels.

during night-time. Related katabatic and drainage effects in AV and from side-valleys, such as Todalen can even have intensified the strong night-time cooling in the valley. Calculating the accumulated cooling after the method described by De Wekker and Whiteman (2006) using the first (1652 UTC) and last (0353 UTC) of the SUMO profiles results in 3.4 MJ m^{-2}. The resulting night-time cooling for snow covered valleys of comparable size and surrounding topography coincides well with the observed temperature decrease of 4-5 K between sunset and sunrise (De Wekker and Whiteman, 2006).

The corresponding temperature profiles from WRF model simulations are shown in Figure 11b). They also reveal the general cooling seen in the observations. The model profiles show a slight warm bias of $\approx$ 2 K, but the amount and rate of cooling at least in the layers II (around 4 K) and IV (around 5 K) are captured well. However, large qualitative and quantitative differences occur in layer III. The model inversion in the late afternoon is by far weaker ($\approx$ 1 K 100 m$-$1) and located about 100 m lower than the observed one. It is weakening toward the morning. During the night the model layer III cools similar to layer IV above. The modeled inversion is getting weaker and rises toward morning. There is no indication of the sharp inversion in the SUMO profiles at around 700 m and the observed temperature decrease in layer III is by far less than predicted by the model. This feature will be discussed in more detaile below.

Figure 12 shows the corresponding wind speed and wind direction profiles. Close to the ground (2-10 m) the wind speed is low ($<$ 4 m s^{-1}) and from easterly to south-easterly directions throughout the whole period. As described in Section 3, no reliable wind data are available from the SUMO system below 200 m. Above, in general northerly winds are prevailing up to 1500 m except for the layer 800-1200 m where a distinct veering occurs throughout the night and at 200-400 m where south-easterly winds are observed in the morning hours. In the

beginning the slight backing of the wind with height indicates cold air advection in the lower atmosphere. The wind speed profiles of late afternoon and evening show two maxima, one in the center of layer II at around 400 m, reaching 6 m s^{-1} and an even more pronounced one reaching 8 m s^{-1} at around 1100 m. Around 800 m, i.e. at the bottom of the strong inversion layer, a minimum wind speed of 2-4 m s^{-1} is observed. The first peak in the wind profiles in layer II can be associated with a weak jet in the valley's center. Towards the morning, the wind speed profile has gradually changed. The lowest accessible layer by SUMO at around 200 m shows now an indication of a low level jet just above the very stable surface layer. Aloft, the wind speed is decreasing close to 0 at around 400 m, slightly speeding up around 600 m before reaching another minimum close to 0 at 800 m. Above that level, the wind increases linearly to about 6 m s^{-1} at 1500 m.

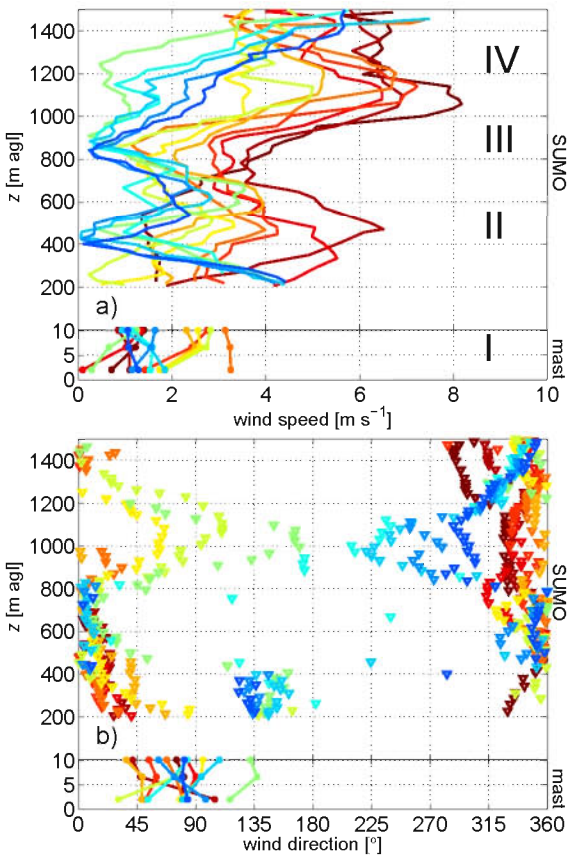

Figure 12 SUMO wind profiles and measurement from the 10 m mast at OAS during case 2. Colour code as in Figure 11a).

The atmospheric profiles taken during the night reveal two interesting features worthwhile to be investigated closer in the following. The first one is the relatively small amount of cooling (< 2 K) in layer III compared to that of layers II and IV, also shown by the average layer temperatures in Figure 13. The second one is the strong and systematic variation of the wind direction during the night in the layer between 900 m and 1100 m. After 2100 the wind in this layer starts to veer from north over east (2200) to south (0130) and finally to west (0330). The situation is visualized in more detail in Figure 14, where the temporal evolution of the average horizontal wind vectors in the layer 900-1100 m are shown. Layer III, roughly at the level of the surrounding mountains, seems to be outstanding by separating the valley from the free atmosphere. The data indicate that the inner-valley air in the layer 0-800 m is decoupled from the free atmosphere above by a strong inversion, leading to a lack of friction between the layers III and IV. Averaging the measured wind components in this altitude region (see Figure 14) shows a distinct and systematic clockwise veering of the horizontal wind vector indicating inertial flow. By theory an inertial period of $2\Pi f{-}1 \approx 12h$ is expected for the measurement location at 78° N, where f represents the corresponding Coriolis parameter. The rotation of the wind vectors in Figure 14, nearly completing a full circle during the observation period of 11 hours, is in good agreement with this theory. The reduced amount of cooling could therefore be an indication for a trapped inertio-gravity wave on top of layer III (900-1100 m). Assuming that the gravitational part of the wave is in its downward moving phase and more or less stationary during the night could explain a compression of the downward moving air against the stable layer in the valley (see the over time downward moving kink in the T-profile (Figure 11a) and Θ-profile (Figure 11c)). The corresponding warming in the 'sandwich'-layer (see black circles in Figure 13 after 2100) that is superimposed to the meso-scale cold-air-advection, results in the observed reduced cooling compared to the layers above and below.

7 Summary and Outlook

During a two weeks field experiment in Arctic environment, SUMO operated reliably and successfully even under very low temperatures. The system proved its potential for atmospheric profiling in such conditions with time resolutions of around 30 minutes. The relatively strict interpretation of the flight permission given by the Norwegian CAA by the local staff at Longyearbyen airport, limited the acquisition of a more complete dataset, e.g. by taking subsequent profiles during the course of a full day. SUMO operations were only allowed when the airport was closed, i.e. usually during

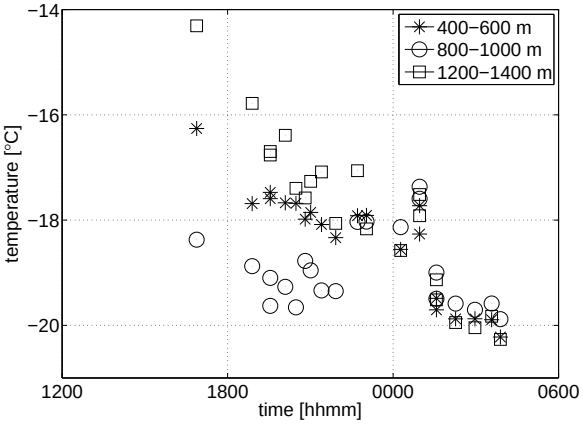

Figure 13 Quasi-timeseries of SUMO mean temperatures in the layers 400-600 m, 800-1000 m and 1200-1400 m during case 2.

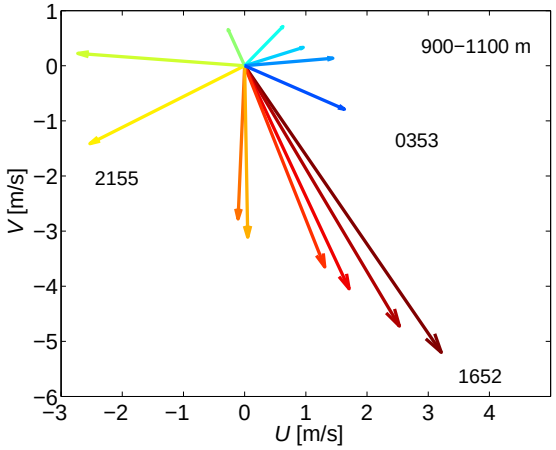

Figure 14 Averaged horizontal wind components shown as vectors for the layer 900-1100 m. Colour code corresponds with the SUMO profiles shown in Figure 11a).

the night time and on the weekends. For future applications routines have to be established that would allow a more frequent profiling, desired and required for advanced observation of ABL evolution and transition processes. Nevertheless, the gathered dataset provided an appropriate and valuable basis for a comparison with parallel tethered balloon ascents and a validation of the WRF model with respect to the performance of different ABL parameterization schemes for strongly stable conditions. Intense measurements during the night of 31. March until 1. April 2009 provided deeper insight in the complex interaction between atmosphere and orography in the stable Arctic ABL.

By operating a tethered balloon system simultaneously to the SUMO aircraft at LYR both measurement systems could be compared with each other. It can be concluded that the SUMO profiles have at least the quality as tethered balloon measurements for levels above ca. 200 m. SUMO outperforms the tethered balloon system in terms of flexibility, transportability and for the penetration of strong inversion layers. The tethered balloon system has its strength at lower levels, providing important information, e.g. with respect to wind information and for temperature measurements in very strong surface inversions. Therefore, it is an ideal tool to bridge the gap between surface measurements (2-10 m) and SUMO profiles in the altitude region of ca. 50-200 m.

In the NWP model part of this paper, we have presented high-resolution WRF runs performed with different ABL schemes. The sensitivity to the choice of ABL scheme and horizontal resolution has been evaluated by using SUMO profile measurements as reference. The QNSE scheme improves the temperature forecast slightly in stable conditions. However, all schemes show a warm bias close to the surface and a cold bias above the ABL.

The possibility to operate SUMO subsequently during one night in AV gave a more detailed picture of thermal and dynamical subgrid processes obviously not captured appropriately in the model integrations. In the surface layer such processes can be night-time cooling due to outgoing longwave radiation and additional drainage processes leading to an extreme surface inversion above the snow covered valley bottom. The obvious presence of an inertial-gravity wave in the atmospheric layer over the valley at the level of the surrounding mountains has not been captured by the model. A higher vertical resolution in these layers and an improved representation of the topography might overcome these shortcomings in the shown NWP model integrations.

Acknowledgements The field work was financed by the Arctic Field Grant 2009 (Svalbard Science Forum RIS ID 3346). Travel expenses for the co-authors M. O. Jonassen and J. Reuder have been covered by Meltzerfondet and an IPY-Thorpex Norwegian Research Council grant number 175992/S30.
Special thanks to Avinor at Longyearbyen airport for a cooperative working environment, and to meteorologikonsulent Torgeir Mørk (DNMI) for kindly providing meteorological data from Longyear airport. The authors are grateful to UNIS for the accessibility of the old Auroral station in Adventdalen as one of the flight basis. Thanks to Andøya Rocket Range for the permssion to use their facilities at Longyear airport. Many thanks to Tor de Lange (GFI) for his great commitment in installing the weather mast in AV in extreme weather conditions. The tethered balloon data was kindly provided by Tiina Kilpeläinen and Miina Manninen. The authors wish to acknowledge the work and commitment of the pilots Martin Müller and Christian Lindenberg. We thank Thomas Spengler for the valuable discussions on boundary-layer dynamics of the case study. Supercomputing resources, on a Cray XT4 computer at Parallab at the University of Bergen, have been made available by the Norwegian Research Council.

References

Brisset P, Drouin A, Gorraz M, Huard P, Tyler J (2006) The Paparazzi solution. MAV2006, Sandestin, Florida

Bromwich D, Hines K, Bai L (2009) Development and testing of Polar Weather Research and Forecasting model: 2. Arctic Ocean. J Geophys Res 114

Chen F, Dudhia J (2001) Coupling an advanced land surface-hydrology model with the Penn State-NCAR MM5 modeling system. Part I: Model implementation and sensitivity. Mon Weather Rev 129(4):569–585

Chou M, Suarez M (1999) A solar radiation parameterization for atmospheric studies. NASA Tech Memo 104606:40

Curry J, Maslanik J, Holland G, Pinto J (2004) Applications of Aerosondes in the Arctic. Bull Amer Meteorol Soc 85(12):1855–1861

De Wekker S, Whiteman C (2006) On the time scale of nocturnal boundary layer cooling in valleys and basins and over plains. J Appl Meteorol Climatol 45(6):813–820

Dethloff K, Abegg C, Rinke A, Hebestadt I, Romanov V (2001) Sensitivity of arctic climate simulations to different boundary layer parameterizations in a regional climate model. Tellus A 53(1):1–26

Galperin B, Sukoriansky S, V P (2007) Implementation of the Quasi-Normal Scale Elimination (QNSE) turbulence model in WRF. 8th WRF Users' Workshop, Boulder CO, June 2007

Hanssen-Bauer I, Førland E (2001) Verification and analysis of a climate simulation of temperature and pressure fields over Norway and Svalbard. Clim Res 16:225–235

Hines K, Bromwich D (2008) Development and Testing of Polar Weather Research and Forecasting (WRF) Model. Part I: Greenland Ice Sheet Meteorology. Mon Weather Rev 136(6):1971–1989

Hines K, Bromwich D, Bai LS, Barlage M, A S (2011) Development and testing of Polar WRF. Part III. Arctic land. J Climate 24:26–48

Hong S, Kim S (2007) Stable boundary layer mixing in a vertical diffusion scheme. The Korea Meteor Soc, Fall conference, Seoul, Korea, Oct 25-26

Hong S, Noh Y, Dudhia J (2006) A new vertical diffusion package with an explicit treatment of entrainment processes. Mon Weather Rev 134(9):2318–2341

Janjic Z (1990) The step-mountain coordinate: Physical package. Mon Weather Rev 118(7):1429–1443

Janjic Z (1996) The surface layer in the NCEP Eta model. 11th Conference on Numerical Weather Prediction, Amer Meteorol Soc pp. 354–355

Janjic Z (2002) Nonsingular implementation of the Mellor-Yamada Level 2.5 Scheme in the NCEP meso models. NCEP Office Note No. 437:61p

Jonassen M (2008) The Small Unmanned Meteorological Observer (SUMO) - Characterization and test of a new measurement system for atmospheric boundary layer research. Master's thesis, Geophysical Institute, University of Bergen

Kilpeläinen T, Vihma T, Ólafsson H (2010) Modelling of spatial variability and topographic effects over Arctic fjords in Svalbard. Tellus A pp. DOI: 10.1111/j.1600–0870.2010.00,481.x

van den Kroonenberg A, Martin T, Buschmann M, Bange J, Vörsmann P (2008) Measuring the wind vector using the autonomous Mini Aerial Vehicle M^2AV. J Atmos Ocean Technol 25:1969–1982

Mahrt L (1998) Nocturnal boundary-layer regimes. Boundary-Layer Meteorol 88(2):255–278

Manninen M (2009) Structure of the atmospheric boundary layer in Isfjorden, Svalbard, in late winter 2009. Master's thesis, University Center in Svalbard

Mayer S, Sandvik A, Jonassen M, Reuder J (2010) Atmospheric profiling with the UAS SUMO: A new perspective for the evaluation of fine-scale atmospheric models. Meteorol Atmos Phys DOI: 10.1007/s00703-010-0063-2

Mckinnon K (1996) Convergence of the Nelder-Mead simplex method to a non-stationary point. Tech. rep., SIAM J. Optim.

Mlawer E, Taubman S, Brown P, Iacono M, Clough S (1997) Radiative transfer for inhomogeneous atmosphere: RRTM, a validated correlated-k model for the longwave. J Geophys Res 102(D14):16,663–16,682

Mölders N, Kramm G (2010) A case study on wintertime inversions in Interior Alaska with WRF. Atmos Res 95(2-3):314–332

Petersson C (2007) An analysis of the local weather around Longyearbyen and an instrumental comparison. Master's thesis, University Center in Svalbard

Reuder J, Brisset P, Jonassen M, Müller M, Mayer S (2009) The Small Unmanned Meteorological Observer SUMO: A new tool for atmospheric boundary layer research. Meteorol Z 18(2):141–147

Reuder J, Ablinger M, Ágústsson H, Brisset P, Brynjólfsson S, Garhammer M, Johannesson T, Jonassen M, Kühnel R, Lämmlein S, de Lange T, Lindenberg C, Malardel S, Mayer S, Müller M, Ólafsson H, Rögnvaldsson O, Schäper W, Spengler T, Zängl G, Egger J (2011) FLOHOF 2007: An overview of the mesoscale meteorological field campaign at Hofsjökull, Central Iceland. Meteorol Atmos Phys DOI: 10.1007/s00703-010-0118-4

Sandvik A, Furevik B (2002) Case study of a coastal jet at Spitsbergen - comparison of SAR and model estimated wind. Mon Weather Rev 130:1040–1051

Schicker I, Seibert P (2009) Simulation of the meteorological conditions during a winter smog episode in the Inn Valley. Meteorol Atmos Phys 103(1):211–222

Seibert P, Beyrich F, Gryning SE, Joffre S, Rasmussen A, Tercier P (2002) Review and intercomparison of operational methods for the determination of the mixing height. Dev Environ Sci 1:569–613

Skamarock W, Klemp J, Dudhia J, Gill D, Barker D, Duda M, Huang XY, Wang W (2008) A Description of the Advanced Research WRF Version 3. NCAR/TN:475+STR

Stull R (1988) An Introduction to Boundary Layer Meteorology. Kluwer Academic Publishers

Sukoriansky S, Galperin B (2008) Anisotropic turbulence and internal waves in stably stratified flows (QNSE theory). Physica Scripta 132:014,036

Tjernström M, Zagar M, Svensson G (2004) Model simulations of the Arctic atmospheric boundary layer from the SHEBA year. AMBIO: J Human Environ 33(4):221–227

Tjernström M, Zagar M, Svensson G, Cassano J, Pfeifer S, Rinke A, Wyser K, Dethlo K, Jones C, Semmler T, Shaw M (2005) Modelling the Arctic Boundary Layer: An Evaluation of Six ARCMIP Regional-Scale Models using Data from the SHEBA Project. Boundary-Layer Meteorol 117:337–381

Troen I, Mahrt L (1986) A simple model of the atmospheric boundary layer; sensitivity to surface evaporation. Boundary-Layer Meteorol 37:129–148

Whiteman CD, Zhong S, Shaw WJ, Hubbe JM, Bian X, Mittelstadt J (2001) Cold pools in the Columbia Basin. Weather and Forecast 16:432–447

Zängl G (2005) Dynamical aspects of wintertime cold-air pools in an Alpine valley system. Mon Weather Rev 133(9):2721

Zilitinkevich S, Baklanov A (2002) Calculation of the height of the stable boundary layer in practical applications. Boundary-Layer Meteorol 105(3):389–409

Paper III

A 'no-flow-sensor' wind estimation algorithm for Unmanned Aerial Systems

Mayer, S. Hattenberger, G. Brisset, P. Jonassen, M. Reuder, J. (2011)

International Journal of Micro Aerial Vehicles
status: submitted

A 'no-flow-sensor' wind estimation algorithm for Unmanned Aerial Systems

Stephanie Mayer, Gautier Hattenberger, Pascal Brisset, Marius O. Jonassen, Joachim Reuder

S. Mayer
Geophysical Institute, University of Bergen
now at: Uni Bjerknes Centre for Climate Research
Allegaten 70
5007 Bergen, Norway
Tel.: +47-55 58 87 13
Fax: +47-55 58 98 83
Email: stephanie.mayer@uni.no

G. Hattenberger
Ecole Nationale de l'Aviation Civil
7, avenue Edouard Belin
31055 Toulouse Cedex 4, France

P. Brisset (†2010)
Ecole Nationale de l'Aviation Civil
7, avenue Edouard Belin
31055 Toulouse Cedex 4, France

M. O. Jonassen
Geophysical Institute, University of Bergen
Allegaten 70
5007 Bergen, Norway

J. Reuder
Geophysical Institute, University of Bergen
Allegaten 70
5007 Bergen, Norway

Abstract

A 'no-flow-sensor' wind estimation algorithm for Unmanned Aerial Systems (UAS) is presented. It is based on ground speed and flight-path azimuth information from the autopilot's GPS system. The algorithm has been tested with the help of the simulation option in the Paparazzi autopilot software using artificial wind profiles. The retrieval accuracy of the predefined profiles by the wind algorithm and its sensitivity to vertical aircraft velocity, diameter of the helical flight pattern and different data sampling methods have been investigated. The algorithm with a correspondingly optimized set of parameters is then applied to various scientific flight missions under real wind conditions performed by the UAS SUMO (Small Unmanned Meteorological Observer). The SUMO wind profiles are compared to measurements of conventional atmospheric profiling systems as radiosondes and piloted balloons. In general, the presented 'no-flow-sensor' wind estimation method performs well in most atmospheric situations and is now operationally used in the post-processing routine for wind profile determination from SUMO measurements.

1 INTRODUCTION

Further progress in atmospheric modeling, important for improved weather forecasts and reliable future climate projections, is inevitably linked to the availability of appropriate data sets for model initialization, model test and validation, and finally model improvement [1, 2, 3]. It is well known that a large portion of the existing model uncertainties can be attributed to an incomplete and unsatisfactory description of relevant atmospheric processes in the atmospheric boundary layer (ABL), i.e. the lowest few kilometres in the atmosphere [4, 5]. As this lower part of the atmosphere is easily accessible by UAS, such systems provide a vast potential to increase the corresponding observational capabilities. Enabling atmospheric profiling and horizontal surveys of the meteorological key parameters pressure, temperature, humidity and wind, in unique spatial and temporal resolution, UAS are expected to be an ideal tool to close the existing observational gap between ground based measurements (e.g. synoptic meteorological network, measurement masts) and satellite observations.

The use of relatively small and therefore cost-efficient UAS as an alternative to conventional meteorological profiling systems (e.g. radiosondes)

in meteorological field campaigns has become more frequent and manifold. Konrad [6] pioneered within this field in the early 1970s with an instrumented and remotely piloted model aircraft. A similar profiling system (KALI), has been developed at the University of Munich in the late 1990s. It has been operated during various field experiments in Nepal, Bolivia and Germany up to 3 km above the ground, in particular for the investigation of orographic effects on atmospheric flow ([7], [8]). Two significant shortcomings of the KALI system are the need of experienced pilots for continuous remote controlled operation of the aircraft and the lack of an appropriate wind measurement system.

Technical progress and electronic miniaturization has triggered the development of UAS equipped with autopilot systems during the last decade (e.g. [9]). Examples for successful application of this concept for atmospheric research are among others, the Aerosonde built in Australia [10], the M^2AV developed in Germany [11], and SUMO [12], developed under the auspices of the Geophysical Institute, University of Bergen in Norway. The larger of these systems have a typical payload of a few kilograms. Therefore it is uncritical to carry a set of sensors for the determination of the meteorological wind speed. The true air speed (TAS) measured by any kind of flow sensor on the airframe can be transformed into the wind speed (u) when the ground speed (GS) and the aircraft's attitude, i.e. the Eulerian angles (yaw, pitch, roll), are known (e.g. [13] and [14]). Small UAS, such as SUMO, have strictly limited payload capacities in the order of a few tenths of grams. Thus, an alternative wind estimation method, without the need of direct flow measurement, but with an accuracy comparable with standard profiling systems such as radiosondes (systematic bias: ± 0.2 m/s; random error: 0.6-3 m/s [15]) has to be designed for small and lightweight platforms.

The Small Unmanned Meteorological Observer
(SUMO) has been designed and developed in cooperation between the Geophysical Institute at the University of Bergen, Norway, Martin Müller Engineering, Germany and the UAS laboratory at ENAC in Toulouse, France. Main design criteria were, the capability of determining meteorological parameters such as pressure, temperature, humidity, wind speed and wind direction with satisfactory accuracy in addition to mobility, flexibility, cost-efficiency and low infrastructural demands for measurements in remote areas. The system is intended to be operated as a 'controllable and recoverable radiosonde' inside and slightly above the ABL. This way, it will help to close the existing gap of in-situ ABL observations covering horizontal scales from

several tenths of meters up to around 10 km. The SUMO UAS system in its current version ([12] and [16]) is based on a modification of the FunJet construction kit by Multiplex and has a wingspan of 80 cm and an overall take-off weight of 580 g. It is electrically powered by a lithium polymer battery (3 cells, 11.4 V, capacity 2100 mAh) driving a pusher-propeller by a 140 W motor in the rear of the airframe. SUMO has a typical endurance of 20 minutes full power motor time, enabling flight missions up to about one hour. For autonomous flight capabilities SUMO is equipped with the Paparazzi autopilot system ([17] and http://paparazzi.enac.fr/wiki/Overview). Paparazzi is an open source autopilot hardware and software project mainly dedicated to the operation of small fixed and rotary wing UAS. It includes the ground control station (GCS) for operation and pre-flight mission planning and simulation. Bi-directional data communication between GCS and aircraft, both for online data transfer to the ground and in-flight mission modification toward the aircraft is implemented by a 2.4 GHz telemetry link. SUMO can easily be used in remote areas without extensive infrastructure. During the last years it has been operated during several field campaigns and successfully performed nearly 300 scientific flight missions (e.g. [12] and [18]). By that it has proven its great value, e.g. for the evaluation of fine scale numerical weather prediction (NWP) models [19].
The 'no-flow-sensor' wind estimation algorithm is introduced in the following Section 2. Paparazzi simulations for testing the method in specific wind conditions are described in Section 3 with the aim to optimize the combination of flight pattern and algorithm parameter configuration. In Section 4, the wind algorithm is tested against simulations for a real föhn situation. Followed by Section 5 where these configurations are applied in the algorithm for the determination of real wind profiles. These wind estimations are compared to conventional atmospheric profiling systems, such as piloted balloon (PiBal) and radiosonde measurements. Finally the study is summarized in Section 6. A short outlook is given in Section 7.

2 WIND ESTIMATION ALGORITHM

2.1 Description

The wind triangle sketched in Fig. 1 describes the wind impact on a flying aircraft. By measuring the true air speed vector (**TAS**) and the ground speed

vector (**GS**) of the aircraft, the atmospheric wind (**u**) can be determined (e.g. [13] and [14]). This implies that both variables have to be measured with very high accuracy since they ususally are of greater magnitude than the variable that has to be calculated. Therefore, sophisticated TAS and Eulerian angle measurement equipment consisting of at least a flow sensor and gyroscope is necessary for a direct wind measurement by using the wind triangle method. As small UAS have a very limited payload capacity, alternative ways for the determination of the horizontal wind have to be developed. In the 'no-flow-sensor' wind estimation method only onboard GPS information (time (t), height above ground (z), flight-path azimuth (χ) and ground speed (GS)) is used to estimate wind speed and wind direction.
The 'no-flow-sensor' method implies a helical (for vertical profiles) or a circular (for horizontal surveys) flight pattern. During flight in a circle the aircraft is influenced by the horizontal wind, thus experiencing tailwind it flies faster and in headwind conditions it is slowed down. Corresponding GS is illustrated in colour code in Fig. 3.

Before the algorithm is explained in detail, some basic variables have to be defined.

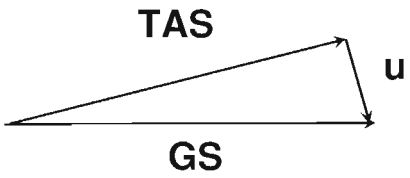

Figure 1: A vector diagram of the wind triangle. TAS: true airspeed, GS: ground speed and u: horizontal wind.

The wind triangle (Fig. 1) is formulated as:

$$\mathbf{TAS} + \mathbf{u} = \mathbf{GS} \tag{1}$$

The mean of the TAS can be calculated by

$$\overline{TAS} = \frac{1}{N} \sum_{i}^{N} \|\mathbf{GS_i} - \mathbf{u}\|. \tag{2}$$

The corresponding variance and standard deviation are defined as:

$$\sigma_{TAS}^2 = \frac{1}{N}\sum_{i}^{N}\left(\|\mathbf{GS_i} - \mathbf{u}\| - \overline{TAS}\right)^2 \tag{3}$$

$$\sigma_{TAS} = \sqrt{\frac{1}{N}\sum_{i}^{N}\left(\|\mathbf{GS_i} - \mathbf{u}\| - \overline{TAS}\right)^2}. \tag{4}$$

For the initialization of the algorithm, the horizontal wind $\mathbf{u}$ is set to [0,0], i.e. **TAS** = **GS**. Flying the aircraft with constant throttle and pitch angle, nearly constant TAS can be assumed. A way to visualize the wind algorithm is to project **GS** and **TAS** in a Cartesian plane. The algorithm fits a circle through the measurement points (see Fig. 2). The circle is found by minimizing the distances (σ_{TAS}) between the measurement points to fit a circle sector with radius r = TAS. This can be achieved by applying a minimization algorithm such as the Nelder-Mead method [20]. This method is known for its computational efficiency and robustness. It is a simplex method for finding a local minimum of a function of several variables. For two variables, a simplex is a triangle, and the method is a pattern search that compares function values at the three vertices of a triangle. The worst vertex, i.e the largest function value, is rejected and replaced with a new vertex. A new triangle is formed and the search is continued. The process generates a sequence of triangles (which can have different shapes), for which the function values at the vertices decrease. The size of the triangles is reduced and the coordinates of the minimum point are found. The algorithm is stated using the term simplex (a generalized triangle in n dimensions) and will find the minimum of a function of n variables [21]. In the example sketched in Fig. 2 a circle with a radius of $TAS \approx 18$ is found. By using the GPS measurement of $\mathbf{GS} = [GS\sin(\chi), GS\cos(\chi)]$ the wind can finally be estimated by the vector difference between **GS** and **TAS**, resulting in $\mathbf{u} = (4.8, 0)$) in Fig. 2.

3 SIMULATIONS

The Paparazzi software incorporates a flight simulation module. This tool has been used to test the algorithm by pre-describing artificial wind conditions. Two different synthetic wind profiles have been applied:

1. constant wind speed $|\mathbf{u}|$ = ws = 10 m/s from 0 to 2000 m above ground

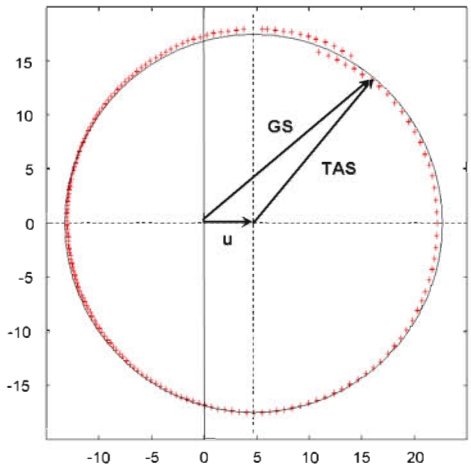

Figure 2: An example of GPS output (red crosses) projected into the Cartesian plane. The black line represents a fit to the respective ground speed values.

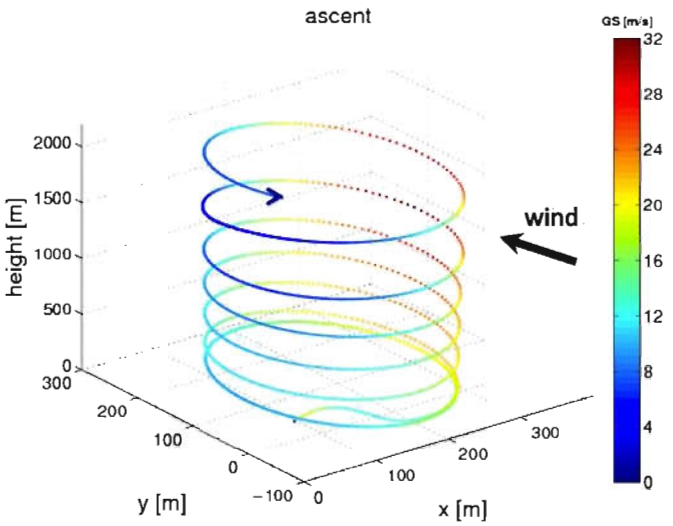

Figure 3: SUMO ascent flight path; colour bar indicates the changing GS [m/s] corresponding to the aircraft encountering headwind (GS small, blue colours) and tailwind (GS high, red colours).

level (agl) and veering (clockwise changing) wind direction with height covering the entire range of 0 ° to 360 ° (see Fig. 4a).

2. constant wind direction (wd = 270 °), and changing wind speed with height (see Fig. 4b)).

The reason for choosing these wind conditions is first of all to clarify if the wind algorithm can cope correctly with all possible wind directions and secondly to see how appropriate it is for the resolution of vertical wind speed gradients (wind shears) changing sharply as indicated in Fig. 4b in z = 1500 m agl.

Both artificial wind profiles have been combined with different flight parameters, such as helix radius and climb speeds, and two different data sampling methods to perform a comprehensive sensitivity study.

3.1 Flight parameters

For ABL studies it is desireable to profile the whole depth of the ABL and even to penetrate capping inversions which can typically reside in heights of 500 m to 2000 m agl. In its current version, the SUMO aircraft motor run time is limited by the battery capacity to approximately 20 min, i.e. with a climb speed of 5 m/s it can reach approximately 3000 m and return safely back to ground. In practice, SUMO climbs in a helix with a radius (r) in the order of 100-200 m (see Fig. 3) with a climb speed (cs) ranging between 2-8 m/s. Accordingly, the algorithm has been tested for a helix with $r_1 = 120$ m and $r_2 = 200$ m, and for $cs_1 = 2$ m/s, $cs_2 = 4$ m/s, and $cs_3 = 8$ m/s.

3.2 Data sampling methods

Two data sampling methods are applied, one representing spatial sampling (1.), the other one temporal sampling (2.):

1. The spatial samples $N = i...n$ are taken for single angular slots (α). Slots of $\alpha = 5$ °, $\alpha = 10$ ° and $\alpha = 15$ ° have been used.

2. The temporal samples $N = i...n$ are taken over a specific time period (p). Periods of $p = 60$ s, $p = 90$ s and $p = 120$ s have been applied.

Mean height intervals Δz are calculated by averaging heights z_i within each sample.

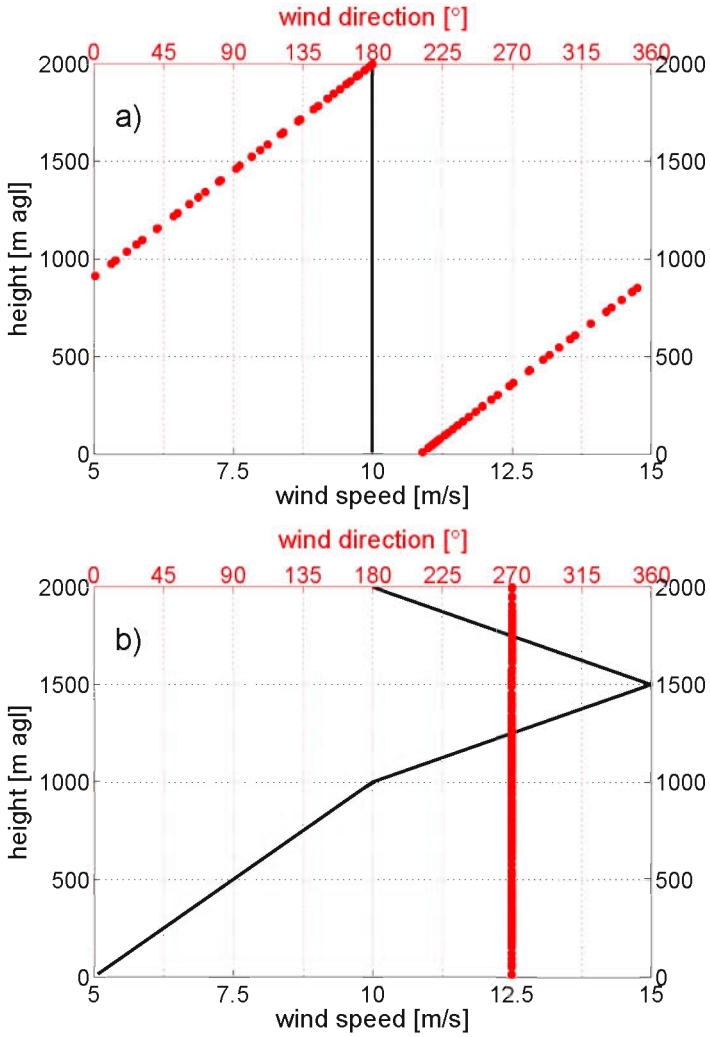

Figure 4: Theoretical wind functions used as references. Bottom axes: wind speed. Top axes: wind direction. a) twisted wind profile with constant wind speed. b) constant wind direction profile with changing wind speed with height.

3.3 Quality tests

As an objective measure of which method is preferable, the average of the root mean squared error ($\overline{\delta}$) is calculated for each configuration:

$$\delta = \sqrt{\frac{1}{n}\sum(t_i - s_i)^2} \tag{5}$$

t: truth and s: simulation. index $i...n$: measurements.

Tables 1-4 summarize the results of the performed sensitivity study. Tables 1 and 2 correspond to the quality of determined wind speed and wind direction using the artificial wind profile 1 (constant wind speed, constant change of wind direction with height). Tables 3 and 4 show the results for wind profile 2 (constant wind direction, continuous wind shear with a maximum wind speed at 1500 m above ground). The results for the wind speed in case 1 (Table 1) show in general a high sensitivity of the retrieval quality from climb speed. The higher the climb speed, the larger $\overline{\delta}(ws)$. The climb speed effect is more pronounced for the temporal sampling. The results also indicate a general increase in $\overline{\delta}(ws)$ toward larger r. The quality of the spatial method seems to be nearly independent of the choice of alpha for the probed sector. These findings are confirmed by the results of the wind speed retrieval for case 2. The only difference is the slightly reduced sensitivity of the temporal method with respect to climb speed and radius of the helical flight path. For the wind direction (Table 2 and 4) the situation is not as clear. Again there is in most cases an increase in $\overline{\delta}(wd)$ with climb speed, except for the spatial method in case 2, where the 8 m/s simulation shows a slightly decreased delta $\overline{\delta}(wd)$. Overall, the 'no-flow-sensor' wind estimation algorithm performs very well in the parameter space of the conducted simulations. $\overline{\delta}(ws)$ is distinctly below 1 m/s, except for some simulations with the 8 m/s climb speed. $\overline{\delta}(wd)$ remains nearly always below 5 °. With this, the algorithm is expected to enable the determination of wind profiles with an accuracy that is comparable to other in situ wind profiling methods. From the presented sensitivity study alone, no clear advice for the preferable use of the spatial or temporal sampling method can be given. Anyway, it is clear that low climb speeds should be favored. Low climb speeds are, however, rather inefficient for reaching high ceiling altitudes required e.g. for a comprehensive profiling of daytime convective boundary layers that can extend vertically over more than 2 km above ground. In such cases, SUMO

is therefore typically operated with high and very efficient climb rates of 8-10 m/s during ascent, but rather low vertical velocities in the order of 2 m/s during descent.

Table 1: Average of root mean squared errors ($\overline{\delta}(ws)$) in m/s for the simulations based on the wind speed profile shown in Fig. 4a. Tested are the estimation methods (spatial method, temporal method) and helix size (r = 120 m, r = 200 m); for different climb speeds (cs).

	cs [m/s]	**spatial [°]**				**temporal [s]**			
		5	10	15	avg.	60	90	120	avg.
120 m	± 2	0.31	0.31	0.32	**0.31**	0.27	0.25	0.22	**0.24**
	± 4	0.36	0.37	0.38	**0.37**	0.28	0.44	0.69	**0.47**
	± 8	0.63	0.65	0.67	**0.65**	0.84	1.57	2.62	**1.68**
200 m	± 2	0.35	0.36	0.37	**0.36**	0.52	0.34	0.34	**0.40**
	± 4	0.52	0.52	0.54	**0.53**	0.57	0.64	0.81	**0.67**
	± 8	1.22	1.23	1.23	**1.23**	1.69	1.84	2.93	**2.15**

Table 2: Average of root mean squared errors ($\overline{\delta}(wd)$) in degrees (°) for the simulations based on the wind direction profile shown in Fig. 4a.

	cs [m/s]	**spatial [°]**				**temporal [s]**			
		5	10	15	avg.	60	90	120	avg.
120 m	± 2	2.16	2.21	2.35	**2.24**	0.90	1.21	1.04	**1.05**
	± 4	2.81	2.88	2.96	**2.88**	1.56	1.59	2.01	**1.72**
	± 8	5.89	7.06	4.10	**5.68**	2.50	2.34	3.46	**2.77**
200 m	± 2	2.33	2.48	2.54	**2.45**	2.58	2.09	1.87	**2.18**
	± 4	3.54	3.61	3.65	**3.60**	4.90	1.84	4.09	**3.61**
	± 8	4.02	4.04	4.10	**4.05**	8.29	2.34	3.21	**4.61**

Table 3: Average of root mean squared errors ($\overline{\delta}(ws)$) in m/s for the simulations based on wind speed shown in Fig. 4b.

	cs [m/s]	spatial [°]				temporal [s]			
		5	10	15	avg.	60	90	120	avg.
120 m	± 2	0.54	0.51	0.51	**0.52**	0.43	0.43	0.44	**0.43**
	± 4	0.55	0.45	0.51	**0.50**	0.54	0.54	0.57	**0.55**
	± 8	0.90	0.88	0.73	**0.84**	0.70	0.81	0.97	**0.83**
200 m	± 2	0.36	0.49	0.42	**0.42**	0.87	0.40	0.39	**0.55**
	± 4	0.91	0.89	0.91	**0.90**	0.75	0.58	0.61	**0.65**
	± 8	1.04	0.95	0.90	**0.96**	0.82	0.82	0.95	**0.86**

Table 4: Root mean squared differences ($\overline{\delta}(wd)$) in degrees (°) for the simulations based on wind direction shown in Fig. 4b.

	cs [m/s]	spatial [°]				temporal [s]			
		5	10	15	avg.	60	90	120	avg.
120 m	± 2	2.55	2.53	2.58	**2.55**	2.37	2.23	2.19	**2.26**
	± 4	2.37	2.48	2.59	**2.48**	1.84	1.86	1.88	**1.86**
	± 8	1.89	1.89	1.93	**1.90**	2.34	2.29	2.29	**3.31**
200 m	± 2	1.77	1.82	2.25	**3.73**	2.86	2.23	2.86	**3.15**
	± 4	3.02	2.95	2.66	**2.88**	4.41	3.31	3.42	**3.71**
	± 8	4.71	4.76	4.70	**4.72**	5.20	5.06	4.98	**5.08**

4 SIMULATION OF A 'FÖHN' CASE

The wind conditions applied in Section 3 are rather artificial. In the next step, the algorithm has also been tested in a simulation based on real wind conditions. For this case, a föhn situation has been selected. The corresponding simulations have been initialized with a wind profile measured by a radiosonde released in Munich, Germany on 26.02.2010 at 00 UTC. The shown wind profile is characterized by a nocturnal low level jet at 250 m above ground, rather constant wind speeds of around 7 m/s between 400 m and 1000 m, and increasing wind speeds above, reaching a maximum wind speed of 15 m/s at 1800 m agl. Aloft, the wind is slightly decreasing to 12 m/s at 3000 m agl. The wind direction is mostly westerly with a slight turn to southerly directions in 1000 to 1500 m agl (see Fig. 5).

The resulting wind profiles derived by the wind algorithm are shown in Fig. 5a for the temporal (p = 60 s) and in Fig. 5b for the spatial sampling method (α = 5 °). The colour indicates the simulations for ascent (blue) and descent (red). In general, the wind estimation algorithm reproduces the initial profile very well. At altitudes below 1300 m both sampling methods fit the initial profile excellent, with an overall better score for the spatial sampling method. The mean score for both sampling methods are $\overline{\delta}(ws) = 2.16$ for the temporal method respectively $\overline{\delta}(ws) = 0.65$ for the spatial method. With higher ambient wind speeds above 1300 m, the temporal sampling method seems to get unstable, resulting in distinct spikes around the measured profile. These are the result of the increasing wind at this altitude reaching nearly the TAS of the aircraft. Looking at a selection of GPS positions during descent, numerous oscillations can be identified, when the aircraft is impacted by strong headwind (see Fig. 6). The spatial sampling method shown in Fig. 5b) does not produce such outliers under headwind conditions. This can be explained by the fact that the temporal data sampling method cannot find an appropriate matching circle due to the aircrafts flight path oscillations while the spatial sampling method overcomes this issue.

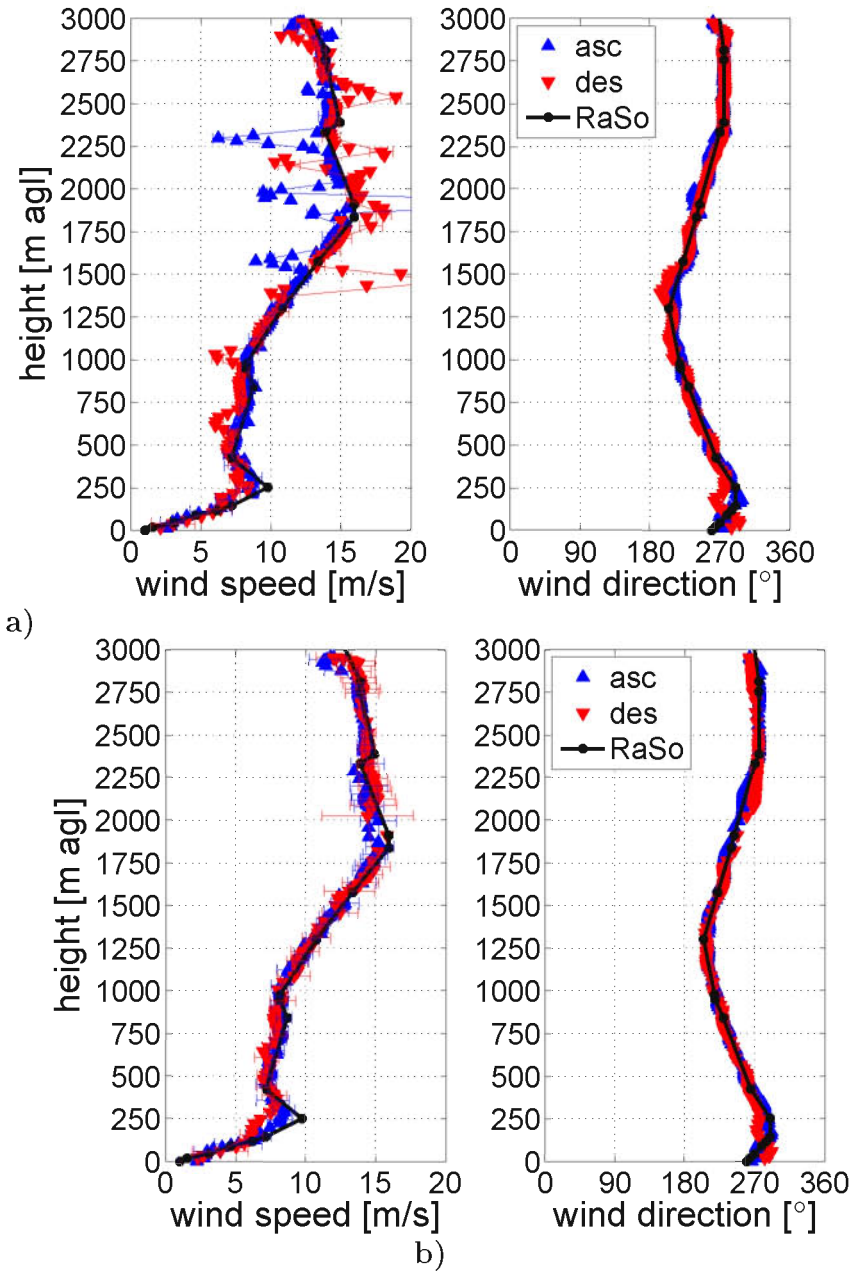

Figure 5: A radiosonde wind profile for a 'föhn' case in Munich, Germany, 26.02.2010 00:00 UTC. a) temporal method has been used. b) using the spatial sampling method. Black line: radiosonde (RaSo); blue: ascent (asc); red: descent (des).

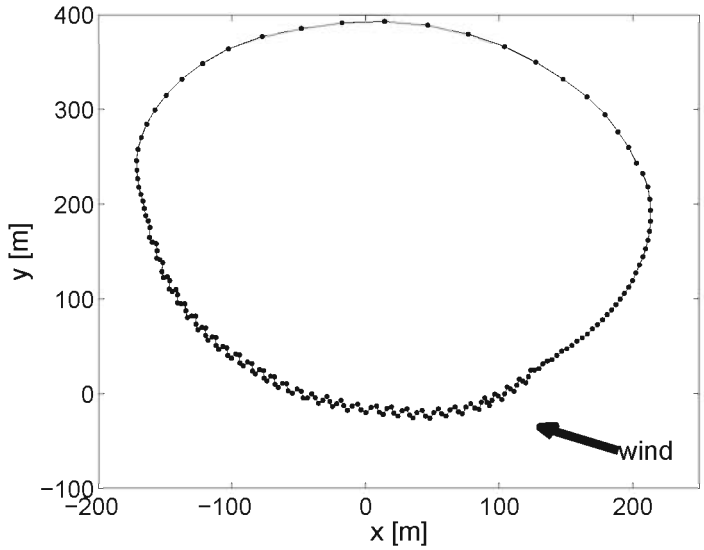

Figure 6: SUMO positions in x-y plane during strong wind conditions. The flight direction is counter-clockwise.

5 APPLICATION TO REAL ATMOSPHERIC MEASUREMENTS

In meteorology, well established in-situ measurement platforms for wind profiles are e.g. radiosondes (RaSo). A radiosonde or rawinsonde is a measurement unit that is attached to a helium filled weather balloon. To date, radiosondes are equipped with a temperature, humidity and pressure sensor and a GPS device. They can penetrate the troposphere and reach high altitudes ($>$ 25 km). Radiosondes are influenced by local wind conditions and therefore they can be quickly blown away from their launch position. Usually they cannot be recovered and thus, they are a rather expensive tool to be used in high frequency. An alternative tool to determine wind speed and wind direction is the method of piloting a small helium filled balloon (PiBal) with two theodolites simultaneously, see e.g. [22]. To investigate the quality of wind profile derivation by the 'no-flow-sensor' wind algorithm in comparison with these conventional in-situ profiling measurement tools, SUMO has been operated in parallel with the aforementioned measurement platforms in several field campaigns. The results are summarized in Table 5. Again both

sampling methods have been applied. For the spatial sampling method, we have chosen a slot of $\alpha = 5\ ^\circ$ and for the temporal sampling method, we have used a period of p = 60 s.

Fig. 7 displays a comparison between PiBal measurement (black line) and a SUMO profile where both the temporal (blue line) and spatial (red line) method have been applied. The PiBal profile is in this case temporally lagged by one hour to the SUMO flight. Both systems show low wind speeds in the order of 2-5 m/s from westerly directions. SUMO data have been averaged between ascent and descent. To enable the direct comparison between both sounding systems, both data sets have been averaged in 50 m height intervals. Both methods show almost identical results in heights z $\geq$ 400 m. Low wind speed ($\leq$ 5 m/s) from westerly to southwesterly directions. Considering PiBal data representing the true state of the atmosphere, the spatial method reduces the root mean squared errors ($\overline{\delta}$) both for wind speed and wind direction quite substantially. The spatial method performs well in low heights ($\leq$ 400 m) compared to the temporal method which fails in this case in heights z $<$ 400 m where SUMO had to leave its helical flight pattern due to switch to manual mode.

Fig. 8 shows SUMO wind estimations in comparison to a RaSo measurement. Both systems have been launched simultaneously from the Norwegian coast guard vessel KV Svalbard. The RaSo sounding registered wind speeds of 15 m/s from northeast in heights of 200 to 600 m above ground. Above, the wind speed decreased to 10 m/s and turned slightly to more easterly directions. The SUMO sounding corresponds very well with the RaSo wind measurement both in wind speed and wind direction. Again, considering the RaSo representing the truth, the spatial method reduces the $\overline{\delta}$ for wind speed (ws) by ca. 40 % and for the wind direction (wd) by 50 % compared to the temporal method.

Fig. 9 presents another example of a SUMO wind profile simultaneously measured with a RaSo ascent in Coburg, Germany. The RaSo measured wind speeds between 6-11 m/s with two minima; one at 200 m agl and a second one at 1000 m agl. A wind speed maximum can be identified in 1400 m agl. Overall, the SUMO measurement match well with the RaSo. The spatial method reduces $\overline{\delta}(ws)$ by approximately 30 %. The wind direction ranges between southeast and east. The SUMO measurement agreed also well with the RaSo measurement. The spatial method reduces $\overline{\delta}(wd)$ by ca. 50 %.

Fig. 10 shows an example of quite strong wind conditions of 8 to 14 m/s measured from the Norwegian coast guard vessel KV Harstad in Andfjorden, Northwestern Norway. The wind speed is almost linearly increasing with height. In this case, SUMO measurements show wind speeds that are in average 1-2 m/s lower compared to the RaSo. This is most likely due to the time lag of almost 2 hours between both launches. Additional discrepancies in the compared wind data can be expected due to the increasing horizontal separation of both systems with altitude, as SUMO is profiling stationary while the RaSo is drifting with the wind. Again, the spatial sampling method reduces $\overline{\delta}(ws)$ by ca. 20 %. The wind direction was mainly west, southwest in lower heights. Both wind direction profiles agree very well. The slots method reduces $\overline{\delta}(wd)$ by approximately 40 %.

Overall, we can state that the spatial sampling method improves the algorithm's performance compared to the temporal sampling method in real wind conditions. This is especially seen for measurements in lower heights. This is quite crucial because thereby reliable wind information can be gained also at lower levels. Using the temporal sampling method, wind data below 200 m would have to be discarded due to poor data quality (high $\overline{\delta}$).

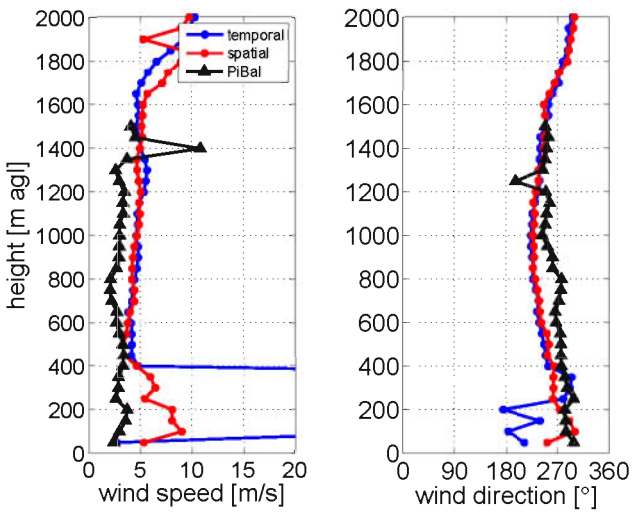

Figure 7: A measured wind profile in Central Iceland, 18.08.2007 17:56 UTC. Black: piloted balloon measurements; blue: wind algorithm using the temporal sampling method with p=60 s; red: wind algorithm using the spatial sampling method with α=5°.

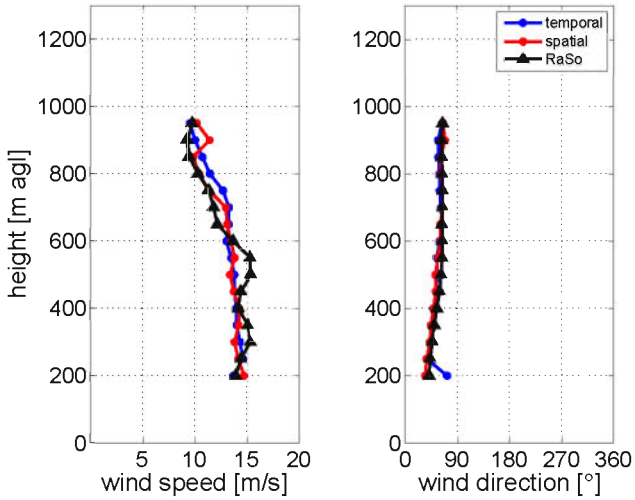

Figure 8: A measured wind profile on Svalbard, 28.02.2008 15:11 UTC. Colour code as in Fig. 7.

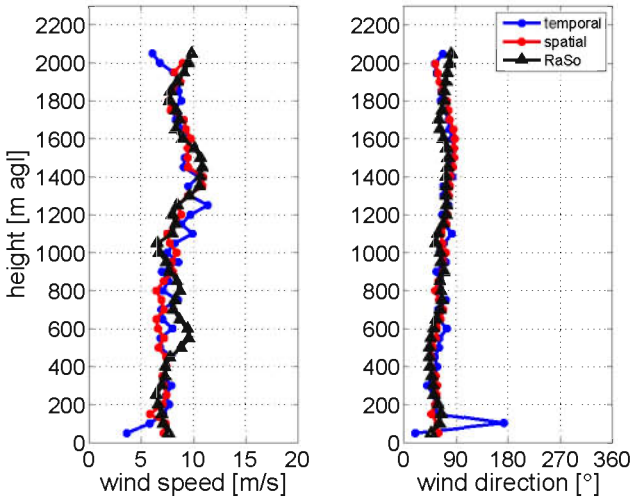

Figure 9: A measured wind profile at Coburg, Germany, 24.07.2008 12:00 UTC.Colour code as in Fig. 7.

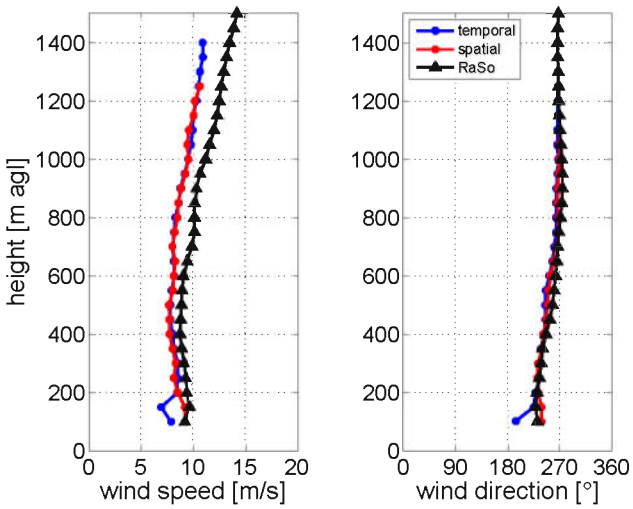

Figure 10: A measured wind profile in Andfjorden, Northern Norway, 27.09.2009 08:28 UTC. Colour code as in Fig. 7.

Table 5: Average of root mean squared errors $\overline{\delta}(ws)$ of the measured wind speed (ws) and wind direction (wd). Wind conditions are indicated in m/s in the right column.

profiles	$\overline{\delta}$(**ws**)		$\overline{\delta}$(**wd**)		wind speed
	temporal	spatial	temporal	spatial	m/s
Iceland, 2007 (Fig. 5)	39.02	2.55	40.98	25.51	< 5
Svalbard, 2008 (Fig. 6)	1.71	1.04	10.82	5.42	10-15
Germany, 2008 (Fig. 7)	1.53	1.10	21.07	10.36	5-10
Norway, 2009 (Fig. 8)	1.92	1.56	9.51	5.46	10-15

6 SUMMARY

In this paper, a 'no-flow-sensor' wind estimation method especially suited for small UAS has been introduced. The algorithm has been tested for different atmospheric conditions by comparing it to simulations and atmospheric measurements. It has been shown that the method can be successfully applied in real atmospheric conditions and that it is appropriate in particular for use with the UAS SUMO. The algorithm has been tested in several configurations, using two different sampling methods (temporal and spatial) as well as different different helix radii (120 m and 200 m) and climb speeds (2, 4, 8 m/s). One important outcome is that best wind data quality can be achieved by operating SUMO with low climb speed. As low climb speed is rather inefficient in reaching high ceiling levels for ABL profiling, SUMO is for this purpose typically operated with high vertical velocity during ascent (8-10 m/s) but distinctly lower values (around 2 m/s) during descent.
The comparison of SUMO wind measurements with PiBal, and RaSo measurements, shows clearly that under real atmospheric conditions the spatial method performs significantly better than the temporal period method especially for low heights. The reason for this is that the spatial method is less sensitive to an exact helical flight pattern compared to the temporal method. Applying the algorithm to a simulation of a föhn case with vertical wind shear showed that the temporal sampling method has its shortcomings in strong headwind conditions when the aircraft's track starts to oscillate. Based on the results of this study the spatial data sampling method used within in the no-flow-sensor wind estimation algorithm has been chosen as an inherent part of the SUMOs data post-processing routine.

7 OUTLOOK

From the meteorological point of view wind measurements closer to the surface (below 200 m) are very important to enable the identification of wind shears and low level jets close to the ground, in particular for investigations of the stable polar boundary layer. For this purpose it is highly desirable to operate SUMO in autonomous mode below that height in future field campaigns. First tests in keeping SUMO in autonomous mode in heights considerably lower as 200 m have given promising results. The SUMO system is under continuous development. Recently it has been equipped with

an inertia measurement unit (IMU) to extend its application range for operations in cloudy conditions and even inside clouds. A pitot tube and 5-hole probe are under integration at the moment. Information from such flow sensors can in the future be used to improve and complement the performance of the presented "sensor-less" algorithm for wind determination. The 5-hole probe, capable for 3D flow measurements with 100 Hz sampling rate, will enable investigations of atmospheric turbulence e.g. for measurements in the wake of wind turbines.

ACKNOWLEDGEMENTS

We would like to dedicate this paper to our colleague Pascal Brisset, one of the fathers and main driving forces behind the Paparazzi project, who tragically died in a climbing accident in May 2010. Our gratitude is directed to the pilots Christian Lindenberg and Martin Müller being a credible part during numerous field campaigns during the last years. We thank the FLOHOF team, the crews of KV Svalbard and KV Harstad. We thank the RaSo team of the Meteorological Institute Munich (MIM) during the field experiment performed in Coburg, Germany. Field grants for M. O. Jonassen and J. Reuder were partly covered by the Arctic Field Grant RiS ID 2902, by the project "Measurement of the energy exchange over sea ice and Arctic leads" (Meltzer foundation, University of Bergen, project number 480627) and IPY/THORPEX (grant number 175992/S30; www.ipythorpex.no).

References

[1] K. Dethloff, C. Abegg, A. Rinke, I. Hebestadt, and V. Romanov, "Sensitivity of Arctic climate simulations to different boundary layer parmeterizations in a regional climate model," *Tellus*, vol. 53A, pp. 1–26, 2001.

[2] D. Stensrud, *Parameterization schemes: Keys to understanding numerical weather prediction models.* Cambridge University Press, 2007.

[3] J. Teixeira, B. Stevens, C. Bretherton, R. Cederwall, J. Doyle, J. Golaz, A. Holtslag, S. Klein, J. Lundquist, D. Randall, A. Siebesma, and P. Soares, "Parameterization of the atmospheric boundary layer: A view

from just above the inversion," *Bulletin of the American Meteorological Society*, vol. 89, no. 4, pp. 453–458, 2008.

[4] L. Mart, "Stratified atmospheric boundary layers and breakdown of models," *J. of Theor. Comp. Fluid Dyn.*, vol. 11, pp. 263–280, 1998.

[5] M. Tjernström, M. Žagar, J. Svensson, J. Cassano, S. Pfeiffer, A. Rinke, K. Wyser, K. Dethloff, C. Jones, S. T., and M. Shaw, "Modelling the Arctic Boundary Layer: An Evaluation of Six Arcmip Regional-Scale Models using Data from the Sheba Project," *Boundary Layer Meteorology*, vol. 117, no. 2, pp. 337–381, 2005.

[6] T. Konrad, M. Hill, J. Rowland, and J. Meyer, "A Small, Radio-Controlled Aircraft As A Platform For Meteorological Sensors," *Appl. Phys. Lab. Tech. Digest*, pp. 11–19, 1970.

[7] J. Egger, S. Bajrachaya, R. Heinrich, P. Kolb, S. Lämmlein, M. Mech, J. Reuder, W. Schäper, P. Shakya, J. Schween, and H. Wendt, "Diurnal Winds in the Himalayan Kali Gandaki Valley. Part III: Remotely Piloted Aircraft Soundings," *Monthly Weather Review*, vol. 130, pp. 2042–2058, 2002.

[8] J. Egger, L. Blacutt, F. Ghezzi, R. Heinrich, P. Kolb, S. Lämmlein, M. Leeb, S. Mayer, E. Palenque, J. Reuder, W. Schäper, J. Schween, R. Torrez, and F. Zaratti, "Diurnal Circulation of the Bolivian Altiplano. Part I: Observations," *Monthly Weather Review*, vol. 133, no. 4, pp. 911–924, 2005.

[9] T. Mueller, "On the Birth of Micro Air Vehicles," *International Journal of Micro Air Vehicles*, vol. 1, no. 1, pp. 1–12, 2009.

[10] G. Holland, P. Webster, J. Curry, G. Tyrell, D. Gauntlett, G. Brett, J. Becker, R. Hoag, and W. Vaglienti, "The Aerosonde Robotic Aircraft: A New Paradigm for Environmental Observations," *Bulletin of the American Meteorological Society*, vol. 82, no. 5, pp. 889–901, 2001.

[11] T. Spiess, J. Bange, M. Buschmann, and P. Vörsmann, "First application of the meteorological Mini-UAV M2AV," *Meteorologische Zeitschrift*, vol. 16, no. 2, pp. 159–169, 2007.

[12] J. Reuder, P. Brisset, M. Jonassen, M. Müller, and S. Mayer, "The Small Unmanned Meteorological Observer SUMO: A new tool for atmospheric boundary layer research," *Meteorol. Z.*, vol. 18, no. 2, pp. 141–147, 2009.

[13] P. Vörsmann, "Ein Beitrag zur bordautonomen Windmessung," *TU Braunschweig Diss.*, 1984.

[14] A. van den Kroonenberg, T. Martin, M. Buschmann, J. Bange, and P. Vörsmann, "Measuring the Wind Vector Using the Autonomous Mini Aerial Vehicle M2AV," *J. Atmos. Oceanic Technol.*, 2008.

[15] WMO, "WMO Guide to Meteorological Instruments and Methods of Observations," Tech. Rep. 8, WMO, 2008.

[16] M. Jonassen, "The Small Unmanned Meteorological Observer (SUMO) - Characterization and test of a new measurement system for atmospheric boundary layer research," *Master thesis at the University of Bergen, Norway*, 2008.

[17] P. Brisset, A. Drouin, M. Gorraz, P. Huard, and J. Tyler, "The Paparazzi Solution," *ENAC*, 2006.

[18] J. Reuder, M. Ablinger, H. Ágústsson, P. Brisset, S. Brynjólfsson, M. Garhammer, T. Johannesson, M. Jonassen, R. Kühnel, S. Lämmlein, T. de Lange, C. Lindenberg, S. Malardel, S. Mayer, M. Müller, H. Ólafsson, O. Rögnvaldsson, W. Schäper, T. Spengler, G. Zängl, and J. Egger, "FLOHOF 2007: An overview of the mesoscale meteorological field campaign at Hofsjökull, Central Iceland," *Meteorology and Atmospheric Physics*, vol. DOI: 10.1007/s00703-010-0118-4, 2011.

[19] S. Mayer, A. Sandvik, M. O. Jonassen, and J. Reuder, "Atmospheric profiling with the UAS SUMO: A new perspective for the evaluation of fine-scale atmospheric models," *Meteorology and Atmospheric Physics*, vol. DOI: 10.1007/s00703-010-0063-2, 2010.

[20] K. I. M. Mckinnon, "Convergence of the Nelder-Mead simplex method to a non-stationary point," tech. rep., SIAM J. Optim, 1996.

[21] J. A. Nelder and R. Mead, "A simplex algorithm for function minimization," *Computer Journal*, vol. 7, no. 4, p. 308313, 1965.

[22] H. Rachele and L. Duncan, "Desirability of using a fast sampling rate for computing wind velocity from pilot balloon data," *Monthly Weather Review*, vol. 95, no. 4, pp. 198–202, 1967.